Uncertainty in Life Cycle Assessments of Well-to-Wheel Greenhouse Gas Emissions of Transportation Fuels Derived from Various Crude Oils

by

Giovanni Roberto Di Lullo

A thesis submitted in partial fulfillment of the requirements for the degree of

Master of Science

in

Engineering Management

Department of Mechanical Engineering
University of Alberta

Edmonton, Alberta

Abstract

Growing concern over climate change has created pressure on the oil and gas industry to reduce their greenhouse gas (GHG) emissions. Several life cycle assessment (LCA) studies have examined various crude oils in an attempt to determine which have the lowest and highest well-to-wheel (WTW) GHG emissions. The majority of these studies published deterministic point estimates with a limited sensitivity analysis. Due to the variation in results between studies and the lack of an uncertainty analysis, the usefulness of the results for policy makers and industry representatives is limited.

The goal of this study is to expand on the previous research by identifying a realistic range of WTW emissions for various crude oils. This research builds on the previously published **FU**N**d**amental **EN**gineering Princip**l****E**s-based Mode**L** for Estimation of **G**reen**H**ouse **G**ases in **C**onventional **C**rude **O**ils (FUNNEL-GHG-CCO). The FUNNEL-GHG-CCO model produced point estimates of the WTW emissions for five North American crude oils. This work makes improvements to the model, adds a Monte Carlo simulation to calculate uncertainty, analyzes additional scenarios to examine the effect of field age on WTW emissions, and expands the model to include three crudes from outside North America. A sensitivity analysis is used to identify sensitive inputs. Then distributions for the sensitive inputs are determined from the literature and used to run the Monte Carlo simulations.

The resulting WTW emission ranges for gasoline are 95.3-99.9 (Saudi Arabia), 99.9-105.5 (Maya), 96.4-104.0 (Mars), 101.6-109.9 (Venezuela Low Steam), 101.1-109.2 (Sirri), 102.5-114.2 (Bow River), 104.6-114.5 (Alaska North Slope (ANS) historical), 105.5-113.2 (Kern historical), 113.6-138.5 (Venezuela High Steam), 133.2-163.2 (ANS current), and 131.5-155.0 gCO_2eq/MJ (Kern current). For ANS and Kern, the current scenarios use lifelong average

production data and the historical scenarios use recent production data to illustrate how the WTW emissions change as the fields age. For the Venezuela crude, two scenarios are used as a wide range of steam-to-oil ratios appear in the literature.

The results of this study will be beneficial to both policy makers and industry representatives. The results identify which pieces of information policy makers would require from industry in order to get accurate WTW emissions estimates. The uncertainty ranges provide a better understanding of how WTW GHG emissions vary between crude oils. This will help policy makers understand the limitations of such models.

Preface

This thesis is original work by Giovanni Di Lullo under the supervision of Dr. Amit Kumar. Chapter 2 and Appendix A were submitted to *Environmental Science and Technology* as Di Lullo, G., Zhang, H., Kumar, A., "Uncertainty in Life Cycle Assessments of Well-to-Wheel Greenhouse Gas Emissions of Transportation Fuels Derived from North American Crudes." Chapter 3 and Appendix B will be submitted to *Applied Energy* as Di Lullo, G., Zhang, H., Oni A., Kumar, A., "Uncertainty in the Life Cycle Assessment Well-to-Wheel Greenhouse Gas Emissions of Transportation Fuels." I was responsible for the concept formulation, data collection, model improvement and validation, and manuscript composition. Dr. Hao Zhang contributed to model validation and manuscript edits. Dr. Abayomi Olufemi Oni contributed to manuscript edits. Dr. Amit Kumar was the supervisory author and was involved with concept formulation, evaluation, assessment of results, and manuscript edits.

This work built on previous work done by Rahman et al. 2014 [1-3] at the University of Alberta. Rahman et al. developed the **FU**N**d**amental E**N**gineering Princip**l** **E**s-based Mode**L** for Estimation of **G**reen**H**ouse **G**ases in **C**onventional **C**rude **O**ils (FUNNEL-GHG-CCO). The FUNNEL-GHG-CCO model performs a life cycle assessment of five North American crude oils. My work used the FUNNEL-GHG-CCO model as a starting point and made improvements to the model calculations as discussed in chapter 2, section 2.2.1. I added a Monte Carlo simulation to the model to calculate well-to-wheel emission ranges rather than deterministic point estimates. I also added three additional crudes to the model from Saudi Arabia, Iran, and Venezuela. I also added two scenarios to study the effect of reservoir age on WTW emissions.

Acknowledgments

I would like to thank Dr. Amit Kumar for providing his continual guidance and support when it was needed. I am especially thankful that he gave me the opportunity to take ownership of the project.

I would like to acknowledge the NSERC/Cenovus/Alberta Innovates Associate Industrial Research Chair in Energy and Environmental Systems Engineering and the Cenovus Energy Endowed Chair in Environmental Engineering for providing financial support for this project. The authors are grateful to representatives from Cenovus Energy Inc., Suncor Energy Inc., Alberta Innovates Energy and Environment Solutions (AI-EES) and Alberta Innovates Bio Solutions (AI-BIO) for their inputs and comments during the course of this study.

I would like to thank Dr. Hao Zhang, a postdoctoral fellow in the Department of Mechanical Engineering at the University of Alberta, for teaching me how to write technical papers and reviewing my research papers. I would like to thank Astrid Blodgett for editorial assistance over the past two years and Dr. Abayomi Olufemi Oni for editorial assistance of this manuscript.

I would like to acknowledge my colleagues at the University of Alberta for their advice and support.

I am grateful to my parents, friends, and girlfriend for their continual support and encouragement. This thesis would not have been possible without them. Thank you.

Table of Contents

List of Tables

List of Figures

Abbreviations

°API	American Petroleum Institute gravity
ANS	Alaska North Slope
CSS	Cyclic steam simulation
EF	Emission factor (gCO_2/MJ)
F-1	Original FUNNEL-GHG-CCO model
F-2	Modified FUNNEL-GHG-CCO model for chapter 2
F-3	Modified FUNNEL-GHG-CCO model for chapter 3
FUNNEL-GHG-CCO	**FUN**damental **EN**gineering Princip**l** **E**s-based Mode**L** for Estimation of **G**reen**H**ouse **G**ases in **C**onventional **C**rude **O**ils
GHG	Greenhouse gas
GOR	Gas-to-oil ratio (m^3/m^3)
GREET	Greenhouse Gases, Regulated Emissions, and Energy Use in Transportation
GWP	Global warming potential
HS	High steam
KYO	Know Your Oil
LCA	Life cycle assessment
LHV	Lower heating value (MJ/kg)
LS	Low steam
MD	Marine diesel
NG	Natural gas
OPGEE	Oil Production Greenhouse Gas Emissions Estimator
OTSG	Once through steam generator
P#	#th percentile
P5	5th percentile
P95	95th percentile
PG	Produced gas
PRELIM	Petroleum Refinery Life Cycle Inventory Model
SF	Steam flood
SI	Supplementary information
SOR	Steam-to-oil ratio (cold water equivalent m^3/m^3)
SP	Surface processing
TTW	Tank-to-wheel (combustion)
ULCC	Ultra-large crude carrier
VFF	Venting, flaring and fugitive
VLCC	Very large crude carrier
WAG	Water-alternating-gas
WF	Water flood
WOR	Water-to-oil ratio (m^3/m^3)
WTR	Well-to-refinery gate
WTT	Well-to-tank
WTW	Well-to-wheel

Chapter 1: Introduction

1.1 Background

Growing awareness of climate change and global pushes for reducing climate change have led to an increased interest in reducing global greenhouse gas (GHG) emissions [4]. Because transportation emissions are responsible for 23% of global CO_2 emissions [5], governments around the world have set carbon emissions reduction targets. For example, the European Union [6] and the California Air Resource Board [7] have implemented polices to reduce transportation fuels carbon intensities by 6% and 10%, respectively, before 2020. One of the solutions to meet these targets is to consume transportation fuels (gasoline, diesel, and jet) with lower upstream emissions.

Upstream emissions from transportation fuels are generated during crude oil production, surface processing, transportation, refining, and distribution. The upstream emissions from crudes vary depending on crude properties and the methods used to produce and process the crude into finished transportation fuels. Heavier crudes usually require more energy to produce and refine than lighter crudes [1, 8].

Crude is a generic term referring to several types of oil. Crude oils are further classified based on their American Petroleum Institute gravity (ºAPI), which is the inverse of a crude's density. For example, water has an API of 10º [9]. Based on their API gravity, crudes are classified as light (>31.1 ºAPI), medium (22.3-31.1 ºAPI), heavy (10-22.3 ºAPI), and extra-heavy (<10 ºAPI) [10].

In order to determine which crudes have higher or lower upstream emissions, life cycle assessments (LCA) can be used to quantify the emission intensities of transportation fuels from various crude oils. LCAs examine the energy used and emissions generated along the life cycle stages from extracting the natural resource to the end of the product life [11]. LCAs are comprised of four main stages: goal and scope definition, life cycle inventory, life cycle impact assessment, and interpretation [12]. Defining the goal and scope sets the context of the study and includes defining a functional unit, system boundaries, assumptions and limitations, and allocation methods. The life cycle inventory stage quantifies the inputs and outputs for each stage. The impact assessment involves classifying and weighting the various impacts into

categories. The interpretation stage is used to verify and effectively communicate the results. By performing LCAs on multiple crudes we can determine which crudes have higher or lower emissions.

1.2 Literature review and research gap

Current literature examines the well-to-wheel (WTW) emissions of transportation fuels, which include the upstream and combustion emissions. The models used for these studies can be divided into two types. Type 1 models, such as Greenhouse Gases, Regulated Emissions, and Energy Use in Transportation (GREET) [13] and GHGenius [14], use a top-down approach wherein high level aggregated facility and country-level data are used to calculate industry average emissions. The use of aggregated data makes it difficult to determine the emission intensity for specific crudes. Type 2 models, such as Jacobs [15, 16], TIAX [17], Oil Production Greenhouse gas Emissions Estimator (OPGEE) [18], Petroleum Refinery Life Cycle Inventory Model (PRELIM) [19], and **FUN**damental **EN**gineering Princip**l****E**s-based Mode**L** for Estimation of **G**reen**H**ouse **G**ases in **C**onventional **C**rude **O**ils (FUNNEL-GHG-CCO) [1-3], use a bottom-up approach wherein energy consumed and emissions generated are calculated using engineering first principles for each stage. Due to lack of information and process complexity, the bottom-up models only examine processes that consume or produce large amounts of energy or pollution and so do not capture all the emissions produced, thus leading to modeling errors. However, a bottom-up model is flexible and can calculate the emissions for specific crudes and provide detailed results for each sub-process.

Various bottom-up models have determined WTW emissions for over 35 crudes; however, the results are difficult to compare due to differences in the boundaries and assumptions used. Additionally, the TIAX and Jacobs models lack transparency and reproducibility as these used confidential data [15-17]. Gordon et al. published a report titled “Know Your Oil” (KYO) that used the PRELIM and OPGEE models to develop WTW estimates for thirty crude oils using consistent boundaries [8]. However, all these models provide deterministic point estimates for the WTW emissions. Without an uncertainty analysis, it is not possible to accurately compare crudes based on their WTW emissions. If the model uncertainty is large compared to the difference in the emissions between two crudes, it would not be accurate to claim that one crude has lower emissions than the other.

1.2 Research motivations

This research was motivated by the following factors:

- The current literature reports WTW emissions as deterministic point estimates; these have limited value and do not convey model accuracy. In order to fairly represent the emissions from each crude uncertainty ranges are required.
- Some of the published reports use confidential information and lack transparency. An independent analysis that uses publically available data is required to verify the results.
- Due to variations across the industry and uncertainty in the publically available data, results should be presented as ranges instead of point estimates for a specific scenario.
- The effect of a crude oil field's age on WTW emissions is not found in current literature.
- The FUNNEL-GHG-CCO model currently evaluates only five crudes. To provide an accurate representation of global transportation fuel production, additional crudes need to be modelled.

1.3 Research objectives

The overall objective of this study is to determine WTW emission ranges for transportation fuels (gasoline, diesel, and jet fuel) derived from various crude oils using publically available data and engineering first principles. This will be accomplished through the following specific objectives:

- Modify the existing **FUN**damental **EN**gineering Princip**l****E**s-based Mode**L** for **E**stimation of **G**reen**H**ouse **G**ases in **C**onventional **C**rude **O**ils (FUNNEL-GHG-CCO) to improve its accuracy and incorporate updated information.
- Use a sensitivity analysis to identify sensitive inputs whose values have significant effect on overall WTW emissions.
- Use publically available data to determine probability distributions for the identified sensitive inputs. This research will use conservative distributions for the inputs due to limited data availability.
- Incorporate a Monte Carlo simulation into the current FUNNEL-GHG-CCO model to determine WTW emission uncertainty ranges for gasoline, diesel, and jet fuel.

- Expand the FUNNEL-GHG-CCO model to include additional crudes from outside North America.
- Identify which inputs have the largest effect on WTW emission uncertainty ranges.
- Compare the results to those in the literature and identify the causes of variation, if any.

The results of this study will be beneficial to both policy makers and industry representatives involved in creating GHG reduction policies. The uncertainty ranges will provide a fair representation of the industry while identifying which crude oils have higher and lower emissions. The uncertainty ranges will help policy makers understand the limitations of such models. Additionally, the results will identify which pieces of data policy makers should collect from industry to improve the accuracy of WTW GHG emission estimates.

1.4 Scope and limitation of the thesis

This study evaluates the GHG emissions from crude production to fuel combustion. Only CO_2, CH_4, and N_2O emissions are examined. Infrastructure emissions are not included due to a lack of data. The current FUNNEL-GHG-CCO model uses a generic refinery model within Aspen HYSYS to determine refinery process unit energy and mass balances. Due to the complexity of the refining process, a more detailed refinery model is outside the thesis scope. The uncertainty analysis does not evaluate the uncertainty in each refinery process unit's energy and mass balances. Only the uncertainty in the heater and boiler efficiencies, along with natural gas and electricity emission factors, are examined for the refinery stage.

1.5 Organization of the thesis

This thesis is a paper format and is written such that each chapter can be read independently; this results in repetition between chapters. There are four chapters and two appendices in this thesis as described below.

Chapter 2, Uncertainty in Life Cycle Assessments of Well-to-Wheel Greenhouse Gas Emissions of Transportation Fuels Derived from North American Crudes: This chapter focuses on an uncertainty analysis in the WTW emissions of transportation fuels previously examined by the original FUNNEL-GHG-CCO model [1-3]. The method and input distributions used to calculate uncertainty ranges are provided. This chapter also examines the effect field age has on WTW

emissions and compares the results to existing literature results. Appendix A contains additional details related to chapter 2 such as modifications made to the original FUNNEL-GHG-CCO model, sampling error calculations, Monte Carlo distribution justifications, source data analysis, and diesel and jet fuel results.

Chapter 3, Uncertainty in the Life Cycle Assessment Well-to-Wheel Greenhouse Gas Emissions of Transportation Fuels: This chapter expands on the work done in chapter 2 by performing an LCA on three additional crude oils from Saudi Arabia, Venezuela, and Iran that have been previously examined by TIAX and Jacobs. After the base case LCA is completed, an uncertainty analysis is performed on the new crudes using the same method as that used in chapter 2. Appendix B contains additional details related to chapter 3 such as sampling error calculations, Monte Carlo distribution justification, and diesel and jet fuel results.

Chapter 4, Conclusions and Recommendations: This chapter summarizes the findings from chapters 2 and 3, and provides recommendations for future work.

Chapter 2: Uncertainty in Life Cycle Assessments of Well-to-Wheel Greenhouse Gas Emissions of Transportation Fuels Derived from North American Crudes

This chapter describes an uncertainty analysis done through the FUNNEL-GHG-CCO model using a Monte Carlo simulation. Alaska North Slope, California's Kern County heavy oil, Mars, Maya, and Bow River heavy oil are examined. For this study, we developed seven scenarios, five historical and two current, the former using lifelong average production data from the oil fields studied and the latter using recent production data to illustrate how WTW emissions change as the fields age.

2.1 Introduction

As climate change becomes a growing concern around the world, there is increased focus on the environmental impact of transportation fuel production. In 2014, the United States' greenhouse gas (GHG) emissions for the petroleum and natural gas sector were 236 million tonnes CO_2eq with an additional 175 million tonnes CO_2eq from refineries [20, 21]. High carbon emissions have led to environmental policies such as the California Low Carbon Fuel Standard, which requires a 10% reduction in California's transportation fuels' 2007 carbon intensity by 2020 [7], and the European Union Fuel Quality Directive, which requires a 6% reduction in transportation fuels' 2010 carbon intensity by 2020 [6]. In order to meet these reductions, the emissions generated during crude production and refining must be reduced.

Crude is a generic term referring to several types of oil. Crude oils are further classified based on their American Petroleum Institute gravity (ºAPI), which is the inverse of a crude's density. For example, water has an API of 10º [9]. Based on the API gravity, crudes are classified as light (>31.1 ºAPI), medium (22.3-31.1 ºAPI), heavy (22.3-10 ºAPI), and extra-heavy (<10 ºAPI) [10].

The well-to-wheels (WTW) emissions from different crudes vary widely depending on the production method used, the crude's properties, refining methods, regional regulations, and industry practices [8]. Additionally, as a crude reservoir ages, its pressure drops, and production

decreases [22, 23]. Enhanced oil recovery methods, such as water flooding, gas injection, artificial pump lift, gas lift and steam flooding, are implemented to improve production rates [23, 24]. However, these methods increase the amount of energy required and emissions generated.

Current transportation fuel life cycle assessments (LCAs) consist of either a high-level top-down analysis to determine industry average emissions or a bottom-up analysis to determine pathway-specific emissions. Top-down models such as the Greenhouse Gases, Regulated Emissions, and Energy Use in Transportation (GREET) [13] and GHGenius [14] use aggregated data, which makes it difficult to compare crudes and identify areas for improvement. Bottom-up models such as the Jacobs [15, 16], TIAX [17], Oil Production Greenhouse gas Emissions Estimator (OPGEE) [18], Petroleum Refinery Life Cycle Inventory Model (PRELIM) [19], **FUN**damental **EN**gineering Princip**l****E**s-based Mode**L** for Estimation of **G**reen**H**ouse **G**ases in the **O**il **S**ands (FUNNEL-GHG-OS [25-27], and **FUN**damental **EN**gineering Princip**l****E**s-based Mode**L** for Estimation of **G**reen**H**ouse **G**ases in **C**onventional **C**rude **O**ils (FUNNEL-GHG-CCO) [1-3] use engineering first principles to calculate the amount of energy required and emissions produced at each stage. Bottom-up models have uncertainties as they focus only on the large pieces of equipment and do not capture every source of emissions; however, the models provide details on the emissions from specific sub-processes. The current transportation fuel LCAs produce deterministic point estimates (versus Monte Carlo, which uses distributions to determine inputs), which vary significantly among models. The variations are due to inconsistent boundaries, assumptions among the models, and differences in the model inputs. The Carnegie Endowment for International Peace published a report titled “Know Your Oil” on the WTW emissions from thirty different crudes with consistent system boundaries using the OPGEE and PRELIM models [8]; however, the report does not include an uncertainty analysis, without which the confidence of the models is not determined. In order to compare crudes and determine which crudes have high and low emissions, a quantified uncertainty range is required. If the uncertainty in the emissions were larger than the difference in emissions between two crudes, it would not be possible to confidently state which crude has lower emissions. Moreover, quantifying the effect each input uncertainty has on the total uncertainty will provide insight into how the model’s accuracy can be improved. Additionally, industry and policy makers are interested in quantifying uncertainty in the emissions, as doing so provides a more accurate representation of the industry.

Thus, a model that can accurately calculate the WTW emissions of various crudes with uncertainty is needed to fill the current gap in the literature.

This study has three objectives. The first is to perform an uncertainty analysis and determine the GHG emissions ranges of the five selected conventional crude oils. The second is to identify what additional data are required to improve the accuracy of the emission estimates of each crude oil. The third is to examine how emissions change as the condition of the crude field declines near the end of its useful life. The results of this study will enhance the understanding of the accuracy of the WTW emission estimates that are used in developing GHG reduction policies. The results showing how emissions increase as a field ages will also be useful to policy makers and industry leaders when assessing whether to keep producing from an aging field.

2.2 Method

This study uses the FUNNEL-GHG-CCO model, published in 2014 [1-3] as the basis for our uncertainty assessment. First, we modified the original model to improve the accuracy of the WTW estimates. Then we performed a sensitivity analysis to identify sensitive inputs and ran a Monte Carlo simulation to determine the uncertainty ranges in each crude's WTW emissions.

2.2.1 Base case model

Since our focus is an uncertainty analysis, this paper only gives a brief overview of the FUNNEL-GHG-CCO model, hereafter referred to as the F-1 model. Readers are encouraged to refer to the previously published work for additional details [1-3].

The F-1 is a bottom-up model that uses engineering first principles to calculate energy use and emissions generated at each stage from raw material extraction to product end use. Figure 1 shows the six main sub-processes within the model boundary. This study uses a functional unit of gCO_2eq/MJ of gasoline produced unless specified otherwise. The paper mainly focuses on gasoline production emissions; diesel and jet fuel emissions are included in section A5. The production stage includes drilling the wells, injecting fluids to maintain reservoir pressure, and lifting the crude to the surface. Surface processing includes crude stabilization, gas treatment, and water treatment. Crude is transported by a combination of pipelines and marine vessels to refineries where it is processed into gasoline, diesel, and jet fuel. The finished products are

distributed to bulk terminals by pipelines, trains, barges, and tankers and then distributed to fueling stations by truck. The final stage is combustion in a vehicle or aircraft.

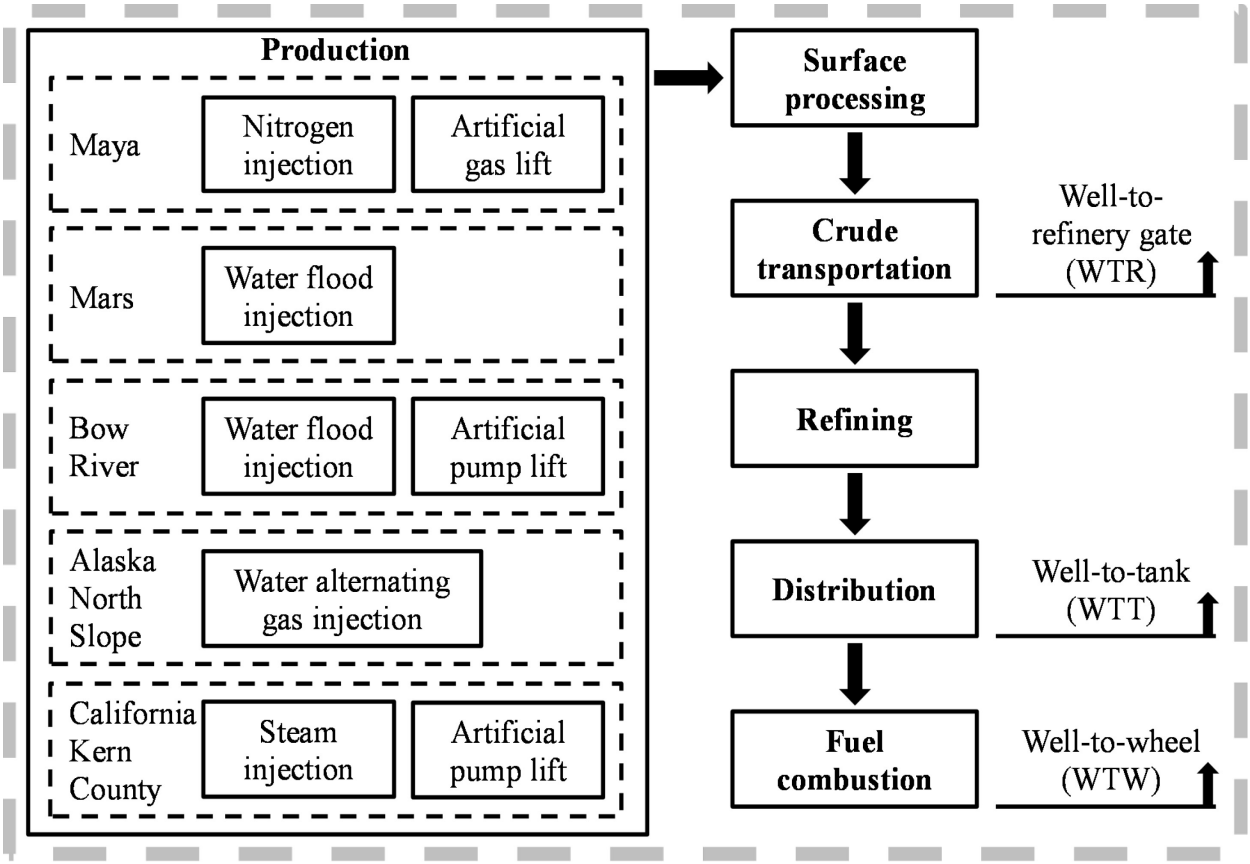

Figure 1: The FUNNEL-GHG-CCO model stages [3]

The F-1 model analyzes five conventional crude oils with each crude oil using a unique production method (see Figure 1). Maya oil is a Mexican heavy crude, 22º API, produced from the Cantrell field located 100 km off the coast of the Yucatan Peninsula [3]. Mars crude is a light, 31.5º API, sour crude produced from an offshore platform in the U.S. Gulf Coast [3]. Bow River oil is a heavy, 23º API, conventional oil produced in Alberta, Canada [3]. Alaska North Slope (ANS) crude is primarily produced from the Prudhoe Bay field and is a medium, 29º API, oil [3]. California Kern County crude is a heavy, 13º API, crude produced primarily from the Midway-Sunset oil field [3]. Table 1 provides a summary of the modeled crudes.

Table 1: Modeled crudes

Crude	API	Country
Maya	22º	Mexico
Mars	31.5º	USA
Bow	23º	Canada
ANS	29º	USA
Kern	13º	USA

This study assumes all crudes are refined in the U.S. The refineries are located in Los Angeles, California for ANS and Kern; Cushing, Oklahoma for Mars and Bow River; and Houston, Texas for Maya [3]. Additionally, the F-1model assumes deep conversion refineries for all crudes as these are typical for North America [3], unlike the model assumptions in "Know Your Oil" [8] which uses different refinery types for each crude.

In order to improve the accuracy of the F-1 model we made five modifications, including using detailed calculations for sub-processes that are large sources of emissions and integrating new sources that are more accurate. The modified model will be referred to as the F-2 model. The modifications are described below.

First, the F-1 model only examined single stage rather than multistage compressors. Using single stage compressors would over-estimate the amount of energy required by the compressor when large compression ratios were required [1-3]. Compressors are used either to inject gas into the reservoir to maintain pressure or to aid in production using a gas lift system. The F-2 model calculations were modified using equations for multistage compressors from the OPGEE model described in the "Know Your Oil" report [8, 18]. The number of compressor stages is chosen such that the compressor ratio of each stage is below 5, as higher compression ratios result in excessive outlet temperatures, thereby decreasing efficiency [18, 28].

Second, the original F-1 model assumed that 100% of California Kern steam is produced via cogeneration within the plant [3]. However, in reality, the cogeneration capacity in the Midway-Sunset field can only provide approximately 30% of the field's steam requirement. A once-through steam generator (OTSG) is added to the model to account for the remaining steam [27].

Third, the F-1 model noted that there was limited data on venting, flaring, and fugitive (VFF) emissions and used a simplistic estimate. Research by Canter et al. determined a range of venting

and fugitive emissions for crude oils by examining several pieces of literature [29]. Canter et al. integrated the VFF ranges into the F-1 model to improve the accuracy of the VFF emissions. We expanded on the work done by Canter et al. and added fugitive emissions for reinjected produced gas.

Fourth, excess produced gas was not considered in the original model. This gas, however, can be used to offset natural gas consumption. The OPGEE model applies a credit for the production of produced gas equal to the natural gas upstream emissions with the transportation emissions excluded [18]. This credit method is integrated in the FUNNEL-GHG-CCO model to align the model boundaries with those in existing literature.

Fifth, the FUNNEL-GHG-CCO model assumed all crudes have the same energy content. The new model calculates the lower heating value (LHV) using a correlation from Speight [30]. This correlation depends on the crude's specific gravity and has been used by the GREET and PRELIM models [19, 31].

Detailed information on the modifications made to the original F-1 model is provided in section A1.

2.2.2 Uncertainty analysis methodology

Output uncertainty in this study has two parts, input uncertainty and input sensitivity [32]. Inputs with high sensitivity and high uncertainty will have a large effect on the output distribution. Hence, a sensitivity analysis was first conducted to identify which inputs should be further examined. Once the sensitive inputs were identified, distributions of these inputs were calculated from values obtained from the literature. Semi-sensitive inputs were also examined in order to determine their level of uncertainty. If their uncertainty was large, they were included in the uncertainty analysis. ModelRisk software was used to run a Monte Carlo simulation and determine the WTW emissions uncertainty [33].

2.2.2.1 Identify sensitive inputs

A +/-25% range of each input base case value was used in the sensitivity analysis on the WTT (well-to-tank) emissions. WTT emissions were analyzed instead of WTW emissions because tank-to-wheel (TTW) emissions (combustion emissions) represent 60%-90% of the total

emissions and the TTW emissions are constant for all of the scenarios and will not be effected by the sensitivity analysis [34]. During the sensitivity analysis, only one input is varied at a time. If an input causes the WTT emissions to change by more than +/-1%, it is defined as a sensitive input. A change of 0.1% to 1% is considered a semi-sensitive input and a change of less than 0.1% is an insensitive input. To identify any inputs that displayed non-linear responses, spider plots were generated. Empirical evidence was used to distribute the semi-sensitive inputs into the sensitive or insensitive groups.

2.2.2.2 Determine distributions for sensitive inputs

Due to the lack of publically available data, a conservative approach was used to determine the sensitive input distributions. Triangle distributions require a most likely, minimum, and maximum estimates to generate. Triangle distributions favor extreme values and result in a wider and more conservative output distribution [35]. Hence, when limited literature or technical documentation is available, triangle distributions are used. For our analysis, in cases where adequate data were available, distribution fitting tools within ModelRisk were used. For dependent inputs, ModelRisk copulas were used to increase the modeling accuracy. A detailed description for each Monte Carlo input is in section A3.Tables 2, 3, and 4 show a summary of the Monte Carlo input distributions and their sources.

2.2.2.3 Determine distributions for insensitive inputs

The insensitive variables individually have little effect on the overall results but their combined effect could have a significant effect. As a result, all the insensitive inputs are assigned a triangle distribution wherein the maximum and minimum values are defined as +/- 10% of the base case value. The output distributions with and without the insensitive input distributions are then compared to determine if ignoring the uncertainty in the insensitive values will have a significant effect on the results. Ideally, every input should have an uncertainty distribution but due to the large number of inputs, this is not practical.

2.3 Monte Carlo simulation

The Monte Carlo simulation ran with 50,000 samples, which ensures that the simulation sampling error has a 99% probability of being less than 0.1 gCO_2eq/MJ. The sampling error calculations and values for each crude are in section A2 [36]. The results are reported using the

5th and 95th percentiles (P5, P95). An iterative approach was used wherein the ModelRisk-generated tornado plots were used to determine which inputs should receive more focus.

The tornado plots are generated by calculating the output mean from a subgroup of Monte Carlo samples. Each subgroup contains only the samples where the input value is within a given percentile range. This study used a 5% range (20 tranches); therefore, the subgroups would be split into ranges of P0-P5, P5-P10, et cetera. The subgroups with the largest and smallest output means are used as the tornado plot's maximum and minimum values [37]. Due to the number of inputs used and the accuracy of the tornado plots, only the sensitive inputs are included. The tornado plots were further filtered to display only the significant inputs. An input was classified as significant if the input's tornado plot variance (maximum – minimum) was greater than 10% of the WTW variance (P95-P5).

Due to the complexity of the refinery portion of the model, an in-depth analysis was not performed for the refinery stage. The F-1 model uses Aspen HYSYS, an advanced refinery modeling software that is used globally by the oil and gas industry [38], to model the refinery. The Aspen model generates energy and mass balances for each process unit in the refinery [3], which are used by the F-1 model to allocate emissions to the transportation fuels. The uncertainty in the process units' mass and energy balances is not examined in this study due to the complexity of the refining process. However, boiler and heater efficiency as well as electricity emission factors (EF) are assigned Monte Carlo input distributions. Refinery emissions are determined using a Monte Carlo simulation that only examines the refinery portion of the model. Refinery output emissions are fed into the main model as Monte Carlo input distributions (Table 5). A second Monte Carlo simulation is run to find the WTW emissions.

2.3.1 Monte Carlo simulation inputs

The inputs with their distributions and sources are listed in Table 2 for general inputs that apply to all crudes and in Table 3 and 4 for the crude-specific inputs. The Monte Carlo distributions use ModelRisk software notation [33]. Emission factors are used to determine the GHG emissions from fuel and electricity consumption. The methane global warming potential (GWP) is used to convert methane emissions into carbon dioxide equivalent emissions. For the surface processing (SP) stage, crude stabilizer temperatures and crude-specific heat correction factors are

used to calculate the energy requirement for crude stabilization, and water-electricity intensities are used to calculate the water filtering energy requirement. For VFF emissions, the flaring volume, flaring efficiency, and produced gas (PG) methane concentration are used to calculate the CO_2eq emissions. The yield factor represents the refinery's conversion efficiency. A yield factor of 1.3 means that 1.3 MJ of crude is required to produce 1 MJ of finished products (gasoline, diesel, and jet fuel); the remaining 0.3 MJ is converted into undesirable products such as fuel oils. The yield factor is important because pre-refinery emissions from production and surface processing are multiplied by the yield factor to determine final gasoline emissions. The "distributed to bulk terminals" input is used to determine which transportation method is used to distribute the gasoline from the refinery to the bulk terminals. Of the five transportation methods available; ocean tanker, barge, pipeline, rail, and truck; rail had the lowest emission intensity and barge had the highest emission intensity. Therefore, a zero means that only rail is used, and a one means that only barges are used.

For Maya, the nitrogen driver efficiency and nitrogen injection volume are used to calculate the energy required to produce and inject nitrogen into the field to maintain reservoir pressure. For Mars, the injection water–to-oil ratio (WOR) and pump discharge pressure are used to calculate the energy required to inject water into the reservoir to maintain pressure. The production WOR and production gas-to-oil ratio (GOR) are used to calculate surface treatment energy requirements and VFF emissions. The well lifetime productivity and well depth are used to calculate the well drilling emissions. For Bow River, the well depth is used to calculate the drilling emissions, and the reservoir pressure and production WOR are used to calculate the artificial pump electricity consumption to lift the crude to the surface. For ANS, the WORs, GORs, and compressor inputs are used to calculate the water alternating gas (WAG) production electricity consumption from the pump and compressor. For Kern, the cogeneration inputs and steam-to-oil ratio (SOR) are used to calculate the steam and electricity emissions generated for the steam flooding production process.

ModelRisk's copulas model dependence between inputs; for example, in the ANS scenario the produced gas volume is dependent on the injected gas volume and a copula is used to link the two distributions. Additional information on how the distributions are determined for each input is in section A3.

Table 2: Monte Carlo general inputs

	Input	Monte Carlo distribution	Units	Source
EF	Methane GWP	Triangle(20.74,34,47.26)		[39, 40]
	NG upstream	Triangle(71.2%,100%,140%)		[31, 41, 42]
	NG boiler comb.	Triangle(97.2%,100%,102.7%)		[31, 41]
	NG turbine comb.	Triangle(96.9%,100%,102.4%)		[31, 41]
Electricity EF	Maya nitrogen compressor	Triangle(330,471,753)	gCO_2eq/kWh	[31, 43]
	Maya & Mars production & SP	Triangle(471,753,1034)	gCO_2eq/kWh	[31]
	Bow River production & SP	Triangle(471,753,1033)	gCO_2eq/kWh	[3, 31, 44]
	ANS production & SP	Triangle(471, 609,1034)	gCO_2eq/kWh	[31, 45, 46]
	ANS & Kern refinery	Triangle(200,318,753)	gCO_2eq/kWh	[31, 45]
	Mars & Bow refinery	Triangle(471,739,1051)	gCO_2eq/kWh	[31, 45]
	Maya refinery	Triangle(471,571,1034)	gCO_2eq/kWh	[31, 45]
Unit Eff.	Boiler	Triangle(62%,75%,88%)		[47-50]
	Heater	Triangle(70%,80%,90%)		[3, 18, 51, 52]
	Low flow pump	Triangle(50%,60%,70%)		[53]
	High flow pump	Triangle(50%,65%,85%)		[1, 15, 18, 53-55]
SP	Specific heat correction factor	Triangle(0.84,1,1.5)		[56]
	Crude stabilizer inlet temp.	Triangle(37.8,48.9,65.6)	ºC	[57]
	Crude stabilizer outlet temp.	Triangle(93.3,173.3,204.4)	ºC	[57, 58]
	Produced water energy intensity	Triangle(0.24,0.36,0.92)	kWh/bbl	[3, 59]
	Imported water energy intensity	Triangle(0.2,0.24,0.62)	kWh/bbl	[3, 59]
VFF and Other	Vented & fugitive gas volumes	Triangle(2.1%,4.6%,7%)		[29]
	Maya flared gas volume	Triangle(0,68.6,131.2)	scf/bbl	[60-63]
	Mars flared gas volume	Triangle(0,13,62.5)	scf/bbl	[60-63]
	Bow flared gas volume	Triangle(0,62.3,145.8)	scf/bbl	[60-63]
	ANS flared gas volume	Triangle(0,190.58,478.99)	scf/bbl	[60-63]
	Kern flared gas volume	Triangle(0,13,62.5)	scf/bbl	[60-63]
	Flaring efficiency	PERT(80%,95%,99%)		[1, 14, 15, 18, 31]
	PG methane concentration	Beta(14.49,2.91,,XBounds(,0.989))	%mol	[18]
	Yield factor	Pert(1.07,1.3,1.49)		[3, 15, 19]
	Distributed to bulk terminals	Uniform(0,1)		[3, 31]

Table 3: Monte Carlo crude-specific inputs: Part 1

	Input	Monte Carlo distribution	Units	Source
Maya	Nitrogen driver efficiency	Triangle(60%,82.3%,95%)		[18, 43, 64, 65]
	Nitrogen injection volume	Triangle(571,822,2727)	scf/bbl	[15, 43, 66-68]
Mars	Injection WOR	Triangle(0.3,0.7,1.5)	bbl/bbl	[8, 15, 69-71]
	Production WOR	Triangle(0.02,0.2,5.5)	bbl/bbl	[8, 15, 69-71]
	Production GOR	Triangle(800,1133,1400)	scf/bbl	[71]
	Well lifetime productivity	Triangle(1.3e5,5.3e5,2.32e7)	bbl/well	[3, 8, 69]
	Well depth	Triangle(4267,4420,5791)	m	[15, 70]
	Pump discharge pressure	Triangle(37.9,42.1,47.2)	MPa	[15, 70, 72]
Bow	Well depth	Triangle(600,1000,1800)	m	[73, 74]
	Reservoir pressure	Triangle(4.1,7.8,17.2)	MPa	[3, 75, 76]
	Production WOR	Triangle(4,15,20)	bbl/bbl	[77, 78]
ANS	Current production WOR	Normal(4.25,0.60, WCopula, XBounds(0.5,6.5))	bbl/bbl	[79, 80]
	Historical production WOR	Normal(0.97,0.137, WCopula, XBounds(0.1,3))	bbl/bbl	[22, 81, 82]
	Current injection WOR	Normal(6.33,1.8,WCopula)	bbl/bbl	[79, 80]
	Historical injection WOR	Normal(1.35,0.38,WCopula)	bbl/bbl	[22, 81, 82]
	Water copula	CopulaBiFrank(5.6,1)		[79, 80]
	Current production GOR	Normal(34100,2195, GCopula)	scf/bbl	[79, 80]
	Historical production GOR	Normal(6390,411, GCopula)	scf/bbl	[22, 81, 82]
	Current injection GOR	Normal(31300,2608, GCopula)	scf/bbl	[79, 80]
	Historical injection GOR	Normal(5841,487, GCopula)	scf/bbl	[22, 81, 82]
	Gas copula	CopulaBiFrank(35,1)		[79, 80]
	Compressor inlet temp.	Triangle(0,15,40)	C	[8, 15]
	Compressor discharge pressure	Triangle(15.5,18.6,21.7)	MPa	[83]
	Compressibility factor	Triangle(0.9,1,1.1)		[84]
	Interstage cooling efficiency	Triangle(60%,80%,100%)		[18]
	Injection gas fugitives emissions	Triangle(0.4,1.3,3.5)	gCO_2eq/scf	[18, 41, 85, 86]

Table 4: Monte Carlo crude-specific inputs: Part 2

	Input	Monte Carlo distribution	Units	Source
California Kern	Current injection SOR	Triangle(4.72,5.74,7.82, WCopula)	bbl/bbl	[87]
	Historical injection SOR	Triangle(1.35,1.64,2.23, WCopula)	bbl/bbl	[87, 88]
	Current production WOR	Triangle(6.6,8,12.1, WCopula)	bbl/bbl	[87]
	Historical production WOR	Triangle(1.58,1.92,2.9, WCopula)	bbl/bbl	[87, 88]
	Water copula	CopulaBiFrank(13,1)		[87]
	Current production GOR	Normal(177.8,18,,XBounds(120,240))	scf/bbl	[87]
	Historical production GOR	Normal(93,9.3,,XBounds(20,180))	scf/bbl	[87, 88]
	Cogen NG consumption	Error(4484,217.6,1,,VseXBounds(3500,5500))	scf/MWh	[88-90]
	Cogen electricity/steam ratio	Normal(0.678,0.037,,VseXBounds(0.4,0.9))	MWh/MWh	[88-90]
	Cogen steam energy required	Triangle(1682,1944,2321)	kJ/kg	[89, 90]
	Cogen steam capacity	Triangle(0%,30%,100%)		[87, 88]
	Cogen electricity credit	Triangle(200,318,471)	gCO_2eq/kWh	[31, 45]

Table 5: Monte Carlo refinery inputs

Crude	Gasoline	Diesel	Jet
Maya	Normal(18.84,1.04)	Normal(15.29,0.83)	Normal(9.55,0.52)
Mars	Normal(16.60,0.93)	Normal(12.52,0.70)	Normal(8.02,0.45)
Bow	Normal(17.43,0.98)	Normal(13.85,0.77)	Normal(9.10,0.51)
ANS	Normal(14.79,0.89)	Normal(10.81,0.65)	Normal(6.89,0.41)
Kern	Normal(16.73,1.02)	Normal(12.19,0.73)	Normal(7.73,0.46)
Units	gCO_2eq/MJ Gasoline	gCO_2eq/MJ Diesel	gCO_2eq/MJ Jet Fuel

2.3.2 Monte Carlo historical and current scenarios

Originally, one Monte Carlo scenario was run for each of the five crudes; however, for the ANS and California Kern crudes the original results were 49 and 11% higher than the previous estimates from the F-1 model, respectively [3]. Additionally, the Kern scenario results were 25 and 41% higher than the Jacobs and TIAX results, respectively [15, 17]. Further investigation found that the discrepancy was from the assumed water and gas injection and production ratios. The ANS and Kern fields have been using enhanced oil recovery for over 20 years [82, 87], and as the fields age the injection and production ratios have increased. Since the WTW emissions are sensitive to the injection and production ratios, two scenarios were developed for these fields, historical and current. The historical scenario uses cumulative ratios, which give an estimate of the weighted average WTW emissions over the entire life of the field. The current scenario uses recent ratios to investigate how the WTW emissions rise as the field ages. Using two scenarios will provide more insight into how the WTW emissions can vary depending on the age of the data used. The only differences between the historical and current scenarios are the inputs for the injection WOR and GOR, and the production WOR and GOR.

ANS injects water and produced gas to maintain reservoir pressure. Table 6 shows ANS' historical annual production and injection GOR and WOR ratios for ANS's Prudhoe oil field [22, 81, 82]. California Kern uses steam injection. Table 7 gives its monthly historical SOR, WOR, and GOR for Kern's Midway Sunset field [87]. As Table 6 and 7 show, the ratios have increased significantly over the last decade. It should be noted that the Jacobs and TIAX studies were published in 2009 and the F-1 model was published in 2014 [3, 15, 17].

Table 6: ANS historical injection and production ratios

Date	Injection GOR	Production GOR	Injection WOR	Production WOR
1980	1,400	1,100	0.02	0.03
1990	3,300	3,200	1.33	0.64
2000	15,700	15,300	3.25	2.39
2010	26,000	28,300	5.74	3.61
Cumulative (2015)	2,200	2,200	0.22	0.33

Table 7: Kern historical injection and production ratios

Date	Injection SOR	Production WOR	Production GOR
Dec-96	2.92	4.42	27
Dec-00	2.63	4.78	37
Dec-05	4.10	5.95	38
Dec-10	4.80	7.81	155
Sep-15	6.60	10.75	190
Cumulative (2009)	1.64	1.92	93

2.4 Results and discussion

As this study focuses on gasoline production from crude oil, only gasoline emissions are presented. Diesel and jet fuel emissions are included in section A5. Results are presented for seven scenarios, one for each crude and two additional scenarios, one for ANS and one for Kern. The additional ANS and Kern scenarios are included to show the effect of reservoir age on the WTW emissions (see Figure 2).

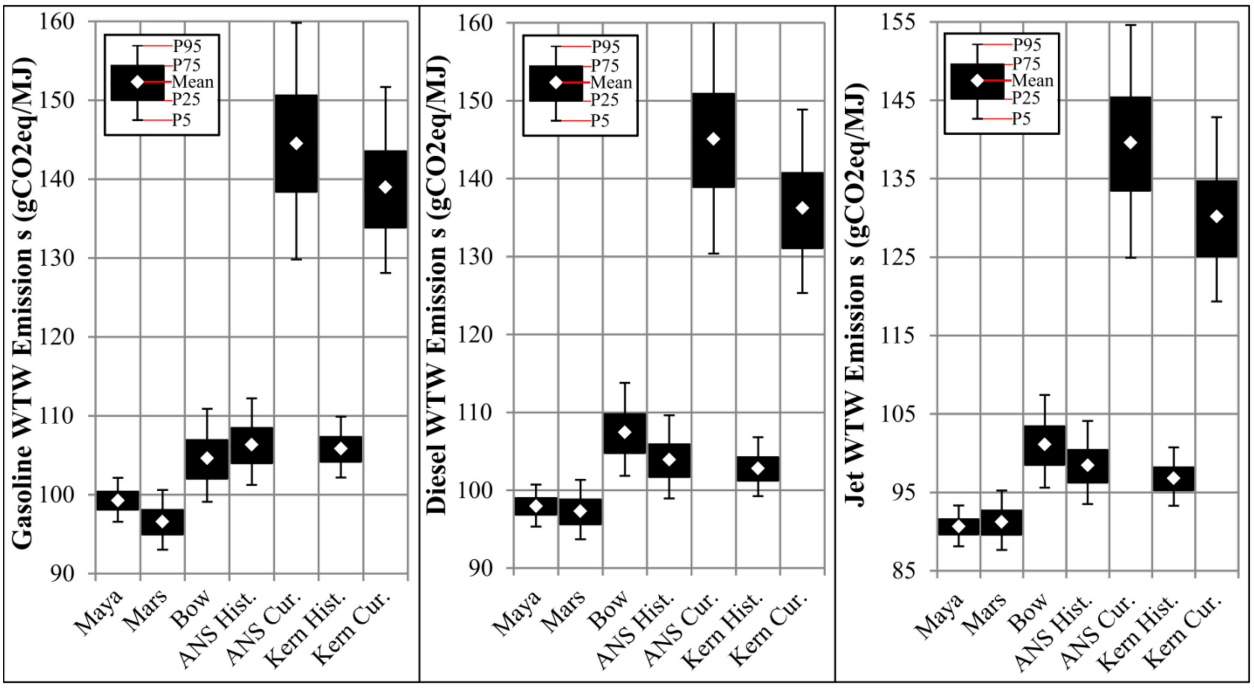

Figure 2: WTW emissions

When the error bars of two crudes overlap, it is not possible to confidently conclude that one crude oil has lower emissions than the other. The results in Figure 2 show an overlap between

most of the crudes studied. This is due to the conservative approach taken in defining input distributions for the Monte Carlo simulation. However, the current ANS and Kern scenarios clearly produce higher emissions than the other scenarios. Additionally, even with the conservative uncertainty, the Kern historical scenario does not overlap the Mars and Maya scenarios.

The inputs that have a significant effect on the gasoline WTW emission uncertainty are shown in tornado plots in Figure 3. A significant effect is defined as having variance (maximum - minimum) greater than 10% of the total WTW variance (P95 - P5). The inputs at the top of the tornado plot have the largest effect on the overall uncertainty while inputs at the bottom are less significant. The results can be further broken down to examine which inputs have the largest effect on the refinery (Figure 4) and VFF emissions (Figure 5 and 6). Some inputs result in larger uncertainties than others. This is due to either a lack of information or a wide range of data in the literature. Additionally, inputs with higher sensitivity will have a larger effect on the WTW uncertainty.

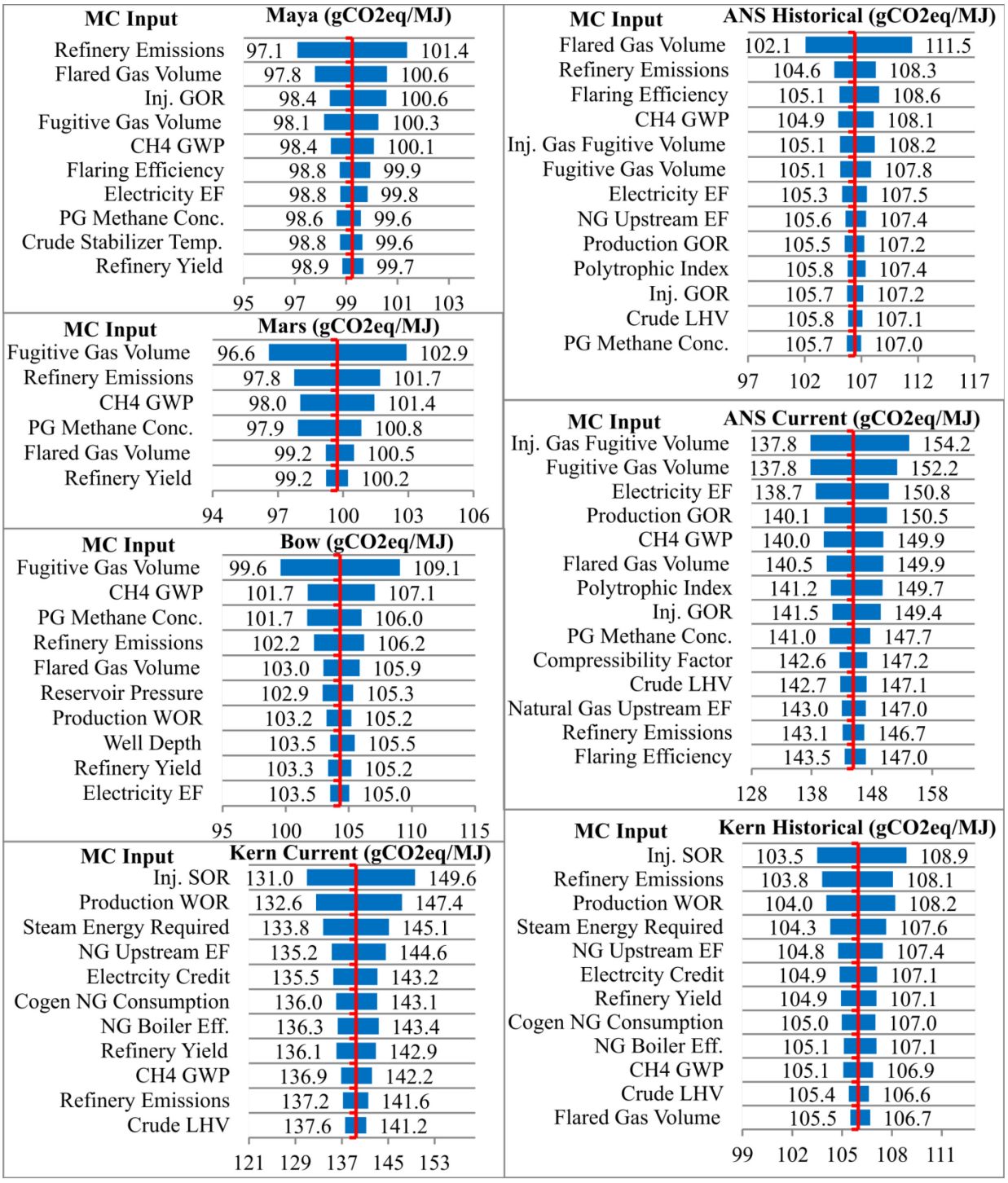

Figure 3: Monte Carlo simulation WTW emission tornado plots for gasoline

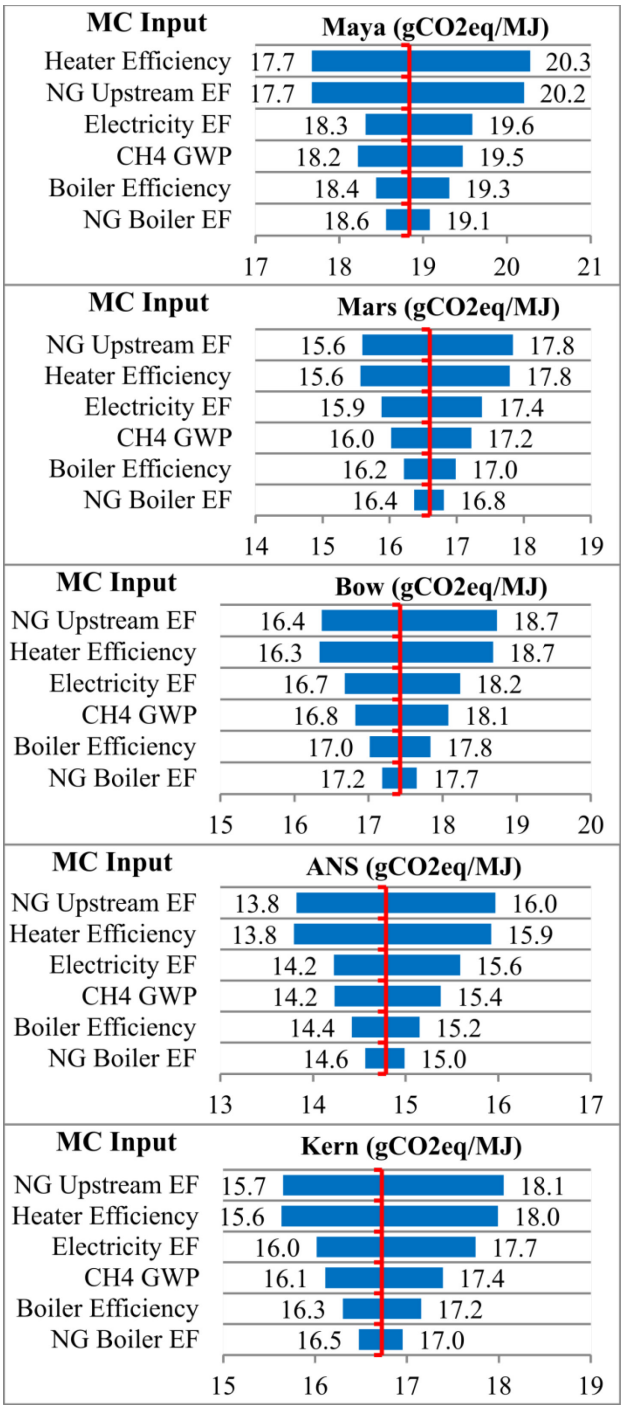

Figure 4: Monte Carlo refinery emission tornado plots for gasoline

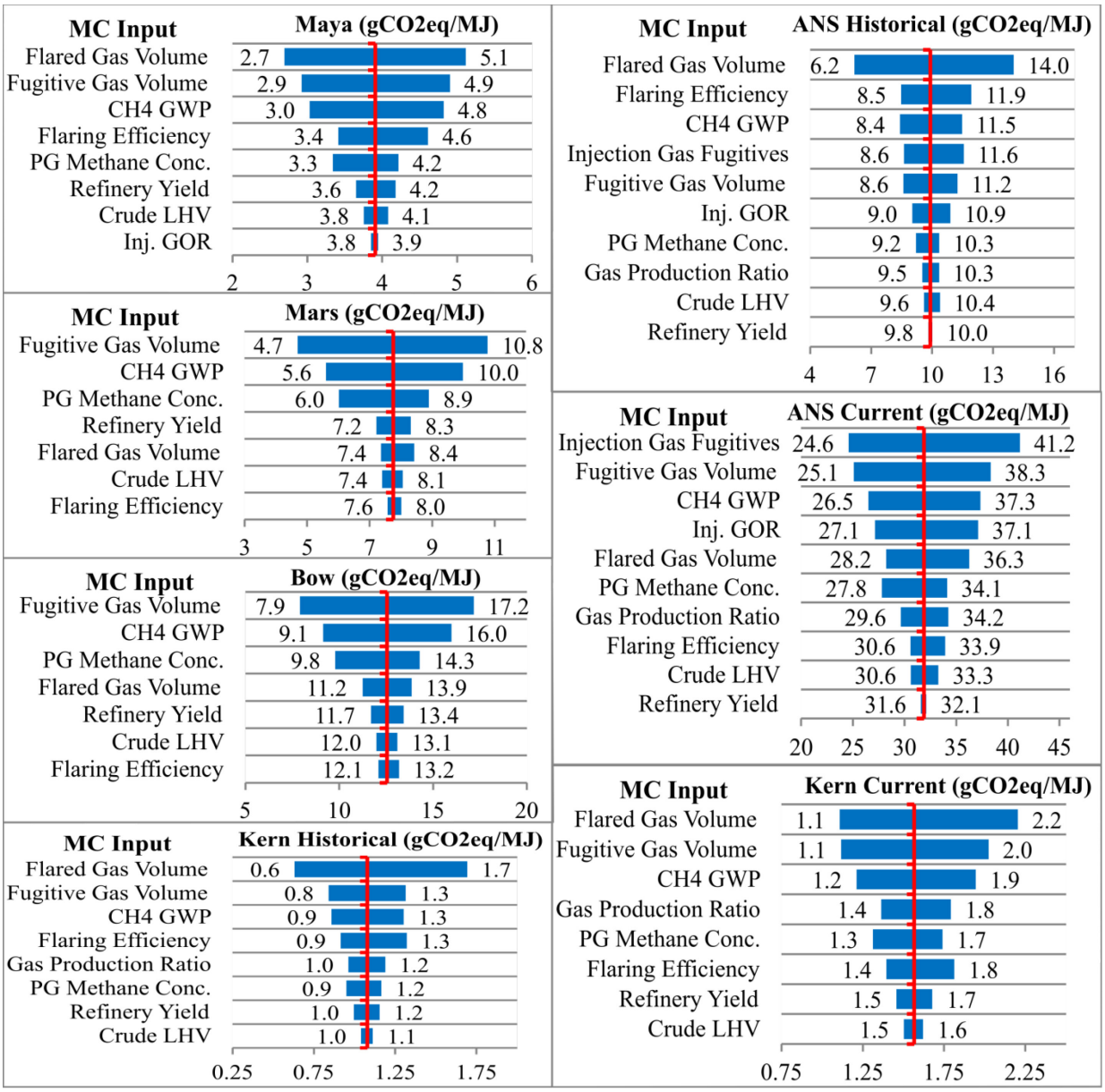

Figure 5: Monte Carlo venting, fugitive, and flaring emission tornado plots

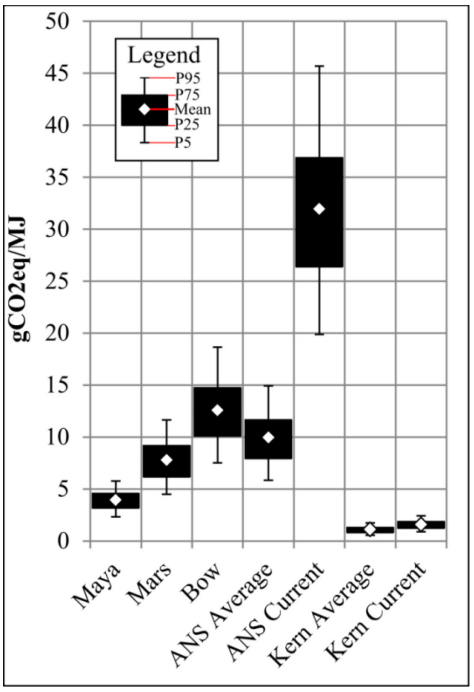

Figure 6: Venting, fugitive, and flaring emissions

2.4.1 Refinery uncertainty

The uncertainty of refinery stage emissions has two main sources, the refinery yield factor and emissions. The refinery yield factor is the ratio of crude oil energy content to the finished product's energy content. The yield factor depends on the crude properties and refinery configuration. For example, the yield factor for ANS from PRELIM varies from 1.07 to 1.53, depending on the refinery configuration [19]. The WTW variance of the yield factor ranges from 2.9 to 4.4 gCO_2eq/MJ for the ANS current and Kern current scenarios, respectively as seen in Figure 3.

Five of the six inputs in the refinery tornado plots (Figure 4) are related to the natural gas consumption, as natural gas is the primary energy source for the refinery. Therefore, efficiency improvements have the potential to significantly reduce the refinery emissions. The natural gas (NG) upstream EF is the largest source of uncertainty for four of the five crudes; therefore, understanding where each refinery gets its natural gas from will have a significant effect on the results.

The large effect the refinery emissions have on the WTW emissions suggests that a more in-depth analysis is required to understand the emissions from the complex refinery processes. Additionally, it should be noted that the refinery yield factor can decrease by using additional conversion processes to further upgrade the bottom-of-the-barrel products, which results in higher emissions [19]. The current model does not include this correlation and provides a conservative range of WTW emissions.

2.4.2 Venting, fugitive, and flaring uncertainty

VFF emissions are a common theme in the tornado plots in Figure 3. VFF uncertainty is primarily due to fugitive volumes, flaring volumes, CH_4 GWP, and PG CH_4 concentrations, as shown in the VFF tornado plots in Figure 5.

The fugitive gas volumes shown in Figure 5 include the vented volumes of gas. Canter et al. studied venting and fugitive gas volumes for North American crudes by examining multiple sources for the oil and gas industry [29]. However, there is a wide range of values in these sources, which rely on approximation methods. There are limited publically available data on directly measured fugitive volumes from crude oil production and refinement [29]. To accurately determine the WTW emissions for the various crudes, more information is needed on the amount of fugitive gas released, especially for gassy oils, as in the ANS current scenario. The injected gas fugitives are calculated specifically for the ANS scenarios and are described in section A3.6. As they are the largest source of uncertainty for the ANS current scenario, more detailed data are required to reduce the uncertainty in the WTW emissions.

Methane GWP values also affect the uncertainty of the model results. Methane GWP values have a ± 35% uncertainty range [39, 40]. Usually a value of 34 is applied to the CH_4 GWP to be converted to GHG emissions (CO_2eq) [39, 40]. However, in an uncertainty analysis of total GHG emissions, a higher CH_4 GWP value will have a relatively larger impact on the total GHG emissions for crudes with large VFF volumes compared to crudes with small VFF volumes.

VFF emissions depend on the concentration of methane in the produced gas. The data analyzed for California showed that methane concentrations could vary from 50-100%, with a mean of 84%. OPGEE and the original F-1 model used 84% for all of the crudes analyzed [3, 18]. Jacobs and TIAX use 75% and 80% methane for their produced gas, respectively [15, 17]. Methane gas

concentrations for each well should be reported to get a better understanding of the produced gas emissions.

Flared gas volumes also have a wide range of uncertainty due to the limited data and range from ± 91% to ± 382% [60]. Though a wide conservative range of 80%-99% flaring efficiency was assumed, it resulted in a relatively small variance of 0.4 to 1.2 gCO_2eq/MJ for five of the seven scenarios (Figure 5). However, for the ANS historical and current scenarios the ranges were 3.4 and 3.3 gCO_2eq/MJ, respectively, as the larger flaring volumes amplified the effect of the flaring efficiency. Therefore, flaring efficiency should be closely monitored for gassy oil.

For the ANS scenarios the injection and production GOR values are significant since the venting and fugitive gas volumes are determined as a percentage of the produced gas volume. The produced gas volume also depends on the injected gas volume and is modelled using ModelRisk copulas.

The distribution of VFF emissions in Figure 6 shows that a significant amount of the uncertainty in WTW emissions is due to VFF emissions. The VFF variance (P95-P5) is over 80% of the WTW variance for the Mars, Bow, and ANS crudes and 61% for Maya. For Kern, the VFF variance is less than 15% as it produces less gas than the other scenarios. This shows that for crudes with a large production GOR, a better understanding of the VFF gas volumes is required to accurately estimate the WTW emissions.

2.4.3 Effect of field age on WTW emissions

As seen in Figure 2, the ANS and Kern current scenarios show emissions increases of 34.8 and 30.4%, respectively, from the historical scenarios. These increases are a result of increased water and gas injection and production rates as discussed in section 3.2.

For the Kern scenario, the increase in emissions is primarily due to the production emissions, while VFF emissions are similar for the current and historical scenarios, as seen in Figure 6. Kern has high production emissions because it requires thermal enhanced oil recovery methods. The other crudes use mechanical enhanced oil recovery methods, which are less energy intensive. The injection SOR, production WOR, steam energy, and NG EFs are the largest sources of uncertainty for the Kern scenarios. For the ANS scenarios, the mean VFF emissions

increased from 9.9 to 31.9 gCO_2eq/MJ, while the mean well-to-refinery (WTR) emissions, excluding the VFF emissions, increased from 7.8 to 24.0 gCO_2eq/MJ. A better understanding of the VFF and production emissions will become increasingly important as ANS gas and water volumes continue to increase.

2.4.4 Effect of insensitive inputs

The Monte Carlo gasoline WTW simulation results in Figure 2 and 6 include the insensitive inputs. A comparison of the WTW emissions with and without the insensitive inputs found that the insensitive inputs had a negligible effect. The insensitive inputs had no detectable effect on the mean, as expected, since the insensitive inputs used symmetric distributions. The differences in the variances (P95-P5) showed that including the insensitive inputs increased the variance by less than 1%. This confirms the original assumption that detailed distributions are not required for the insensitive inputs as the effect will be negligible.

2.4.5 Model comparison with published literature

This study used an uncertainty analysis to determine the most likely range of emissions for each crude using a range of values for various inputs. If the input ranges used in this study cover all reasonable values, then the results from another model with the same model boundaries should be within the output ranges found in this study. Figure 7 compares the WTW emissions for gasoline from this study, Jacobs, TIAX, "Know Your Oil" (KYO), and the original F-1 model. The models in Figure 7 do not have the same boundaries; as a result, some of the WTW emissions are outside the range found in this study. The Jacobs and TIAX, F-1, and KYO models were developed in 2009, 2014, and 2015, respectively, and so did not use the same emission factors and CH_4 GWP [3, 8, 15, 17]. The gasoline combustion emissions are 73.2, 73.9, 73.6, 73.0, and 73.6 gCO_2eq/MJ for the F-2, F-1, Jacobs, TIAX, and KYO models, respectively [3, 8, 15, 17]. The F-2 model and the KYO model use 34 as the CH_4 GWP and the others use 25 [3, 8, 15, 17].

The TIAX emissions results are significantly lower than the other models'. This is because TIAX uses a simpler approach than the others when modeling WTR emissions and focuses more on the refining emissions. Since the current F-2 model included additional fugitive emissions for the reinjected gas, the F-1 emissions are 7 and 31% lower than the ANS current and historical

scenarios, respectively. The KYO and Jacobs results, except for the Jacobs Mars results, were within the range of values reported for all the crudes in this study. For the Kern scenario, the KYO and F-1 model results line up with the lower end of our current scenario. This makes sense since these models use SORs of 5.79 and 5.13 m^3/m^3 while our scenario uses a mean SOR of 5.74 m^3/m^3 with a minimum of 4.72 m^3/m^3. It was initially unclear why the Jacobs Kern scenario is 18% lower than our current scenario as it uses a SOR of 5 m^3/m^3. Further investigation found that the variation was due to the refinery and electricity emissions. The Jacobs refinery emissions were lower due to differences in the refinery configurations used. The electricity emissions for the F-2 model were higher because the cogenerated electricity had a higher emission intensity than the grid electricity, which was used by Jacobs [91]. For Mars, the Jacobs results are higher than ours due to the produced gas credit and the water injection ratio. This study calculated a 3.7 gCO_2eq/MJ gas credit. Jacobs does not use a gas credit for produced gas, and it used a water injection ratio of 5.5 m^3/m^3, which is the highest water production ratio in our study [91]. The F-1 results differ from the F-2 results primarily due to the new VFF emissions.

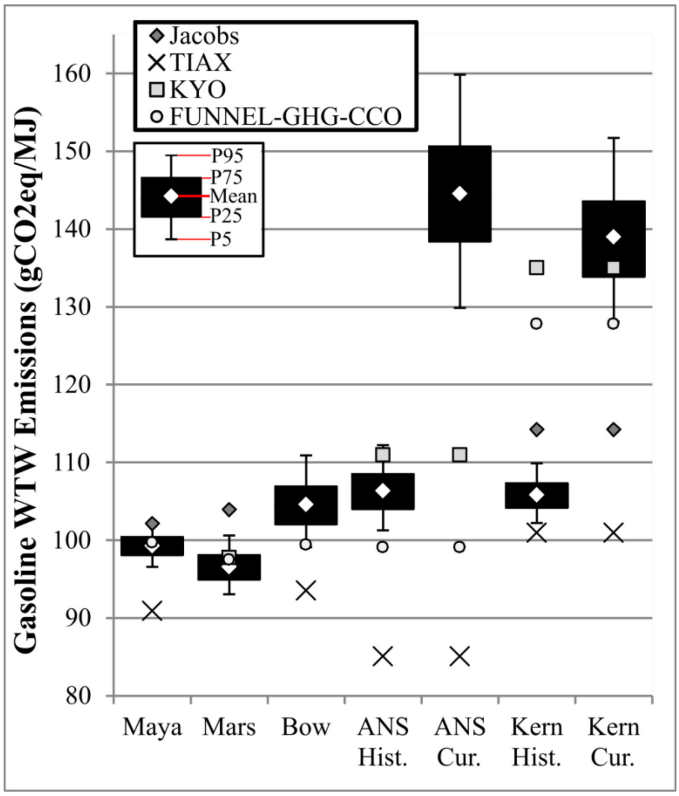

Figure 7: Comparison of gasoline WTW emissions from the literature

2.5. Conclusion

In previous published literature, the WTW emissions of various crudes are compared using point estimates without uncertainty. In order to compare crudes and determine whether one has higher or lower emissions than another, the uncertainty in the emissions is required. A sensitivity analysis was used to identify which sensitive inputs would have the largest effect on the WTW emissions. Distributions were then determined for the sensitive inputs and a Monte Carlos simulation was performed to calculate the uncertainty in the WTW emissions. Using conservative distributions, we found that while there is significant overlap between the scenarios it is still possible to distinguish the highest- and lowest-emission crudes. For example, Mars' gasoline WTW emissions were the lowest and ranged from 96.4-104.0 gCO_2eq/MJ, while the ANS current gasoline WTW emissions were the highest and ranged from 133.2-163.2 gCO_2eq/MJ. WTW emissions ranges for the remaining scenarios are 99.9-105.5 (Maya), 102.5-114.2 (Bow River), 104.6-114.5 (ANS historical), 105.5-113.2 (Kern historical), and 131.5-155.0 gCO_2eq/MJ (Kern current). Further analysis determined that the following inputs have the largest effect on the WTW emission ranges and require further investigation:

1. Venting, flaring, and fugitive emissions, especially for gassy crudes such as ANS
2. Refinery emissions, focusing on natural gas consumption and process unit efficiencies
3. Refinery yield factor
4. Natural gas upstream emission factors, especially when thermal recovery is used (Kern)
5. Injection and production gas-to-oil ratios and water-to-oil ratios

Policy makers interested in estimating the WTW emissions of a crude oil should focus on getting accurate data related to the inputs listed above. Currently the venting, fugitive, and flaring gas volumes show the largest potential for improvement due to their large uncertainty and lack of accurate publicly available data.

The current scenarios for ANS and Kern show that as fields age their production emissions can grow significantly. Furthermore, a carbon tax would increase the historical scenarios' gasoline cost for the ANS and Kern current scenarios, illustrating that the variation between scenarios is large enough to have a significant effect on the field's economics.

Chapter 3: Uncertainty in the Life Cycle Assessment Well-to-Wheel Greenhouse Gas Emissions of Transportation Fuels

This chapter presents a life cycle assessment of three crudes from Saudi Arabia, Venezuela, and Iran done through the modified FUNNEL-GHG-CCO model. Once the base case LCA was completed, a Monte Carlo simulation was run to determine the uncertainty in WTW emissions using the same method described in chapter 2.

3.1 Introduction

Growing awareness of climate change and global pushes for carbon taxes have led to increased interest in reducing global greenhouse gas (GHG) emissions [4]. Because transportation emissions are responsible for 23% of the global CO_2 emissions, governments have set strategic carbon emission reduction targets. For example, the European Union and California Air Resource Board have implemented polices to reduce the carbon intensity of transportation fuels by 6% and 10%, respectively, before 2020 [6, 7]. One solution to meet these targets is to consume transportation fuels (gasoline, diesel and jet) with lower upstream emissions.

The upstream emissions from transportation fuels are generated during crude oil production, surface processing, transportation, refining, and distribution. Life cycle assessments (LCAs) have been used to quantify emission intensity (emissions produced per unit of product produced) by examining the energy used and emissions generated along the life cycle stages from extraction of natural resources to the end of the product life [11]. By performing an LCA on multiple crudes, we can compare their GHG emissions. The upstream emissions from different crudes will vary depending on the crude properties and the methods used to produce and process the crudes into finished transportation fuels.

Current literature examines well-to-wheel (WTW) emissions of transportation fuels, which includes the upstream to combustion emissions, through models. These models can be divided into two types. Type 1 models, such as Greenhouse Gases, Regulated Emissions, and Energy Use in Transportation (GREET) [13] and GHGenius [14], use a top-down approach in which high level aggregated facility- and country -level data are used to calculate industry average

emissions. However, the use of aggregated data makes it difficult to determine emission intensity for specific crudes. Type 2 models, such as Jacobs [15, 16], TIAX [17], Oil Production Greenhouse gas Emissions Estimator (OPGEE) [18], Petroleum Refinery Life Cycle Inventory Model (PRELIM) [19], and **FUN**damental **EN**gineering Princip**l****E**s-based Mode**L** for Estimation of **G**reen**H**ouse **G**ases in **C**onventional **C**rude **O**ils (FUNNEL-GHG-CCO) [1-3], use a bottom-up approach wherein energy consumed and emissions generated are calculated using engineering first principles for each stage. Due to the lack of information and process complexity, the bottom-up models only examine processes that consume or produce large amounts of energy or pollution, and so they do not capture all the emissions produced and may lead to modeling results with limited accuracy. However, a bottom-up model can calculate the emissions for specific crudes and provide detailed results for each sub-process.

Various bottom-up models have determined the WTW emissions for over 35 crudes; however, the results are difficult to compare due to differences in the boundaries and assumptions used. Additionally, the TIAX and Jacobs models lack transparency and reproducibility as they were conducted by consulting companies and used confidential data [15-17]. Gordon et al.'s report "Know Your Oil" (KYO) used the PRELIM and OPGEE models to develop WTW estimates for thirty crude oils using consistent boundaries [8]. However, all these models provide deterministic point estimates for the WTW emissions. Without an uncertainty analysis, it is not possible to accurately compare crudes based on their WTW emissions. If model uncertainty is high compared to the difference in the emissions between two crudes, it would not be accurate to claim that one crude has lower emissions than the other.

Chapter 2 examined the uncertainties in five North American crudes using an updated version of the FUNNEL-GHG-CCO model and found that the uncertainties in WTW emissions ranged from ±2.6 to ±10.4%. Although uncertainty ranges could be large, it was still possible to differentiate between the highest- and lowest-emitting crudes.

There are two main gaps in the previously published work. First, the Jacobs [15, 16] and TIAX [17] models lack transparency, and reproducibility. Second, the published literature only examines uncertainty in 5 out of the 35 crudes studied. Both gaps are important to policy makers and industry representatives because quantifying the uncertainty in WTW emissions will provide a more accurate representation of the industry.

The general objective of this study is to determine the WTW emission uncertainties for Saudi Arabia, Iran, and Venezuela oils. The specific objectives are to:

1. Conduct a transparent and reproducible LCA on crude oils from Saudi Arabia, Iran, and Venezuela previously examined by Jacobs and TIAX with the FUNNEL-GHG-CCO model
2. Determine the WTW emission uncertainty by performing a Monte Carlo simulation

These crudes were chosen as Saudi Arabia and Venezuela represent 17% and 11% the crude imported to the USA from 2011 to 2015 [92], a significant portion of the USA's imports. While the USA does not currently import any Iranian oil, this oil was included due to the potential for imports as a result of the lifting of the Iranian trade embargo in 2016 [92, 93].

The uncertainty ranges determined from this study will provide a fair representation of the industry and a GHG emission comparison among the three crude oils. The results will help policy makers understand the limitations of LCA models and will help identify data gaps from industry in order to improve the accuracy of the WTW GHG emission estimates.

3.2 Method

This study was conducted in two stages. In the first stage we performed an LCA of the WTW emissions for crude oils from Saudi Arabia, Iran, and Venezuela. Data were collected and fed into a modified version of the FUNNEL-GHG-CCO model to complete the LCA. The scope of this LCA comprises of site preparation, production, surface processing, crude transportation, refining, distribution, and combustion stages. The study's second stage was an uncertainty analysis on the LCA WTW emissions. First, a sensitivity analysis was used to identify sensitive inputs that would have a significant effect on the results. Uncertainty distributions were then determined for the sensitive inputs and were used in a Monte Carlo simulation to determine the uncertainty. The Monte Carlo simulations are run using ModelRisk which is a Microsoft Excel add-in [33].

3.2.1 Base case model

The original FUNNEL-GHG-CCO model was created by Rahman et al. in 2014 and uses engineering first principles to perform a bottom-up analysis [1-3]. This model was used to study five conventional North American crudes (Maya, Mars, Bow River, Alaska North Slope, and

California Kern) and determine deterministic point estimates for the WTW emissions of each crude. The crudes were produced using water flooding, nitrogen gas injection, water-alternating-gas (WAG) injection, and steam injection. The FUNNEL-GHG-CCO model focuses on crudes refined and used within the USA and uses a functional unit of gCO_2eq/MJ of gasoline/diesel/jet fuel. This article focuses on gasoline production; diesel and jet fuel production emissions are included in appendix B4. Figure 8 gives a high level overview of the seven main stages.

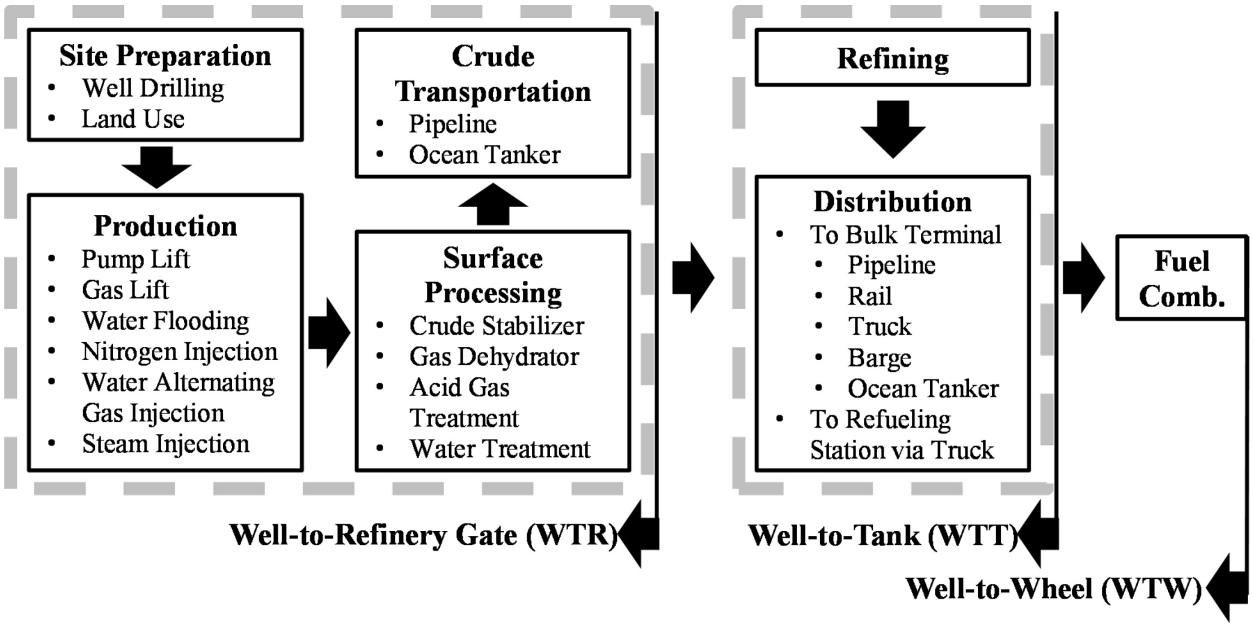

Figure 8: FUNNEL-GHG-CCO model boundary

The model used by Di Lullo et al. [94] will be referred to as the F-2 model, and the original FUNNEL-GHG-CCO model will be referred to as the F-1 model. This study made four additional modifications to the F-2 model to accommodate the new crudes and provide additional accuracy improvements; this study's model used in this paper is referred to as the F-3 model.

The modifications to the F-3 model are these: First, the F-1 and F-2 models used values (emission factors [EFs] and energy densities) from the 2013 version of GREET while the F-3 model uses the 2015 version of GREET. Second, the electricity emission factors have been updated to use consistent boundaries. Earlier versions did not include upstream EFs for the regional grid emission factors. Third, the water treatment in the original and F-2 model assumed that injected water would use treated produced water first and only import sea water if there was insufficient produced water available. The F-3 model allows the user to specify whether the

produced water is reused or if all the injected water is imported. Fourth, this model updated the distributions used for the crude transportation stage to improve accuracy. Further details on the modified electricity EFs and crude transportation distributions are in appendix B3.

3.2.2 Overview of new crude oils

Crude oil properties vary significantly around the world and are classified by their American Petroleum Institute gravity (ºAPI) as light (>31.1 ºAPI), medium (22.3-31.1 ºAPI), heavy (10-22.3 ºAPI), and extra-heavy (<10 ºAPI). The API gravity is related to the inverse of the crude's density with water being 10ºAPI [9]. This study performs an LCA on light crudes from Saudi Arabia, heavy crude from Venezuela, and medium crude from Iran. The Saudi Arabia and Venezuela crudes were chosen as they represent a significant portion of the USA's imports. Iranian oil, this oil was included due to the potential for imports as a result of the lifting of the Iranian trade embargo in 2016 [92, 93]. Additionally, earlier studies on these crudes lacks transparency with respect to data inputs, and do not incorporate an uncertainty analysis [15-17]. Table 8 shows a summary of the crude oils.

3.2.2.1. Saudi Arabia

The Gwahar oil field is over 2,000 square miles and is split into multiple zones. The Ain Dar and Uthmaniyah zones both produce oil from the Arab-D formation and produce a majority of the field's oil [95, 96]. As a result, this study focuses on Saudi Arabian light crude (Arab Light) from the Arab-D formation. The crude from the northern Ain Dar zone has an API of 34º [97], and the crude from the lower Uthmaniyah zone has an API of 32.6º [95]. The entire Gwahar field produced approximately 5 million bpd in 2003 [96]. The field currently uses water injection to maintain reservoir pressure. The produced oil is gathered at Abqaiq for surface processing [96]. The stabilized crude is then transported through the 1200 km Petroline to the Yanbu terminal, where it is loaded onto very large crude carriers (VLCC) and ultra-large crude carriers(ULCC) for transport to the USA [98].

3.2.2.2 Venezuela

Bachaquero crude is produced in the Bolivar oilfield on the east coast of Lake Maracaibo [99]. The heaviest cut of Bachaquero crude was used to align with the Jacobs study and has an API of 11.7º [15, 100]. Steam flooding (SF) and cyclic steam simulation (CSS) are used to produce the

heavy crude using offshore platforms [99-103]. It is assumed that the crude is then transported via pipeline to the Gulf of Venezuela coast where it is loaded onto a crude tanker.

3.2.2.3 Iran

The Alvand, Nosrat, Sivand, and Dena oilfields are located off the coast of Sirri Island in the Persian Gulf [104, 105]. Water injection is used to produce medium 31º API oil from offshore platforms [106]. This study focuses on the Sirri C&D fields due to data availability. The crude undergoes surface treatment on Sirri Island and is then loaded onto ultra-large crude carriers(ULCC) moored offshore [104, 107].

Table 8: Summary of crude oil fields

Crude Name	ºAPI	Country	Field	Production technique
Arab Light	32.6	Saudi Arabia	Arab-D section of the Gwahar field	Water flooding
Vene	11.7	Venezuela	Bachequero-13	Steam flooding and cyclic steam simulation
Sirri	31	Iran	Sirri C&D	Water flooding

3.3 Life cycle assessment of WTW greenhouse gas emissions

This section covers the LCA of the study. Each life cycle stage is described, followed by the LCA results.

3.3.1 Goal and scope definition

As described in section 3.2, this study examines the WTW emissions of transportation fuel production. A bottom-up analysis is used to quantify the energy and mass balances for each life cycle stage. A functional unit of gCO_2eq/MJ crude is used for pre-refinery emissions and gCO_2eq/MJ gasoline/ diesel/jet fuel for the WTW emissions.

3.3.2 Life cycle inventory

This section provides the inputs used for the LCA of the new scenarios. Only a high level description of the calculations used is given in this study; for additional details on the calculations readers are encouraged to read the previous works from Rahman et al. and chapter 2 [1-3].

3.3.2.1 Site preparation

Site preparation emissions are those from well drilling and land alteration. Diesel fuel used to run the drill is the primary pollution source [3]. The amount of drilling emissions is dependent on the drilling depth and the well lifetime productivity (as shown in Table 9). The lifetime well productivity is approximated from the total oil recovered and the number of wells drilled [25].

The land use emissions are a result of carbon from the soil and biomass being oxidized during well construction and from the land's reduced ability to sequester carbon after being disrupted [108, 109]. The land use emissions depend on the carbon richness of the ecosystem and the drilling intensity [108]. Since Sirri and Venezuela production occurs offshore and Saudi Arabia is a desert, low carbon richness was assumed for all three crudes. A moderate drilling intensity was assumed for all scenarios. The land use emissions were taken from OPGEE using a 30 year time period [108].

Table 9: Drilling stage inputs

Crude	Vene	Sirri	Arab Light
Average depth (m)	914[100]	2,438 [106]	2,042 [96]
Well lifetime productivity (m^3/well)	537,021[a]	364,876[b]	36,567[c]
[a] Approximated from initial oil-in-place of 7.04e9 bbl, 300 wells and 14.4% oil recovery factor [100] [b] Approximated from initial oil-in-place of 27e6 bbl, 2 wells and 17% oil recovery factor [106] [c] Approximated from 345e6 bbl 2008 cumulative production and active 1500 wells [110, 111]			

3.3.2.2 Production and surface processing

The production and surface processing emissions are primarily dependent on the injection and production steam-to-oil (SOR), water-to-oil (WOR), and gas-to-oil (GOR) ratios (shown in Table 10). The Venezuela SF and CSS production emissions are calculated from the amount of steam required and the energy required to heat the steam. The Venezuelan base case assumes 1924 kJ/kg of energy are required to produce the 75% quality steam required for injection [90, 100]. Steam energy calculations are provided in appendix B2.2. Due to the wide range of SORs found in the literature, both a high steam (HS) scenario and a low steam (LS) scenario are used for the Venezuelan crude; the only difference between the two scenarios is the steam injection ratio, as seen in Table 10. Sirri and Arab Light water flooding (WF) production emissions are calculated from the amount of energy required for the injection pump. An injection pump

discharge pressure of 27.6 and 20.7 MPa is used for the Sirri and Arab Light scenarios based on their reservoir pressures [106, 112, 113]; additional detail is in appendix B2.

The surface processing stage uses the same calculations as those in the F-1 and F-2 models [1-3]. There are no crude-specific inputs other than the water injection and production ratios. The Sirri scenario is unique as the produced water is not reinjected but disposed of into the ocean [114], resulting in a larger volume of water requiring treatment. Further details are given in appendix B2.3.

Table 10: Injection and production ratios

Crude	Production technology	Inj. WOR (m^3/m^3)	Inj. SOR (m^3/m^3)	Prod. WOR (m^3/m^3)	Prod. GOR (m^3/m^3)
Vene low steam	Steam flooding and cyclic steam simulation	N/A	0.25	2.0	98.0
Vene high steam	Steam flooding and cyclic steam simulation	N/A	2.10	0.3	98.0
Sirri	Water flooding	2.7	N/A	1.0	133.6
Arab Light	Water flooding	1.8	N/A	0.7	101.5

3.3.2.3 Venting, fugitive, and flaring emissions

During the crude production, surface processing, transportation, and refining stages, hydrocarbon gas is either vented or leaks into the atmosphere; this gas is known as venting and fugitive emissions. The F-2 model used previous work by Canter et al. [29] that calculated the venting and fugitive gas volumes as a percentage of the produced gas volume for North American crudes. As there is no additional information available for crudes outside of North America, the same percentage of 4.6% is used for this study in chapter 2.

Flaring emissions occur when the produced gas (PG) is combusted as it is vented to the atmosphere. The flaring rate is calculated from the respective countries' annual flaring and oil production volumes and results in flaring rates of 6.5, 14.8, and 46.5 m^3 PG/m^3 crude for the Arab Light, Vene, and Sirri scenarios, respectively. Further details are provided in appendix B3.1.

The produced gas composition is used to determine the EF for the vented, fugitive, and flared (VFF) gas. All crudes except for Arab Light use the default gas composition from the F-1 and F-

2 models, which is derived from OPGEE due to lack of data [3, 18]. The Arab Light scenario uses crude-specific gas composition from the northern Ain Dar field, which has a lower methane concentration (44.3 vs. 84.0 mol%) [113]. The full gas composition is provided in Table B2.

The F-2 model introduced a produced gas credit. The credit is defined as the natural gas production and processing emissions, as the produced gas can be used to offset the natural gas consumption. This model assumes all produced gas that is not reinjected or lost is sold as produced gas.

3.3.2.4 Crude transportation

The crudes are transported from the production and surface processing sites to the refinery in three stages. First, the crude is transported from the surface processing site to the coast via pipeline, then it is transported to the USA via tanker, and finally it is transported inland to the refineries via pipeline. It is assumed that all three crudes are refined in Houston, as 98% and 65% of Venezuelan and Persian Gulf crude are imported to PADD 3 [115].

The pipeline calculations are unchanged from the F-2 version and use scenario-specific inputs (provided in Table 11) to calculate the pumping energy required to overcome frictional losses. Additional information on how the pipeline velocities and throughputs are determined is in appendix B3.2.

Table 11: Crude pipeline transportation data

Crude	Origin	Destination	Distance (km)	Velocity (m/s) [54, 116, 117]	Throughput (m^3/d) [117]	Kinematic viscosity (cSt)
Vene	Bachaquero	Gulf of Venezuela	125[a]	1.4	63,500	48.6 [118]
Sirri	Platform	Sirri Island	50[b]	3.3	63,500	20.3 [119]
Arab Light	Abqaiq	Yanbu	1,200[c]	3.3	476,962	10 [120, 121]
USA	Houston port	Houston refineries	80[d]	1.4/2[e]	63,500	Crude specific

[a] Google map's distance from Bachaquero to coast
[b] Farthest field from Sirri Island [105]
[c] Length of the Petroline [54]
[d] From F-1 model, approximate distance from port to refineries [1-3]
[e] 1.4 m/s for Vene, 2 m/s for Sirri and Arab Light [54, 116, 117]

Using the GREET calculation method, we approximated the marine tanker emissions from the tanker capacity, travel distance, velocity, and load factors [13]. The tanker capacity is determined

from the origin port limitations, and the distances between the ports are determined from Sea-Distance-org; both are shown in Table 12 [13]. The load factors refer to the average engine load, the delivery trip uses a load factor of 0.83, and the return trip uses 0.70 [13]. The tanker velocity is assumed to be 15 knots for all scenarios [13].

Table 12: Crude marine tanker transportation data

Crude	Origin	Distance (km) [122]	Capacity (DWT)
Vene	Maracaibo City	3,408	240,000[a]
Sirri	Sirri Island	22,561	240,000[a]
Arab Light	Yanbu	22,743	315,000[b]
[a] Typical VLCC and ULCC vary from 160,000 to 330,000 DWT; this research used the average as the default [107, 123] [b] Typical tankers range from 280,000 to 350,000 DWT; this research used the average as the default [124]			

3.3.2.5 Refining

The refinery emissions are calculated using the Aspen HYSYS model previously used in the F-1 and F-2 models. The crude assays for Arab Light [120], Venezuela Bachaquero Heavy [118], and Sirri offshore [119] were input into the Aspen model to determine the refinery emissions and refinery yield factor. Mass-based allocation was used to track the emissions through the refinery to determine each product's share of the refinery emissions. The refinery yield factor is used to convert pre-refinery emissions from gCO_2eq/MJ crude to gCO_2eq/MJ gasoline/diesel/jet. It represents the inverse of the refinery conversion efficiency. If the refinery yield factor is 1.25, then 1.25 MJ of crude is required to produce 1 MJ of desired products, where gasoline, diesel, and jet fuel are the desired products. The remaining 0.25 MJ is either lost or converted to undesirable products such as coke or heavy fuel oils. The pre-refinery emissions are multiplied by the refinery yield since more than 1 MJ of crude must be produced and transported to the refinery to produce 1 MJ of desired end product.

3.3.2.6 Distribution and vehicle combustion

The final products are distributed from the refinery to bulk terminals using a combination of ocean tankers, barges, pipelines, and trucks. Trucks are then used to distribute the products from the bulk terminals to the fueling stations. As all the crudes examined are refined in North America there is no variation in the distribution and combustion emissions between scenarios.

3.3.3 LCA emission factors

This section provides the key EFs used in the analysis; full details on how the EFs are calculated from the reference values are provided in appendix B3. The NG Upstream EF is the only Fuel EF in Table 13 not taken directly from GREET; it is determined from work by Weber et al. [41] that examined uncertainty in NG upstream emissions. The marine residual oil LHV is 39.5 MJ/kg [13]. Electricity EFs are calculated using GREET values and regional electricity grid mixes [13]. The fuel upstream emissions and 6.5% transmission losses are included in the values provided in Table 14. The final product distribution EFs are taken from GREET and vary for each product as shown in Table 15. Vehicle combustion EFs are 73.3, 75.9, and 72.9 gCO_2eq/MJ for gasoline, diesel, and jet fuel, respectively [13].

Table 13: Fuel emission factors [13] (gCO_2eq/MJ)

Emission source	Value
Stationary diesel engine comb.	73.43
Industrial NG boiler comb.	56.52
NG turbine comb.	56.32
Diesel upstream	15.74
NG upstream [41]	17.96
PG credit	12.52
Marine residual oil comb.	80.84
Marine diesel upstream	12.75

Table 14: Electricity emission factors (gCO_2eq/kWh)

Electricity Use	EF	Sources
Vene production & pipeline 1[a]	531	[125, 126]
Sirri production & pipeline 1[a]	877	[127]
Saudi Arabia production	869	[128, 129]
Saudi Arabia pipeline 1	767	[130]
Pipeline 2[b] & Houston refinery	656	[45]

[a] Pipeline 1 carries crude from the production site to the origin marine port
[b] Pipeline 2 carries crude from destination marine port to the refinery

Table 15: Final product distribution to end user EF [13] (gCO_2eq/MJ)

Method	Gasoline	Diesel	Jet
Ocean tanker	0.544	0.262	0.260
Barge	0.623	0.372	0.369
Pipeline	0.240	0.208	0.206
Rail	0.100	0.330	0.325
Truck	0.140	0.142	0.141

3.3.4 LCA results

The LCA analysis found that the heavy Venezuelan crudes had the highest emissions and Arab Light the lowest (shown in Figure 9). This is expected, as the heavier crude requires a more energy intensive production and refining process. The difference in emissions between the gasoline, diesel, and jet fuels is a result of the different refinery, distribution, and combustion emissions for each product; the pre-refinery emissions (WTR) are the identical for gasoline, diesel, and jet fuel.

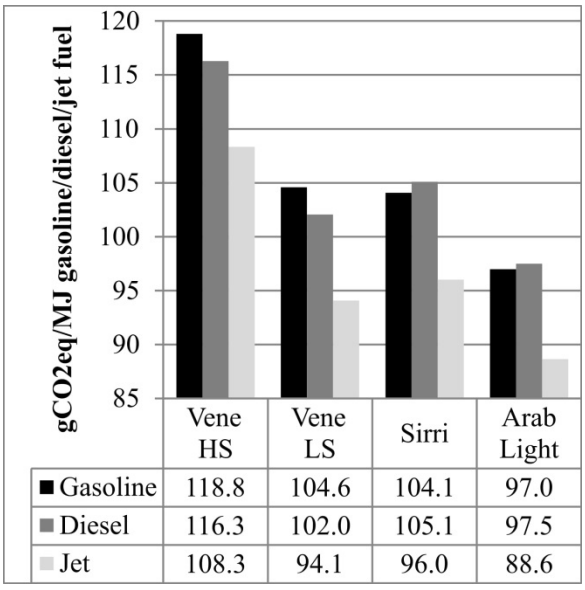

Figure 9: LCA well-to-wheel emissions

3.3.4.1 Well to refinery gate LCA results

Figure 10 shows the breakdown of well-to-refinery gate (WTR) emissions for gasoline, diesel, and jet fuel production. The results show that the production, VFF, and crude transportation stages are the primary emissions sources. All emissions are shown in terms of gCO_2eq/MJ of

crude for pre-refinery emissions. The site preparation emissions range from 0.13 to 0.21 gCO_2eq/MJ for Vene and Arab Light, respectively. The land-use emissions are 0.13 gCO_2eq/MJ for all four scenarios and contribute to the majority of the site preparation emissions. The drilling emissions for Vene are negligible due to the high well lifetime productivity. The production emissions are from steam generation for the Vene scenarios and water injection for the Sirri and Arab Light scenarios. The Sirri emissions are higher than the Arab Light emissions because of the higher water injection ratio and injection pressure used. The Vene scenarios have the highest emissions as the thermal production method is more energy intensive. The surface processing emissions range from 0.72 to 0.78 gCO_2eq/MJ for Vene and Sirri, respectively; the crude oil stabilizer contributes to 85-91% of the surface treatment emissions. Sirri has the highest VFF emissions due to its high GOR and large flaring volumes (see Table 16). Arab Light has the lowest VFF emissions because its produced gas has a low methane concentration and a low flaring rate. Even though the Sirri scenario has a larger GOR, the Arab Light scenario has a larger gas credit because Sirri flared a larger portion of its produced gas. The crude transportation emissions are low, 0.48 gCO_2eq/MJ for Vene, as the marine transportation distance is shorter (3,400 versus 23,000 km for Sirri and Arab Light). Table 17 provides a breakdown of the crude transportation emissions. The pipeline emissions were small due to the relatively short transportation distances.

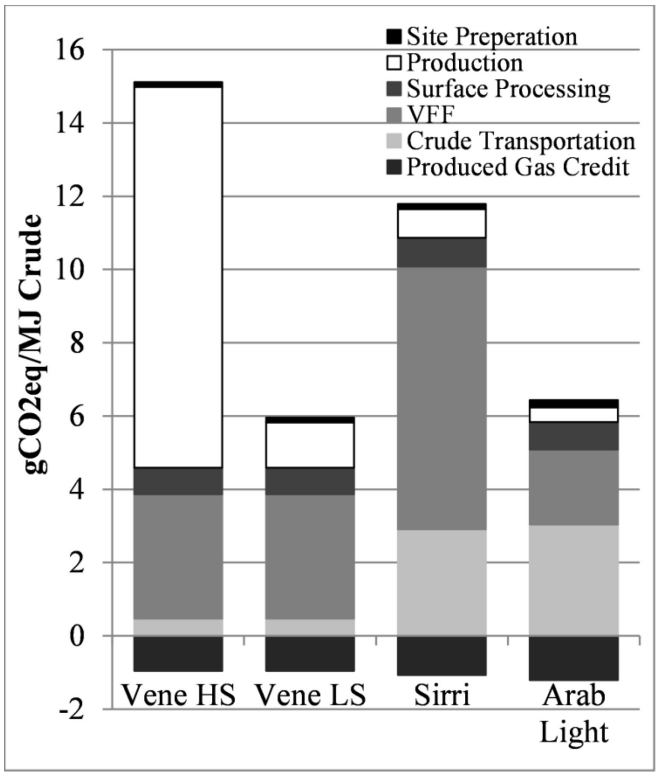

Figure 10: LCA well-to-refinery gate emissions

Table 16: LCA VFF and PG credit emissions (gCO_2eq/MJ)

Crude	Vene HS	Vene LS	Sirri	Arab Light
Venting and fugitive	2.28	2.28	3.37	1.39
Flaring	1.11	1.11	3.80	0.66
% Flaring	32.8%	32.8%	53.0%	32.1%
PG credit	-0.95	-0.95	-1.07	-1.20

Table 17: LCA crude transportation emissions breakdown (gCO_2eq/MJ)

Crude	Vene HS	Vene LS	Sirri	Arab Light
Pipeline 1[a]	0.02	0.02	0.07	0.38
Marine	0.45	0.45	2.82	2.65
Pipeline 2[b]	0.01	0.01	0.01	0.02
Total	**0.48**	**0.48**	**2.90**	**3.05**

[a] Pipeline 1 carries crude from the production site to the origin marine port
[b] Pipeline 2 carries crude from destination marine port to the refinery

3.3.4.2 LCA refinery, distribution, and combustion emissions

Refinery emissions vary for each crude and final product (see Table 18.) Jet fuel is made of the light ends of the crude feedstock that go through mild treatment and as a result have the lowest emissions. For the lighter crudes, Sirri and Arab Light, the diesel emissions are higher than the gasoline emissions, while for the heavy crude the opposite is true; this is a result of the crude composition and refinery configuration. The refinery yield factors are 1.55, 1.33, and 1.25 for the Vene, Sirri, and Arab Light scenarios, respectively. The Vene scenario has the highest yield factor because it is a heavier crude and will produce larger amounts of undesirable products such as residual oil. The pre-refinery emissions in gCO_2eq/MJ crude are multiplied by the refinery yield factor to get emissions in gCO_2eq/MJ gasoline/diesel/jet fuel. Since all the crudes are refined and distributed in North America, distribution and combustion emissions are the same for all the crudes. Distribution emissions for gasoline, diesel, and jet fuel are 0.50, 0.44, and 0.43 gCO_2eq/MJ and combustion emissions are 73.27, 75.86, and 72.89 gCO_2eq/MJ. The combustion emissions represent 61 to 82% of the total WTW emissions.

Table 18: LCA refinery emissions by product fuel (gCO_2eq/MJ)

Crude	Gasoline	Diesel	Jet
Vene	23.03	16.50	11.50
Sirri	16.06	13.12	7.02
Arab Light	16.68	13.15	7.26

3.4 Uncertainty analysis of WTW emissions

This section covers the method and results of the uncertainty analysis. Only an overview is provided here; detailed technical information can be found in appendix A. The uncertainty analysis uses a functional unit of gCO_2eq/MJ gasoline/diesel/jet fuel. Only a breakdown of the gasoline WTW emissions is provided in the main report. The diesel and jet fuel results are in appendix B4.

3.4.1 Uncertainty analysis methods

The uncertainty in the model output is due to sensitivity and uncertainty in the model inputs. Hence, a sensitivity analysis was used to identify sensitive inputs. Distributions were then

generated for each of the sensitive inputs from the available literature. Finally, a Monte Carlo simulation was used to quantify the uncertainty for each scenario.

3.4.1.1 Sensitivity analysis

Since tank-to-wheel (TTW) emissions are constant across all scenarios they are not included in the sensitivity analysis; instead well-to-tank (WTT) emissions are used. In order for an input to be deemed sensitive, a ±25% change in the input value must result in a change of ±1% or greater in the WTT emissions. A change of ±0.1% to ±1% is considered semi-sensitive and a change of less than ±0.1% is deemed insensitive. Even if an input is deemed insensitive, the output uncertainty could be significant if the input uncertainty is significantly larger than ±25%. Hence in this study, the lists of semi-sensitive and insensitive inputs were reviewed and any inputs that were identified as having large uncertainties were reclassified as sensitive inputs See Tables 19, 20, and 21 in section 3.4.2 for a full list of the sensitive inputs.

3.4.1.2 Determining distributions for sensitive inputs

In order to create a statistical distribution, a significant amount of data is required. When limited data are available, this study uses triangular distributions that require a most likely, minimum, and maximum estimate to generate. Additionally, triangular distributions are more conservative as they favor extreme values [131]. ModelRisk copulas are used to model dependence between inputs to produce a more conservative result [33, 35].

3.4.1.3 Determining distributions for the insensitive inputs

Even though the insensitive inputs individually have an insignificant effect, they can collectively impact the WTW emissions. As a result, the insensitive inputs are assigned a triangular distribution with a minimum and maximum value of 90% and 110% of the base case value. This will give a wider, more conservative output distribution.

3.4.1.4 Monte Carlo simulation parameters

To ensure the sampling error is less than 0.1 g/MJ, 50,000 samples are used for each scenario. Sampling error calculations are in appendix B1. Reported results use the 5% and 95% percentiles (P5, P95) to capture the extreme estimates.

ModelRisk tornado plots were used to identify which inputs had the largest contribution to the overall uncertainty. The tornado plots were generated using the conditional mean and 20 tranches. This means that the Monte Carlo samples are divided into 20 subgroups based on the value of the input being examined. For example, subgroup 1 includes all samples where input X's value is in the P0-P5 range of its distribution. The mean of each subgroup is calculated, and the tornado plot displays the minimum and maximum subgroup mean. Due to the number of inputs modeled and limited accuracy of the tornado plots, only the significant inputs are displayed. Significant inputs have a tornado plot variance (maximum - minimum) that is greater than 10% of the WTW variance (P95-P5). Spider plots were also used to identify any non-linear responses.

This study does not include an in-depth analysis of the uncertainty in the refinery process. The F-1 model uses Aspen HYSYS to model a typical North American refinery and this model is used unchanged in the current work [1-3]. The Aspen model outputs mass and energy balances for each refinery unit and these values are used to allocate emissions to each sub process using mass-based allocation [1-3, 38]. In order to determine refinery emissions, the energy balances are multiplied by heater and boiler efficiencies and fuel EF. This study includes uncertainty ranges for the efficiencies and EFs only and does not consider uncertainty in the mass and energy balances for each process unit. The refinery uncertainty is then fed into the WTW model as an input uncertainty to estimate the WTW uncertainty.

3.4.2 Monte Carlo inputs

Table 19, 20, and 21 show the distributions used for common and crude-specific inputs. Most of the common inputs have been taken unchanged from the F-2 model. The EF ranges were determined using GREET as the most likely value and uncertainty ranges from Weber and Calvin [41]. The electricity EFs were defined using the regional grid electricity mix and GREET defaults. The unit efficiencies, surface processing (SP), and crude transport distributions were determined by examining several references and using judgment to define probable ranges. The venting and fugitive emissions distributions were determined from work by Canter et al. [29]. The flared gas volume distributions used the measurement error specified by the NOAA data [60]. Data from OPGEE and other sources were used to define probable ranges for the flaring efficiency and PG methane concentration [18]. The refinery yield factor range is based on the

authors' judgment from reviewing variations in the Aspen model results with various crude assays and work from PRELIM [19, 38]. Additional details can be found in chapter 2 and appendix B2 and B3.

3.4.3 Uncertainty analysis results

Only the gasoline emissions are examined here; the diesel and jet fuel results are in section B4. Figure 11 shows that even when considering uncertainty, the Vene HS scenario clearly has higher WTW emissions than the remaining scenarios, since there is no overlap in the uncertainty ranges. However, it is not possible to conclude whether the Vene LS or Sirri scenario has higher or lower emissions as their uncertainty ranges have a significant amount of overlap. The Monte Carlo simulation was run twice for each scenario, once with the insensitive input distributions included and once with constant insensitive inputs. The difference between the two results was within sampling error, verifying that the insensitive inputs did not have a significant effect on the final results.

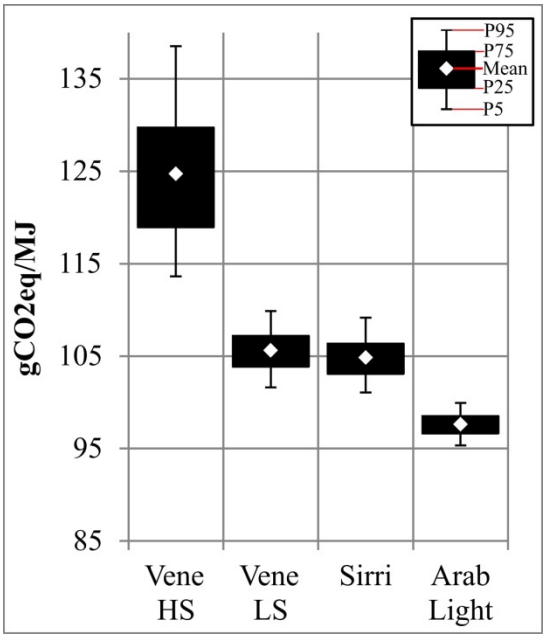

Figure 11: Uncertainty in gasoline WTW emissions

Table 19: Common Monte Carlo input distributions: Part 1

	Input	Monte Carlo Distribution	Units	Source
EF	Methane GWP*	Triangle(20.74,34,47.26)		[39, 40]
	NG upstream*	Triangle(71.2%,100%,140%)		[13, 41, 42]
	NG boiler comb.*	Triangle(97.2%,100%,102.7%)		[13, 41]
	NG turbine comb.*	Triangle(96.9%,100%,102.4%)		[13, 41]
Electricity EF	Arab Light production	Triangle(502,869,1200)	gCO_2eq/kWh	[13, 132]
	Arab Light pipeline 1	Triangle(690,767,844)	gCO_2eq/kWh	[13, 130]
	Vene production & pipeline 1	Triangle(254,531,803)	gCO_2eq/kWh	[13, 126]
	Sirri production & pipeline 1	Triangle(699,877,1105)	gCO_2eq/kWh	[13, 127]
	Pipeline 2 + Houston refinery	Triangle(502,656,804)	gCO_2eq/kWh	[13, 45]
Unit Eff.	Boiler*	Triangle(62%,75%,88%)		[47-50]
	Heater*	Triangle(70%,80%,90%)		[3, 18, 51, 52]
	Low flow pump*	Triangle(50%,60%,70%)		[53]
	High flow pump*	Triangle(50%,65%,85%)		[1, 15, 18, 53-55]
	Pipeline pump	Triangle (75%, 85%, 92%)		[54, 55, 133, 134]
SP	Specific heat correction factor*	Triangle(0.84,1,1.5)		[56]
	Crude stabilizer inlet temp.*	Triangle(37.8,48.9,65.6)	ºC	[57]
	Crude stabilizer outlet temp.*	Triangle(93.3,173.3,204.4)	ºC	[57, 58]
	Produced water energy intensity*	Triangle(1.51,2.26,5.79)	kWh/ m^3	[3, 59]
	Imported water energy intensity*	Triangle(1.26,1.51,3.90)	kWh/ m^3	[3, 59]
Crude Transport	Heavy crude pipeline velocities	Triangle(0.8,1.4,2.0)	m/s	[117]
	Light/medium crude pipeline velocities	Triangle(1.3,2.0,3.1)	m/s	[117]
	Middle Eastern light crude pipeline velocities	Triangle(2.0,3.3,3.8)	m/s	[54, 116, 117]
	Pipeline throughput	Triangle(15900,63600,127200)	m^3/d	[117]
	Marine distances	Triangle(90%,100%,110%)		
	Arab Light ocean tanker capacity	Triangle(280000,315000,350000)	DWT	[124]
	Sirri and Vene ocean tanker capacity	Triangle(160000,240000,320000)	DWT	[123]
	Tanker velocity	Triangle(22.2,27.8,31.5)	km/hr	[123, 135-137]
	Marine fuel comb. EF	Triangle(95%,100%,105%)		[13]
	Residual oil energy density	Triangle(37.7,39.5,41.6)	MJ/kg	[13]
*From F-2 model in chapter 2				

Table 20: Common Monte Carlo input distributions: Part 2

	Input	Monte Carlo Distribution	Units	Source
VFF and Other	Vented & fugitive gas volumes*	Triangle(2.1%,4.6%,7%)		[29]
	Arab light flared gas volume	Triangle(2.16,6.50,10.85)	m^3/m^3	[60]
	Vene flared gas volume	Triangle(0.66,14.82,28.98)	m^3/m^3	[60]
	Sirri flared gas volume	Triangle(37.10,46.52,55.94)	m^3/m^3	[60]
	Flaring efficiency*	PERT(80%,95%,99%)		[1, 13-15, 18]
	PG methane concentration*	Beta(14.49,2.91,,XBounds(,0.989))	%mol	[18]
	Refinery yield factor	Triangle(190%,100%,110%)		[19]
	Distributed to bulk terminals*	Uniform(0,1)		[3, 13]
*From F-2 model in chapter 2				

Table 21: Crude-specific Monte Carlo input distributions

	Input	Monte Carlo Distribution	Units	Source
Arab Light	Production GOR	ModPERT(37.58,98.85,214.25,15)	m^3/m^3	[97, 113]
	Injection WOR	Triangle(1,1.8,5,WCopula)	m^3/m^3	[17, 97]
	Production WOR	Triangle(0,0.72,5, WCopula)	m^3/m^3	[15, 97]
	Water copula	CopulaBiFrank(10,1)		
	Water injection pressure	Triangle(17.9,20.7,23.4)	MPa	[15, 113]
	PG methane concentration	Triangle(36.7%,44.3%,54.4%)	%mol	[113]
	Petroline throughput	Triangle(4.29e5,4.77e5,5.25e5)	m^3/d	
Vene	Production GOR	Triangle(53.43,97.96,178.1)	m^3/m^3	[101, 103]
	HS injection SOR	Triangle(1,2.1,5, WCopula)	m^3/m^3	[99, 100, 102]
	LS injection SOR	Triangle(0.01,0.25,0.7, WCopula)	m^3/m^3	[99, 100, 102]
	Production WOR	Triangle(0.3,2,3, WCopula)	m^3/m^3	[99]
	Water copula	CopulaBiFrank(10,1)		
	Steam energy required	Triangle(1675,1924,2349)	kJ/kg	[90, 100-102]
Sirri	Production GOR	Triangle(53.43,133.58,195.91)	m^3/m^3	[106, 112, 138]
	Injection WOR	Triangle(0.5,2.7,5.7, WCopula)	m^3/m^3	[106, 112, 139]
	Production WOR	Triangle(0.5,1,5.7, WCopula)	m^3/m^3	[106]
	Water copula	CopulaBiFrank(10,1)		
	Water injection pressure	Triangle(17.9,27.6,31.0)	MPa	[106, 112]
	Produced water treatment	Triangle(0.31,0.63,1.26)	kWh/m^3	[3, 59, 114, 140]

3.4.3.1 Sources of uncertainty in WTW emissions

The tornado plots in Figure 12 identify which input distributions had the largest effect on WTW emission uncertainty. The refinery emissions had the largest effect in every scenario except in the Vene HS scenario; there, the injection SOR had the largest effect. Hence a more detailed analysis of the refinery emissions is recommended to improve the model's accuracy, especially for the Arab Light scenario where the refinery emissions were the dominating source of uncertainty. For the Vene HS scenario, the injection SOR, steam energy required, and NG boiler efficiency are the dominating factors. This is expected as the LCA showed that thermal production methods produce higher emissions due to the large amount of energy required. The marine diesel (MD) upstream EF had a significant effect due to the long transportation distances. The transportation emissions are small, but for the Arab Light scenario, where the WTW emissions are low, the transportation inputs have a measurable effect. Therefore, for low emission crudes a detailed analysis of the transportation emissions is required to further reduce uncertainty in WTW emissions. The tornado plots are not able to accurately represent dependent variables. In all scenarios, the production WOR and injection WOR/SOR are dependent; as a result, the production WOR appears to be more significant than it actually is.

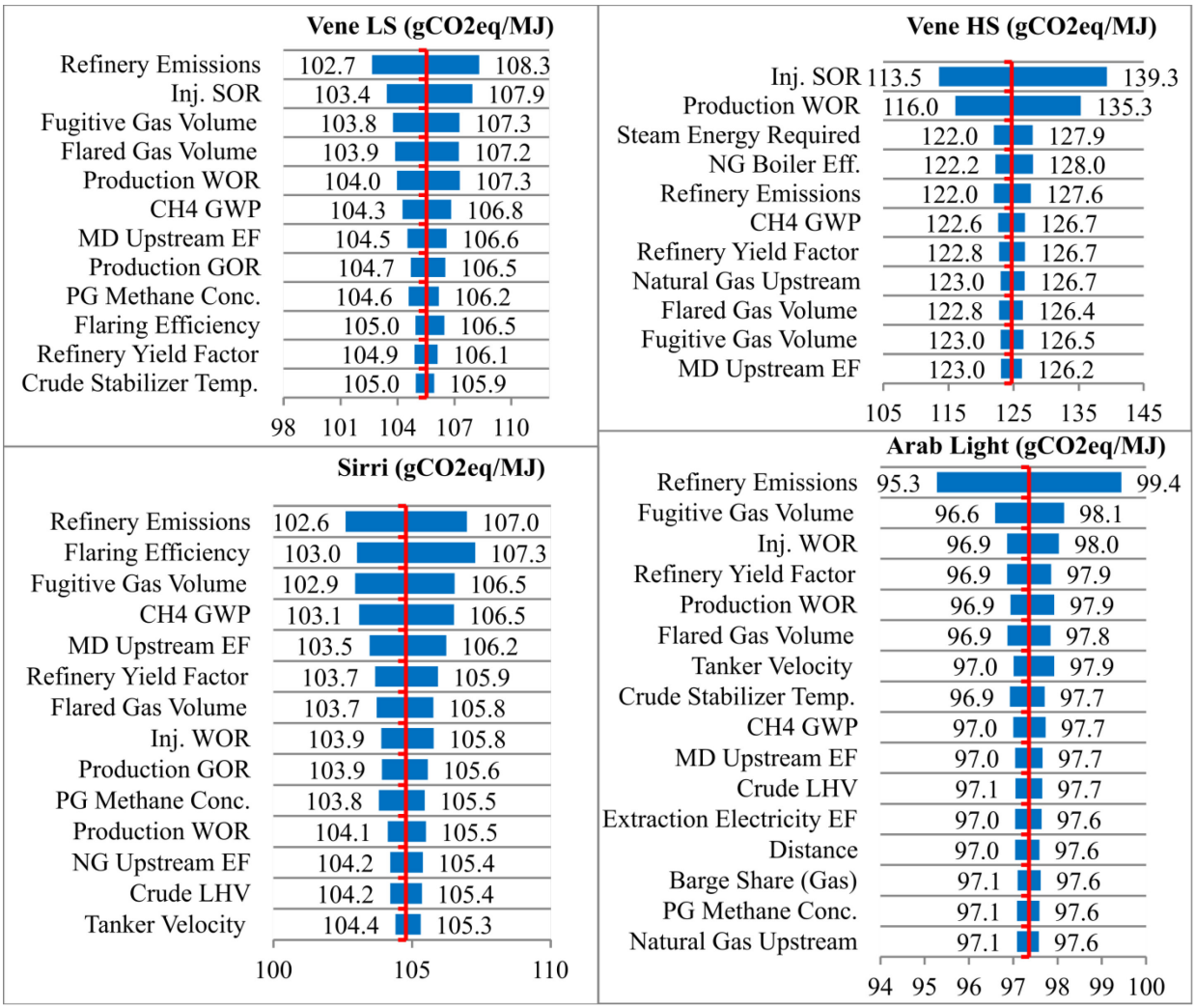

Figure 12: Gasoline WTW tornado plots

3.4.3.2 Sources of uncertainty in VFF emissions

As Figure 12 shows, the inputs related to the VFF emissions are a significant source of uncertainty. Further investigation shows that the uncertainty in the VFF emissions ranges from ±30% to ±55%, as shown in Figure 13. For the Vene LS and Sirri scenarios, the VFF variances (P95-P5) are 5.8 and 7.1 gCO_2eq/MJ, while the WTW variances are 8.3 and 8.1 gCO_2eq/MJ, respectively. This means that a significant portion of the overall uncertainty is due to the VFF emissions. For Arab Light and Vene HS, the VFF uncertainty is not as significant with the VFF variance at 2.2 and 5.9 gCO_2eq/MJ, while the WTW variances are 4.6 and 24.9 gCO_2eq/MJ, respectively. For the Vene HS scenario, the injection SOR reduces the impact from the VFF

emissions. For the Arab Light scenario, the overall low VFF emissions reduce their effect on WTW uncertainty.

Figure 14 provides additional detail on which input has the largest effect on the VFF uncertainty. For the Vene scenarios, the production GOR and flaring and fugitive volumes have the largest effect due to their wide uncertainty ranges. For the Sirri scenario, the flaring efficiency and CH_4 global warming potential (GWP) are more significant due to the large flaring volumes seen in Iran. For the Arab Light scenario, the low methane concentration and flared volume reduces the significance of the flaring efficiency, flared gas volume, and CH_4 GWP.

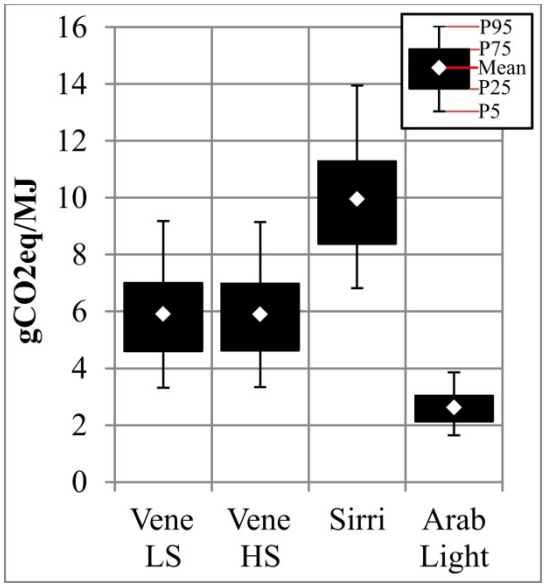

Figure 13: Uncertainty in VFF emissions

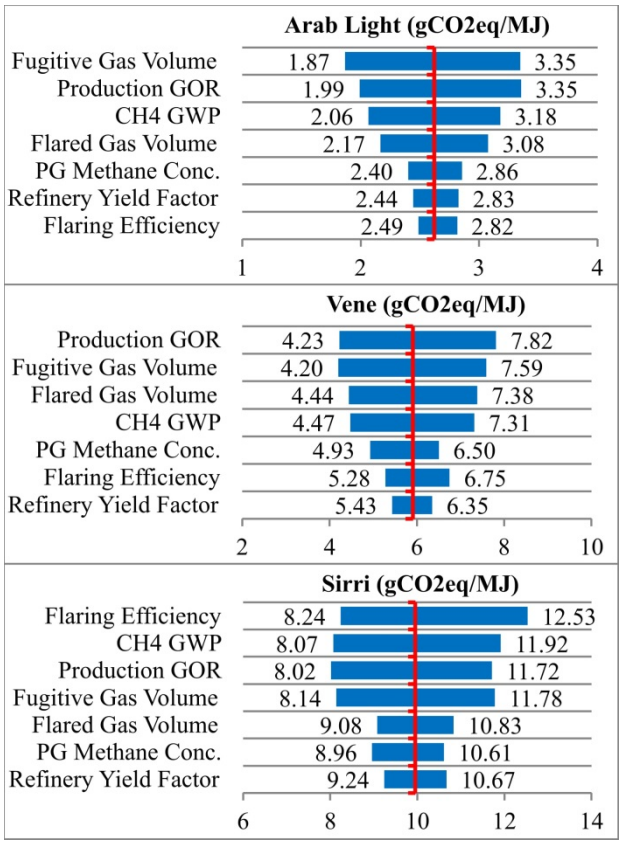

Figure 14: VFF tornado plots

3.4.3.3 Sources of uncertainty in refinery emissions

Figure 15 shows that the natural gas upstream EF has the largest effect on refinery emissions uncertainty. Thus examining the refinery's source of natural gas would improve estimates' accuracy. The variation between the three scenarios is a result of the crude composition affecting flow rates to each process unit. For example, heavier crudes will have higher flow rates through the vacuum distillation tower.

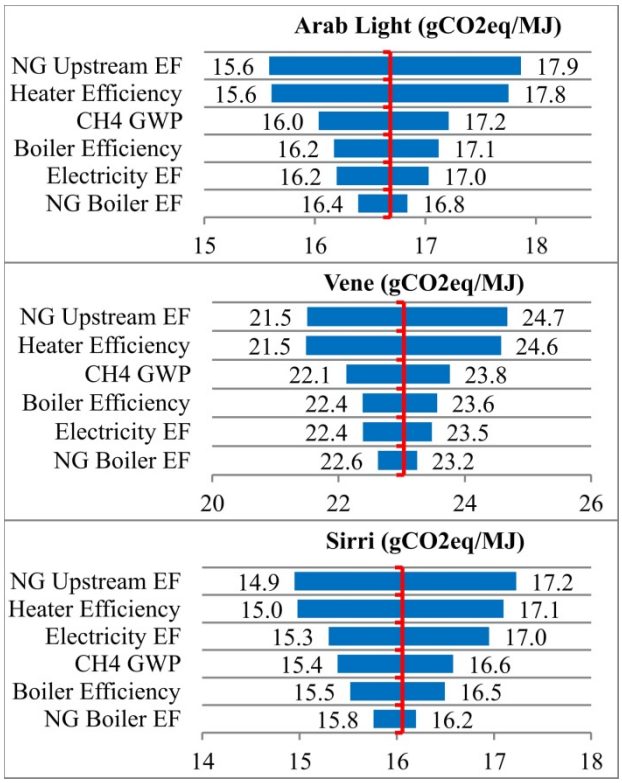

Figure 15: Refinery tornado plots

3.5 Discussion

In this section, this study's results are compared with those in published literature. Then the F-2 and F-3 results are compared to show the differences in WTW emissions of North American and imported crudes (Figure 16).

3.5.1 Comparison to published literature

Since this work uses a wide range of values for the inputs, the results from this study should encompass the results from previous studies if consistent boundaries are used. However, the boundaries are not consistent across all the models and hence the results vary. In order to verify that this study's results are nonetheless in agreement with those in the previous literature, the variation is explained.

Figure 16 shows that the Jacobs North American results are within this study's uncertainty ranges [15]. For the Vene LS scenario, the Jacobs N.A. results are on the lower end of this study's distribution as Jacobs uses a production WOR of 0.25 and a production GOR of 16.0

m^3/m^3 compared to this studies 2.0 and 101.5 m^3/m^3. The low GOR used by Jacobs represents the field's original GOR while the current production GOR used here is from current wells. For the Arab Light scenario, the Jacobs N.A. results use Arab medium oil. This study examined Arab Light due to data availability; as a result, the Jacobs emissions should be lower than our results. However, the Jacobs study used a higher injection WOR (2.3 vs. 1.8 m^3/m^3) and production GOR (115.8 vs. 101.5 m^3/m^3), which increased the emissions.

The Jacobs EU study assumed the crudes would be refined in Europe and use medium conversion refineries, while this study and assumes deep conversion refineries, which have higher energy intensities [16]. As a result, the European results tend to be lower than the North American results, as seen from the Jacobs EU and N.A. results for the Arab Light scenario. For the Sirri scenario, the Jacobs EU refinery emissions are 7.4 gCO_2eq/MJ compared to this study's results of 16.1 gCO_2eq/MJ. As deep conversion refineries are the most GHG intensive refinery configuration, it makes sense that the Jacobs EU results are lower than this study's results.

TIAX performs a high level analysis that is not as detailed as the analyses done by Jacobs N.A. or this study. Therefore, its results are lower than results from Jacobs and this study [17]. The largest source of variation between TIAX and this study is in refinery and VFF emissions. The TIAX refinery emissions are 4.3 and 1.4 gCO_2eq/MJ lower than our results for the Vene and Arab Light scenarios and the VFF emissions are 4.1 and 2.4 gCO_2eq/MJ lower. The refinery variation is a result of the TIAX model using aggregated data from the United States to represent a typical refinery rather than using a deep conversion refinery. Overall, TIAX's limited scope and high level analysis resulted in lower estimates when compared to Jacobs and this study.

Comparing this study's results to the previous literature showed that the main source of variation between the modeled results was the refinery configuration. However, the variations caused by the assumed input values were included in this study's uncertainty ranges. This is important for policy makers as it shows this study's results give a fair representation of each crude's WTW emissions. Additionally, the use of input distributions reduces the F-3 model's sensitivity to author bias (unintentional or intentional).

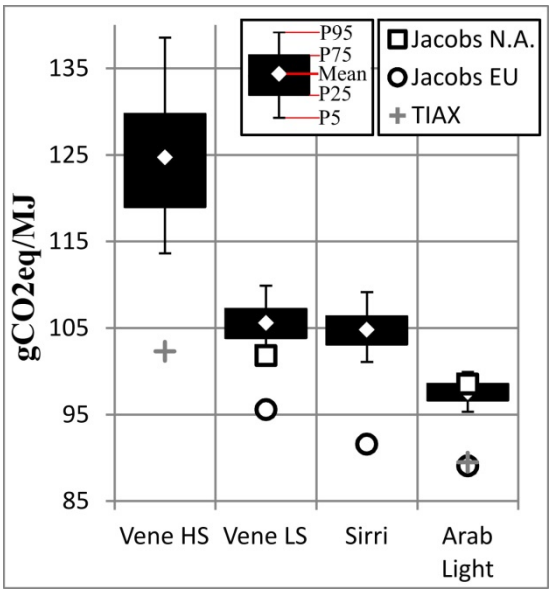

Figure 16: WTW emissions comparison to previous literature

3.5.2 Comparison to F-2 model results

To provide a better understanding of the uncertainty in the WTW emissions of various crudes, this study's results are compared to the F-2 model results for North American crudes from chapter 2. The purpose of this comparison is first to verify that the results are reasonable; if two crudes have similar properties and production methods. Then their WTW emissions should be similar. Second, the combined results are analyzed to determine if it is possible to group crudes based on their WTW emissions. If the uncertainty ranges are too large, it will not be possible to confidently state if one crude has higher emissions than another.

The results from the F-2 model have been updated to ensure that the model boundaries are consistent with the new F-3 model; additional information is in section B3. In Figure 17, the historical scenarios for Alaska North Slope (ANS) and Kern use lifetime averaged data for the injection and production ratios while the current scenarios use recent data to show how the WTW emissions change as the fields age. Table 22 provides a brief summary of the F-2 and F-3 crudes.

Vene HS and Kern current both use steam injection to produce heavy oil, but the Kern scenario has higher emissions due to the injection SOR used, 7.8 m^3/m^3 for Kern vs. 2.1 m^3/m^3 for Vene HS. Sirri, Arab Light, Bow River, and Mars all use water injection to maintain reservoir

pressure. Bow River has the highest emissions as it is heavier crude and uses a higher injection WOR. The Sirri scenario has similar emissions to Bow even though it is a lighter crude due to its high injection pressure. Mars emissions are lower as it uses a lower injection WOR and has a lower flared gas volume. Arab Light has the lowest emissions due to its small VFF emissions and low energy intensity production. Overall there were no unexpected variations in the results.

The results in Figure 17 allow the crudes to be separated into three general groups based on their WTW emissions. Group A contains the high emission crudes, ANS Current, Kern Current, and Vene HS. Group B contains medium emission crudes, Bow River, ANS Historical, Vene LS, Kern Historical, and Sirri. Group C contains the low emission crudes, Maya, Arab Light, and Mars. The uncertainty ranges show that it is not possible to confidently state if a crude has higher or lower emissions than another crude within its group. However, crudes in Group A have no overlap in their uncertainty ranges with Group B and C crudes. There is overlap between Group B's and C's 5^{th} and 95^{th} percentile ranges; however, there is no overlap between the 25^{th} and 75^{th} percentile ranges. To reduce the uncertainty ranges, either additional data are required or each crude should be further divided into specific production sites.

Table 22: Summary of F-2 and F-3 crudes

Crude	ºAPI	Production technology	Crude location	Refinery location
Maya	22.0	N_2 injection & gas lift	Mexico	Houston, TX
Mars	31.5	Water injection	U.S. Gulf Coast	Cushing, OK
Bow River	24.7	Water injection and pump lift	Canada	Cushing, OK
ANS	31.9	Water-alternating-gas injection	Alaska	Los Angeles, CA
Kern	13.0	Steam injection and pump lift	California	Los Angeles, CA
Vene	11.7	Steam injection	Venezuela	Houston, TX
Sirri	31.0	Water injection	Iran	Houston, TX
Arab Light	32.6	Water injection	Saudi Arabia	Houston, TX

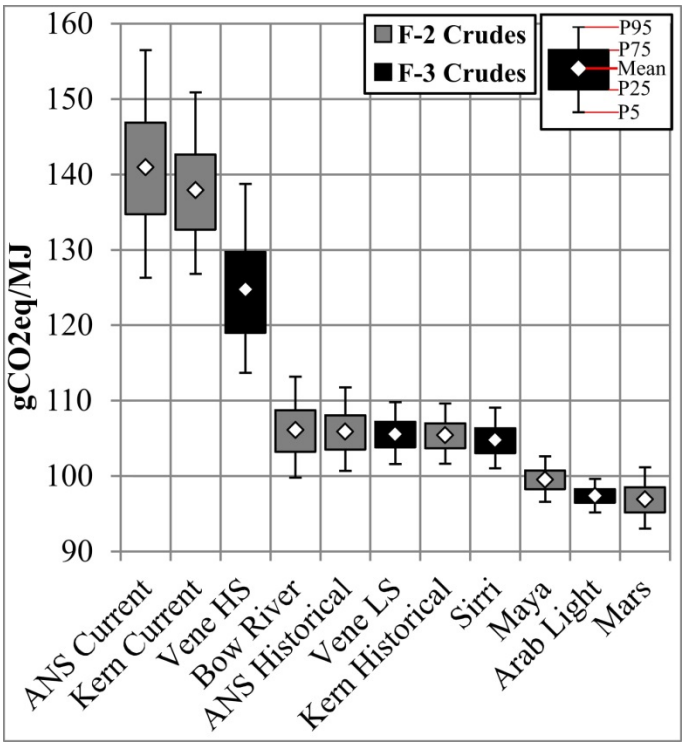

Figure 17: Comparison of F-2 and F-3 gasoline WTW emissions

3.6 Conclusion

The existing literature on the well-to-wheel (WTW) greenhouse gas (GHG) emissions of transportation fuels produced limited point estimates. This study used Monte Carlo simulations to quantify the uncertainty in the WTW emissions for three crudes from Saudi Arabia, Venezuela, and Iran. An updated version of the **FUN**damental E**N**gineering Princip**l**E**s**-based Mode**L** for Estimation of **G**reen**H**ouse **G**ases in **C**onventional **C**rude **O**ils (FUNNEL-GHG-CCO (FUNNEL-GHG-CCO) was used to perform a transparent life cycle assessment (LCA) for the three crudes previously studied by consulting companies.

The results showed that the Vene HS scenario clearly had the highest emissions at 113.6-138.5 gCO_2eq/MJ as its uncertainty range did not overlap with the remaining crudes. The Vene LS and Sirri scenarios had similar WTW emissions of 101.6-109.9 and 101.1-109.2 gCO_2eq/MJ, respectively. The Arab Light scenario uncertainty range did not overlap with any of the other crudes and had the lowest WTW emissions at 95.3-99.9 gCO_2eq/MJ.

The largest sources of uncertainty in WTW emissions were the VFF, refining, and injection SOR inputs. To reduce uncertainty in refining emissions, additional information from industry is required to develop an in-depth refinery model. To reduce uncertainty in VFF emissions, site-specific rather than aggregated country-wide data are required. VFF emissions require extensive on-site measurements as the current literature is limited. For example, flaring volume measurements use satellite images that have limited accuracy and do not differentiate between oil fields. For the Vene HS scenario, limited data availability for the injection SOR resulted in a wide conservative range being assumed; improved data availability could narrow this range.

The uncertainty ranges produced in this study will give policy makers and industry representatives a better understanding of the limits of bottom-up LCA models. Using a range of inputs will also give readers insight into how the assumed input values can affect the WTW emissions and also will give policy makers more confidence when using the numbers as they will not need to ask how emissions will change if input numbers change. Furthermore, this study's results are not as sensitive to author bias (intentional or unintentional) as they might be because the input ranges include a wide range of values taken from multiple sources. Additionally, the results of this study can be used to identify areas for potential GHG emission reductions and set realistic climate change policy targets.

Chapter 4: Conclusions and Recommendations for Future Work

4.1 Conclusion

This study investigated uncertainty in well-to-wheel (WTW) greenhouse gas (GHG) emissions of eight crudes through life cycle assessments. Five of the crudes, Maya, Mars, Bow River, Alaska North Slope (ANS), and California Kern County, were previously examined through the original **FUN**damental E**N**gineering Princip**l****E**s-based Mode**L** for Estimation of **G**reen**H**ouse **G**ases in **C**onventional **C**rude **O**ils (FUNNEL-GHG-CCO). Three crudes from Saudi Arabia, Venezuela, and Iran were included in this study. Earlier published literature examined WTW GHG emissions of transportation fuels, but these studies present deterministic point estimates. Adding a Monte Carlo simulation to calculate uncertainty helped provide a more realistic representation of the industry.

The previously published FUNNEL-GHG-CCO model was used as starting point for this work. The model's accuracy was improved through modifications that allowed us to use more detailed calculations and newer data. For the three new crudes, a full life cycle assessment was performed. This included gathering data related to the field properties, crude properties, production process, and crude transportation process. The surface processing, refining, finished product distribution, and fuel combustion stages were the same as the previously published FUNNEL-GHG-CCO crudes and required minimal additional data. For all scenarios a sensitivity analysis was performed that examined the sensitivity of each input. If a ±25% change in the input's value causes the well-to-tank (WTT) emissions to change by more than ±1%, it is defined as a sensitive input. Distributions were then determined for each of the sensitive inputs. A Monte Carlo simulation used the input distributions to calculate the uncertainty in the WTW emissions.

4.1.1 LCA GHG WTW emissions

A base case life cycle assessment of the three new crudes was performed using the updated FUNNEL-GHG-CCO model. The results showed that WTW emissions were highest for the Venezuela high steam (HS) and low steam (LS) thermal production scenarios at 118.8 and 104.6 gCO_2eq/MJ, respectively. The non-thermal production crudes, Sirri and Arab light, had lower emissions at 104.1 and 97.0 gCO_2eq/MJ, respectively.

4.1.2 Uncertainty in the LCA GHG WTW emissions

The resulting WTW emission ranges for gasoline are 95.3-99.9 (Saudi Arabia), 99.9-105.5 (Maya), 96.4-104.0 (Mars), 101.6-109.9 (Vene LS), 101.1-109.2 (Sirri), 102.5-114.2 (Bow River), 104.6-114.5 (ANS historical), 105.5-113.2 (Kern historical), 113.6-138.5 (Vene HS), 133.2-163.2 (ANS current), and 131.5-155.0 gCO_2eq/MJ (Kern current). Overall, the uncertainty in the WTW emissions ranged from ±2% to ±11% with the higher emission crudes having larger uncertainties. As the tank-to-wheel (TTW) emissions are constant for all crudes, the uncertainty in the WTT emissions gives a better representation of the overall model uncertainty. WTT uncertainty ranges from ±27% to ±9%. Overall the uncertainty ranges made it impossible to differentiate between the WTW emissions for Bow River, ANS historical, Vene LS, Kern historical, and Sirri (group B). However, the ANS current, Kern current, and Vene HS scenarios (group A) clearly had higher emissions than the group B and C scenarios as there was no overlap in the uncertainty ranges. The Maya, Arab light, and Mars scenarios (group C) had the lowest emissions, but their 95^{th} percentile uncertainty ranges overlapped with group B crudes' 5^{th} percentile uncertainty ranges; however, there was no overlap between group B's 25^{th} percentile and group C's 75^{th} percentile ranges.

The current and historical scenarios for ANS and Kern show that as the fields age their WTW emissions can grow rapidly as larger water and gas injection ratios are required to maintain reservoir pressure. The WTW emissions for the ANS and Kern current scenarios were 34.8% and 30.4% higher than the historical scenarios, respectively.

4.1.3 Sources of uncertainty

The largest source of uncertainty is from general areas: venting, fugitive, and flaring (VFF) volumes, refinery emissions, and injection and production fluid ratios. The uncertainty in the VFF volumes is due to a lack of high quality, publically available data. The currently available data are aggregated and use inaccurate approximation methods [29, 60, 108]. Site-specific measurements and continual monitoring of VFF volumes are required to improve the WTW emission estimates. The refinery emissions results are uncertain due to modeling limitations. A rigorous refinery model is required to get accurate energy consumption and mass yields for each process unit. The uncertainty in the fluid injection and production ratios is a result of both limited publically available data and natural variations from well to well. Additional data could

be used to define a more accurate input distribution, but the natural variation from well to well will limit how small the uncertainty range can be.

4.1.4 Study implications

The uncertainty ranges show that the WTW emissions cannot be approximated as a function of the crude API. Bow River (24.7º API) has higher emissions than Arab Light (32.6º API), but lower emissions than ANS (31.9º API). Similarly, the WTW emission ranges are not grouped based on production technology. The Bow River, ANS and Kern historical, Vene LS, and Sirri scenarios all have similar emissions even though they use different production technologies.

The main factor that separates the high emission crudes from the low emission crudes is the injection and production fluid volume ratios. Crudes that inject large volumes of water or gas per barrel of crude produced require more energy, thereby increasing their emissions. However, injecting a barrel of steam will require more energy than injecting a barrel of water. Additionally, crudes that produce large volumes of gas per barrel of crude tend to have higher VFF emissions, which result in higher WTW emissions. Thus collecting more accurate information related to fluid injection, production volume ratios, and VFF volume ratios will help policy makers obtain more accurate WTW emission estimates.

Although there is overlap between the WTW emission ranges, it is still possible to differentiate between the high and low emission crudes. These emission uncertainty ranges will give policy makers and industry representatives a better understanding of an LCA model's accuracy and limitations. Policy makers and industry representatives can use the results of this study to set realistic climate change policy targets. Policy makers interested in improving the accuracy of the WTW emission estimates should focus on getting accurate data from industry related to the key inputs identified in this study.

4.2 Recommendations for future work

The following recommendations have been made to improve the model's accuracy:

1. Currently, the Aspen refinery model represents a generic North American deep conversion refinery using petroleum shift reactors. This is a simplistic model that relies on linear equations to approximate process unit energy use and product yields. In order to improve the model's accuracy, a rigorous Aspen refinery model is needed, with an uncertainty analysis of the process unit energy use and product yields.
2. The current refinery model uses a deep conversion refinery with a fluid catalytic cracking and gas-oil hydrotreater. Additional research should examine the effect of different refinery configurations on the WTW emissions.
3. Due to a lack of available data, the current model uses conservative input distributions. Input from industry and technical experts would reduce the uncertainty in the input distributions and improve the model's accuracy.
4. Currently, all the refinery emissions are allocated to the desired end products (gasoline, diesel, and jet fuel). However, the undesirable byproducts, such as coke and fuel oils, are not examined. Further research should examine the effects of the undesirable byproducts on the well-to-wheel emissions.

Bibliography

[1] M. M. Rahman, C. Canter, and A. Kumar, "Greenhouse gas emissions from recovery of various North American conventional crudes," *Energy,* vol. 74, no. pp. 607-617, Sept. 2014. [Online]. Available: http://dx.doi.org/10.1016/j.energy.2014.07.026. [Accessed: June 14, 2016]

[2] M. M. Rahman, C. Canter, and A. Kumar, "Well-to-wheel life cycle assessment of transportation fuels derived from different North American conventional crudes," *Applied Energy,* vol. 156, no. pp. 159-173, Oct. 2015. [Online]. Available: http://dx.doi.org/10.1016/j.apenergy.2015.07.004. [Accessed: June 14, 2016]

[3] M. M. Rahman, "Life Cycle Assessment of North American Conventional Crudes for Production of Transportation Fuels," MSc. thesis, University of Alberta, Edmonton, 2014.

[4] The World Bank, "Carbon Pricing: It's on the move," *The World Bank*, Nov. 30, 2015 [Online]. Available: http://www.worldbank.org/en/news/feature/2015/11/30/carbon-pricing-its-on-the-move. [Accessed: Apr. 12, 2016].

[5] International Energy Agency, "CO2 Emissions from Fuel Combustion Highlights," *International Energy Agency*, 2015 [Online]. Available: https://www.iea.org/publications/freepublications/publication/CO2EmissionsFromFuelCombustionHighlights2015.pdf. [Accessed: Apr. 13, 2016].

[6] The European Parliament and the Council of the European Union, "Directive 2009/30/EC," *Official Journal of the European Union,* vol. 52, no. pp. 88-113, June 2009. [Online]. Available: http://dx.doi.org/10.3000/17252555.L_2009.140.eng. [Accessed: June 14, 2016]

[7] "Low Carbon Fuel Standard Program Background," *arb.ca.gov,* Feb. 2, 2016. [Online]. Available: http://www.arb.ca.gov/fuels/lcfs/lcfs-background.htm [Accessed: Feb. 11, 2016]

[8] D. Gordon, A. Brandt, J. Bergerson, and K. Jonathan, "Know Your Oil: Creating a Global Oil-Climate Index," *Carnegie Endowment for International Peace*, 2015 [Online]. Available: http://carnegieendowment.org/files/know_your_oil.pdf. [Accessed: Feb. 18, 2016].

[9] "API gravity," *wikipedia.org,* May 8, 2016. [Online]. Available: https://en.wikipedia.org/wiki/API_gravity [Accessed: June 14, 2016]

[10] "Crude Oil," *viscopedia.com,*[Online]. Available: http://www.viscopedia.com/viscosity-tables/substances/crude-oil/ [Accessed: Feb. 22, 2016]

[11] "Defining Life cycle Assessment," *gdrc.org,*[Online]. Available: http://www.gdrc.org/uem/lca/lca-define.html [Accessed: Apr. 14, 2016]

[12] International Organization for Standardization., "ISO 14040," 2010 [Online]. Available: http://www.iso.org/iso/catalogue_detail?csnumber=37456. [Accessed: June 14, 2016].

[13] GREET1, ver. 2015, Argonne National Laboratory, Argonne, IL. [Online]. Available: https://greet.es.anl.gov/ [Accessed: June 14, 2016]

[14] GHGenius, ver. 4.02, (S&T)^2 Consultants Inc, Delta, BC. [Online]. Available: http://www.ghgenius.ca/downloads.php [Accessed: May 16, 2016]

[15] W. Keesom, S. Unnasch, and J. Moretta, "Life Cycle Assessment Comparison of North American and Imported Crudes prepared for Alberta Energy Research Institute," *Jacobs Consultancy*, AERI 1747, July 2009 [Online]. Available: http://eipa.alberta.ca/media/39640/life%20cycle%20analysis%20jacobs%20final%20report.pdf. [Accessed: June, 14, 2016].

[16] B. Keesom, J. Blieszner, and S. Unnasch, "EU Pathway Study: Life Cycle Assessment of Crude Oils in a European Context," *Jacobs Consultancy*, Mar. 2012 [Online]. Available: http://www.energy.alberta.ca/Oil/pdfs/OSPathwayStudyEUjacobsRept2012.pdf. [Accessed: June 14, 2016].

[17] J. Rosenfeld, J. Pont, K. Law, D. Hirshfeld, and J. Kolb, "Comparison of North American and Imported Crude Oil Lifecycle GHG Emissions - Final Report Prepared for Alberta Energy Reseach Institute," *TIAX LLC*, TIAX Case No. D5595, July 6, 2009 [Online]. Available: http://eipa.alberta.ca/media/39643/life%20cycle%20analysis%20tiax%20final%20report.pdf. [Accessed: Mar. 25, 2016].

[18] OPGEE ver. 1.1 Draft E, Stanford School of Earth, Energy & Enviromental Sciences, Stanford, CA. [Online]. Available: https://pangea.stanford.edu/researchgroups/eao/research/opgee-oil-production-greenhouse-gas-emissions-estimator [Accessed: May 16, 2016]

[19] Petroleum Refinery Life Cycle Inventory Model, ver. 1.0, University of Calgary, Calgary, AB. [Online]. Available: http://ucalgary.ca/lcaost/prelim [Accessed: May 16, 2016]

[20] Enviromental Protection Agency, *Greenhouse Gas Reporting Program: Refineries,* EPA [Online]. Available: http://www.epa.gov/ghgreporting/ghgrp-2014-refineries. [Accessed: Nov. 11, 2015].

[21] Enviromental Protection Agency, *Greenhouse Gas Reporting Program: Petroleum and Natural Gas Systems,* EPA [Online]. Available: http://www.epa.gov/ghgreporting/ghgrp-2014-petroleum-and-natural-gas-systems. [Accessed: Nov. 11, 2015].

[22] Alaska Oil and Gas Conservation Commission, *Prudhoe Bay Feild, Prudhoe Oil Pool - EOR Injection,* Alaska Department of Administration, 2004 [Online]. Available: http://doa.alaska.gov/ogc/annual/2004/Oil_Pools/Prudoe%20Bay%20-%20Oil/Prudhoe%20Bay,%20Prudhoe%20Bay/Cht_Inj_EOR.pdf. [Accessed: Apr. 29, 2016].

[23] Wikipedia. "Oil depletion," Mar. 18, 2016. [Online]. Available: https://en.wikipedia.org/wiki/Oil_depletion [Accessed: June 28, 2016]

[24] Rigzone. "What Is EOR, and How Does It Work?,"[Online]. Available: http://www.rigzone.com/training/insight.asp?insight_id=313 [Accessed: June 28, 2016]

[25] B. Nimana, C. Canter, and A. Kumar, "Energy consumption and greenhouse gas emissions in the recovery and extraction of crude bitumen from Canada's oil sands," *Applied Energy,* vol. 143, no. pp. 189-199, Apr. 2015. [Online]. Available: http://dx.doi.org/10.1016/j.apenergy.2015.01.024. [Accessed: June 28, 2016]

[26] B. Nimana, C. Canter, and A. Kumar, "Energy consumption and greenhouse gas emissions in upgrading and refining of Canada's oil sands products," *Energy,* vol. 83, no. pp. 65-79, Apr. 2015. [Online]. Available: http://dx.doi.org/10.1016/j.energy.2015.01.085. [Accessed: June 28, 2016]

[27] B. Nimana, C. Canter, and A. Kumar, "Life cycle assessment of greenhouse gas emissions from Canada's oil sands-derived transportation fuels," *Energy,* vol. 88, no. pp. 544-554, Aug. 2015. [Online]. Available: http://dx.doi.org/10.1016/j.energy.2015.05.078. [Accessed: June 14, 2016]

[28] A. J. Kidnay, W. R. Parrish, and D. G. McCartney, "Compression," in *Fundamentals of Natural Gas Processing*, 2nd ed. Boca Raton, Fl: CRC Press, 2011, pp. 185-210.

[29] C. Canter and A. Kumar, "Impact of fugitive emissions on the greenhouse gas emissions of conventional crudes," presented at *AIChE Annual Meeting*, Nov. 16-21, 2014, Atlanta. 2014.

[30] J. G. Speight, The Chemistry and Technology of Petroleum, 4th ed. Hoboken: CRC Press, 2014.

[31] GREET1, ver. 2013, Argonne National Laboratory, Argonne, IL. [Online]. Available: https://greet.es.anl.gov/ [Accessed: May 16, 2016]

[32] D. P. Loucks, E. van Beek, J. R. Stedinger, J. P. M. Dijkman, and M. T. Villars, "Model Sensitivity and Uncertainty Analysis," in *Water Resources Systems Planning and Management: An Introduction to Methods, Models and Applications,* Paris: UNESCO, 2005. [Online] Available: https://www.utwente.nl/ctw/wem/education/afstuderen/Loucks_VanBeek/09_chapter09.pdf

[33] ModelRisk Software, ver. 5.3, Vose Software, Belgium. [Online]. Available: http://www.vosesoftware.com/ [Accessed: May 16, 2016]

[34] G. Di Lullo, M. M. Rahman, and A. Kumar, "Uncertainty analysis of transportation fuels from North American conventional oils GHG emissions," presented at *65th Canadian Chemical Engineering Conference*, Oct. 4-7, 2015, Calgary, Canada. 2015.

[35] M. van Hauwermeiren and D. Vose, "A Compendium on Distributions," in Ghent, Belgium: Vose Software, 2009. [Online] Available: http://www.vosesoftware.com/content/ebookmr4.pdf

[36] G. Angevine and V. Oviedo, "Ensuring Canadian Access to the Oil Markets in the Asia-Pacific Region," *Fraser Institute*, July 17, 2012 [Online]. Available: https://www.fraserinstitute.org/studies/ensuring-canadian-access-oil-markets-asia-pacific-region. [Accessed: Feb. 18, 2016].

[37] "Tornado plots," *vosesoftware.com,*[Online]. Available: http://www.vosesoftware.com/ModelRiskHelp/index.htm#Presenting_results/Other_plots/Tornado_charts.htm [Accessed: Feb. 26, 2016]

[38] Aspen HYSYS Refiney Wide Model.hsc, ver. 8.4, [Online]. Available: http://www.aspentech.com/products/aspen-hysys/ [Accessed: May 16, 2016]

[39] G. Myhre, D. Shindell, F.-M. Bréon, W. Collins, J. Fuglestvedt, J. Huang*, et al.*, "Anthropogenic and Natural Radiative Forcing Supplementary Material," in *Climate Change 2013: The Physical Science Basis. Contribution of Working Group to the Fifth Assessment Report of the Intergovernmental Panel on Climate Change,* Cambridge and New York: Cambridge University Press, 2013. [Online] Available: https://www.ipcc.ch/pdf/assessment-report/ar5/wg1/supplementary/WG1AR5_Ch08SM_FINAL.pdf

[40] G. Myhre, D. Shindell, F.-M. Bréon, W. Collins, J. Fuglestvedt, J. Huang*, et al.*, "Anthropogenic and Natural Radiative Forcing," in *Climate Change 2013: The Physical Science Basis. Contribution of Working Group to the Fifth Assessment Report of the Intergovernmental Panel on Climate Change,* Cambridge and New York: Cambridge University Press, 2013. [Online] Available:

[41] C. L. Weber and C. Clavin, "Life cycle carbon footprint of shale gas: Review of evidence and implications," *Environmental Science & Technology,* vol. 46, no. 11, pp. 5688-5695, June 2012. [Online]. Available: http://dx.doi.org/10.1021/es300375n. [Accessed: June 14, 2016]

[42] U.S. Energy Information Administration, *Natural Gas Gross Withdrawals and Production,* U.S. EIA, July 31, 2015 [Online]. Available: http://www.eia.gov/dnav/ng/ng_prod_sum_dcu_NUS_a.htm. [Accessed: Feb. 11, 2016].

[43] L. Turanskyj and K. B.A., "Turbomachinery for the world's largest nitrogen plant: Enhanced Oil Recovery to increase the output in the Cantarell oil feild, Mexica," *MAN*, June 2001 [Online]. Available: https://www.yumpu.com/en/document/view/16563813/turbomachinery-for-the-worlds-largest-nitrogen-man-turbo-india/3. [Accessed: Mar. 25, 2016].

[44] Goverment of Canada., *National Inventory Report: Part 3,* United Nations Framework Convention on Climate Change, Table A11-9 & Table A11-10, Apr. 17, 2015 [Online]. Available: http://unfccc.int/national_reports/annex_i_ghg_inventories/national_inventories_submissions/items/8812.php. [Accessed: Feb. 18, 2016].

[45] Enviromental Protection Agency., *eGRID Data Files,* Energy and the Environment, Jan. 4, 2016 [Online]. Available: http://www.epa.gov/energy/egrid. [Accessed: Feb. 11, 2016].

[46] U.S. Energy Information Administration, *Alaska - State Profile and Energy Estimates,* EIA, Feb. 18, 2016 [Online]. Available: http://www.eia.gov/state/?sid=AK#tabs-4. [Accessed: Mar. 25, 2016].

[47] Cleaver Brooks., "Boiler Efficiency Guide: Facts about Firetube Boilers and Boiler Efficiency," *Cleaver Brooks*, CB-7767, Mar. 2010 [Online]. Available:

http://www.cleaver-brooks.com/reference-center/insights/boiler-efficiency-guide.aspx. [Accessed: June 14, 2016].

[48] C. Stark, "Reducing Energy Cost Through Boiler Efficiency," *Department of Poultry Science North Carolina State University*, 2015 [Online]. Available: https://www.ncsu.edu/project/feedmill/pdf/E_Reducing%20Energy%20Cost%20Through%20Boiler%20Efficiency.pdf. [Accessed: Mar. 25, 2016].

[49] Energy Technology Systems Analysis Program., "Industrial Combustion Boilers," *International Energy Agency*, IEA ETSAP - Technology Brief I01, May 2010 [Online]. Available: http://www.iea-etsap.org/web/e-techds/pdf/i01-ind_boilers-gs-ad-gct1.pdf. [Accessed: June 14, 2016].

[50] Council of Industrial Boiler Owners., "Energy Efficiency & Industrial Boiler Efficiency: An Industry Perspective," *Council of Industrial Boiler Owners*, 2015 [Online]. Available: http://www.swagelokenergy.com/download/EEIBE.pdf. [Accessed: Feb. 18, 2016].

[51] "Our Heaters," *devcoheaters.com,*[Online]. Available: http://www.devcoheaters.com/our-heaters/ [Accessed: Feb. 16, 2016]

[52] F. Wildy, "Fired Heater Optimization," *AMETEK Process Instruments* [Online]. Available: http://www.etaassociates.com/Fired%20Heater%20Optimization%20ISA%20AD.pdf. [Accessed: Mar. 25, 2016].

[53] J. Evans, "Centrifugal Pump Efficiency—What Is Efficiency?," *Pumps & Systems*, 2012 [Online]. Available: http://www.pumpsandsystems.com/topics/pumps/pumps/centrifugal-pump-efficiency-what-efficiency. [Accessed: March 30, 2016].

[54] I. J. Karassik, J. P. Messina, P. Cooper, and C. C. Heald, "2.1 Centrifugal Pump Theory," in *Pump Handbook,* New York: McGraw Hill Professional, 2015. [Online] Available: http://accessengineeringlibrary.com/browse/pump-handbook-fourth-edition

[55] J. M. Campell, Gas Conditioning and Processing vol. 2: The Equipment Modules. Norman, OK: Campell Petroleum Series, 1984.

[56] W. Wright, "Simple Equations to Approximate Changes to the Properties of Crude Oil with Changing Temperature," *John M. Campbell Consulting*, Apr. 1, 2014 [Online]. Available: http://www.jmcampbell.com/tip-of-the-month/2014/04/simple-equations-to-approximate-changes-to-the-properties-of-crude-oil-with-changing-temperature/. [Accessed: Feb. 17, 2016].

[57] F. S. Manning and R. E. Thompson, Oilfield Processing of Petroleum: Crude Oil vol. 2. Tulsa, OK: PennWell Books, 1995.

[58] M. Stewart and K. Arnold, "Chapter 2 - Crude Stabilization," in *Emulsions and Oil Treating Equipment* Burlington: Gulf Professional Publishing, 2009, pp. 81-106.

[59] N. Vlasopoulos, F. A. Memon, D. Butler, and R. Murphy, "Life cycle assessment of wastewater treatment technologies treating petroleum process waters," *Science of The Total Environment,* vol. 367, no. 1, pp. 58-70, Aug. 2006. [Online]. Available: http://dx.doi.org/10.1016/j.scitotenv.2006.03.007. [Accessed: June 14, 2016]

[60] National Oceanic and Atmospheric Administration, *Global/Country Results 1994-2010,* NOAA, BCM_Global_20110223.xlsx, Feb. 23, 2011 [Online]. Available: http://ngdc.noaa.gov/eog/interest/gas_flares.html. [Accessed: Mar. 25, 2016].

[61] U.S. Energy Information Administration, *International-Total Petroleum and Other Liquids Production,* EIA [Online]. Available: http://www.eia.gov/beta/international/?fips=MX#pet. [Accessed: Feb. 17, 2016].

[62] U.S. Energy Information Administration, *Crude Oil Production,* EIA [Online]. Available: http://www.eia.gov/dnav/pet/pet_crd_crpdn_adc_mbbl_a.htm. [Accessed: May 20, 2016].

[63] National Energy Borard, *ARCHIVED - Estimated Production of Canadian Crude Oil and Equivalent,* NEB, 2016 [Online]. Available: https://www.neb-one.gc.ca/nrg/sttstc/crdlndptrlmprdct/stt/archive/stmtdprdctnrchv-eng.html. [Accessed: Feb. 18, 2016].

[64] Modern Power Systems, "Integrated solution key to success of world's largest oil-field N2 plant," *Global Trade Media*, Nov. 16, 2001 [Online]. Available: http://www.modernpowersystems.com/features/featureintegrated-solution-key-to-success-of-world-s-largest-oil-field-n2-plant/. [Accessed: Mar. 25, 2016].

[65] M. A. Cerce and V. P. Patel, "Selecting steam turbines for pump drivers," *in Proc. of the Twentieth International Pump Users Symposium, Mar. 17-20, 2003, Houston, TX*, [Online]. Texas: Turbomachinery Laboratory of the Texas A&M University, 2003. Available: http://turbolab.tamu.edu/proc/pumpproc/P20/12.pdf [Accessed: May 20, 2016].

[66] T. Limón-Hernández, G. Garza-Ponce, and C. Lechuga-Aguiñaga, "Status of the Cantarell field development program: An overview," *in Proc. of the Offshore Technology Conference, Apr. 30 - May 3, 2001, Houston, TX*, [Online]. Texas: Offshore Technology Conference, 2001. Available: https://www.onepetro.org/download/conference-paper/OTC-13175-MS?id=conference-paper%2FOTC-13175-MS [Accessed: May 16, 2016].

[67] J. Clemente, "Cantarell is not Mexico's only oil production problem," *Pipeline & Gas Journal,* no. August, 2008, pp. 52-54, Aug. 2008. [Online]. Available: http://www.peakoil.net/files/Cantarell%20Is%20Not%20Mexico%E2%80%99s%20Only%20Oil%20Production%20Problem.pdf. [Accessed: May 16, 2016]

[68] S. Weeden, "Meteoric History Of Cantarell Field Continues For Pemex," *Hart Energy*, May 1, 2015 [Online]. Available: http://www.epmag.com/meteoric-history-cantarell-field-continues-pemex-792716#p=full. [Accessed: Feb. 17, 2016].

[69] L. d. Sousa, "Deepwater GOM: Reserves versus Production - Part 1: Thunder Horse & Mars-Ursa," *The Oil Drum*, Sept. 30, 2011 [Online]. Available: http://www.theoildrum.com/pdf/theoildrum_8366.pdf. [Accessed: Mar. 25, 2016].

[70] J. Lach, "IOR for Deepwater Gulf of Mexico " *Research Partnership to Secure Energy for America*, 07121-1701.FINAL, Dec. 15, 2010 [Online]. Available: http://www.knowledge-reservoir.com/pdf/rpsea_report.pdf. [Accessed: Feb. 18, 2016].

[71] Bureau of Safety and Environmental Enforcement, *Oil and Gas Operations Reports - Part A (OGOR-A) Well Production 1996 - 2015,* BSEE, 2016 [Online]. Available:

https://www.data.bsee.gov/homepg/pubinfo/freeasci/product/freeprod_ogora.asp. [Accessed: Feb. 18, 2016].

[72] J. Weiland, M. Azari, F. Suparman, P. E. Fox, and D. F. Dorffer, "Case history review of the application of pressure transient testing and production logging in monitoring the performance of the Mars deepwater Gulf Of Mexico field," *in Proc. of the SPE Annual Technical Conference and Exhibition, Sept. 21-24, 2008, Denver, Colorado*, [Online]. Texas: Society of Petroleum Engineers, 2008. Available: http://dx.doi.org/10.2118/115591-MS. [Accessed: May 19, 2016].

[73] Alberta Energy Regulator, *Alberta's Energy Reserves & Supply/Demand Outlook,* AER, ST98, 2015 [Online]. Available: https://www.aer.ca/data-and-publications/statistical-reports/st98. [Accessed: Feb. 18, 2016].

[74] National Energy Board, *Conventional Heavy Oil Resources of the Western Canada Sedimentary Basin,* NEB, Aug. 2011 [Online]. Available: https://www.neb-one.gc.ca/nrg/sttstc/crdlndptrlmprdct/rprt/archive/cnvntnlhvylrsrcs2001/TRhvylWCSB2001-eng.pdf. [Accessed: Feb. 18, 2016].

[75] C. Galas, A. Clements, E. Jaafar, O. Jeje, D. Holst, and R. Holst, *Identification of Enhanced Oil Recovery Potential in Alberta - Phase 2 Final Report,* Energy Resource Conservation Board, 4208.18158, Mar. 2012 [Online]. Available: http://www.ags.gov.ab.ca/publications/pdf_downloads/ercb-eor-report2.pdf. [Accessed: Feb. 18, 2016].

[76] L. Fedenczuk, P. Pedersen, and M. Pedersen, "Analyzing waterflood responses for Pekisko B," *in Proc. of the Digging Deeper, Finding a Better Bottom Line, June 14-18, 1999, Calgary, AB*, [Online]. Texas: The Petroleum Socitey, 1999. Available: https://www.onepetro.org/download/conference-paper/PETSOC-99-46?id=conference-paper%2FPETSOC-99-46 [Accessed: May 16, 2016].

[77] G. Renouf and P. Nakutnyy, "Success of Heavy Oil Waterfloods - Factors and Predictions Phase II," *Petroleum Technology Research Centre*, May 2009 [Online]. Available: http://steps.ptrc.ca/concrete/files/8914/0554/3411/SRC-001-00094_Final_Report_Phase_I.pdf. [Accessed: Mar. 25, 2016].

[78] G. Renouf, M. Sheidaei, K. E. Gebhardt, and D. Soveran, "Heavy Oil Waterflooding Scoping Study," *Petroleum Technology Research Centre*, May 2004 [Online]. Available: http://steps.ptrc.ca/concrete/files/3514/0546/3331/Heavy_Oil_Waterflooding_Scoping_Study_-_Final_Report.pdf. [Accessed: Mar. 25, 2016].

[79] Alaska Oil and Gas Conservation Commission, *Monthly Production Reports,* Alaska Department of Administration, 2015 [Online]. Available: http://doa.alaska.gov/ogc/production/pindex.html. [Accessed: Apr. 29, 2016].

[80] Alaska Oil and Gas Conservation Commission, *Alaska Oil and NGL Production - December 2015,* Alaska Department of Administration, Feb. 2, 2016 [Online]. Available: http://doa.alaska.gov/ogc/ActivityCharts/Production/2015_12-ProdChart.pdf. [Accessed: Apr. 29, 2016].

[81] Alaska Oil and Gas Conservation Commission, *Prudhoe Bay Feild, Prudhoe Oil Pool - Production,* Alaska Department of Administration, 2004 [Online]. Available:

http://doa.alaska.gov/ogc/annual/2004/Oil_Pools/Prudoe%20Bay%20-%20Oil/Prudhoe%20Bay,%20Prudhoe%20Bay/Cht_Production.pdf. [Accessed: Apr. 29, 2016].

[82] Alaska Oil and Gas Conservation Commission, *AOGCC Pool Statistics - Prudhoe Bay Unit, Prudhoe Oil Pool,* Alaska Department of Administration, 2004 [Online]. Available: http://doa.alaska.gov/ogc/annual/current/18_Oil_Pools/Prudhoe%20Bay%20-%20Oil/Prudhoe%20Bay,%20Prudhoe%20Bay/1_Oil_1.htm. [Accessed: Apr. 29, 2016].

[83] Alaska Oil and Gas Conservation Commission, *Conservation Order 341D,* Alaska Department of Administration, Nov. 30, 2001 [Online]. Available: http://doa.alaska.gov/ogc/orders/co/co300_399/co341d.htm. [Accessed: Apr. 29, 2016].

[84] PetroWiki. "Real gases," *petrowiki.org,* June 4, 2015. [Online]. Available: http://petrowiki.org/Real_gases [Accessed: Feb. 18, 2016]

[85] B. Kaltenbach, C. Walsh, C. Foerster, T. Walsh, J. MacDonald, P. Stokes*, et al.*, *North Slope of Alaska Facility Sharing Study,* Alaska Department of Natural Resources, May 2004 [Online]. Available: http://dog.dnr.alaska.gov/publications/Documents/OtherReports/NorthSlope_Facility_Sharing_Study.pdf. [Accessed: Feb. 18, 2016].

[86] $(S\&T)^2$ Consultants Inc., "Shale Gas Update for GHGenius," *Natural Resources Canada Office of Energy Efficiency*, Aug. 31, 2011 [Online]. Available: http://www.ghgenius.ca/reports/ShaleGasUpdateFinalReport.pdf. [Accessed: June 14, 2016].

[87] Division of Oil, Gas & Geothermal Resources, *Monthly Oil and Gas Production and Injection Reports 01/2013-09/2015,* California Department of Conservation, 2015 [Online]. Available: ftp://ftp.consrv.ca.gov/pub/oil/monthly_production_reports/. [Accessed: Feb. 18, 2016].

[88] Division of Oil, Gas & Geothermal Resources, *2009 Annual Report of the State Oil & Gas Supervisor,* California Department of Conservation, 2010 [Online]. Available: http://www.conservation.ca.gov/dog/pubs_stats/annual_reports/Pages/annual_reports.aspx. [Accessed: Feb. 18, 2016].

[89] R. Edmond, D. W., and T. Nass Chas, "Cogeneration improves thermal EOR efficiency," *Oil and Gas Journal,* vol. 88, no. 42, Oct. 1990. [Online]. Available: http://www.ogj.com/articles/print/volume-88/issue-42/in-this-issue/production/cogeneration-improves-thermal-eor-efficiency.html. [Accessed: May 16, 2016]

[90] Y. Çengel and M. A. Boles, Thermodynamics: An Engineering Approach, 7th ed. New York: McGraw-Hill, 2011.

[91] W. Keesom, S. Unnasch, and J. Moretta, "Life Cycle Assessment Comparison of North American and Imported Crudes prepared for Alberta Energy Research Institute," *Jacobs Consultancy*, AERI 1747, 2009 [Online]. Available: http://www.eipa.alberta.ca/media/39640/life%20cycle%20analysis%20jacobs%20final%20report.pdf. [Accessed:

[92] U.S. Energy Information Administration, *Weekly Preliminary Crude Imports by Top 10 Countries of Origin (ranking based on 2013 Petroleum Supply Monthly data),* EPA, June 6, 2016 [Online]. Available: http://www.eia.gov/dnav/pet/pet_move_wimpc_s1_w.htm. [Accessed: June 14, 2016].

[93] A. Asghedom, *Iran's petroleum production expected to increase as sanctions are lifted,* U.S. Energy Information Administration, Jan. 19, 2016 [Online]. Available: http://www.eia.gov/todayinenergy/detail.cfm?id=24592. [Accessed: May 3, 2016].

[94] G. R. Di Lullo, "Uncertainty in Life Cycle Assessments of Well-to-Wheel Greenhouse Gas Emissions of Transportation Fuels Derived from Various Crude Oils," MSc. thesis, University of Alberta, Edmonton, AB, 2016.

[95] S. M. Al-Mutairi and M. Al-Harbi, "Water production management strategy in North Uthmaniyah area, Saudi Arabia," *in Proc. of the Europec/EAGE Annual Conference and Exhibition, June 12-15, 2006, Vienna*, [Online]. Texas: Society of Petroleum Engineers, 2006. Available: http://dx.doi.org/10.2118/98847-MS. [Accessed: June 14, 2016].

[96] M. R. Simmons, Twilight in the Desert: The Coming Saudi Oil Shock and the World Economy. Hoboken, New Jersey: Wiley, 2005.

[97] A. H. H. Alhuthali, H. H. Al-Awami, A. Soremi, and A. I. Al-Towailib, "Water management in North 'Ain Dar, Saudi Arabia," *in Proc. of the 14th Middle East Oil & Gas Show and Conference, Mar. 12-15, 2005, Bahrain*, [Online]. Texas: Society of Petroleum Engineers, 2005. Available: http://dx.doi.org/10.2118/93439-MS. [Accessed: June 15, 2016].

[98] A. Al-Ahmed, A. Bond, and D. Morillo, "Security Threats to Saudi Arabia's Oil Infrastructure," *The Institute for Gulf Affairs*, 2013 [Online]. Available: http://www.gulfinstitute.org/wp-content/uploads/2013/11/Threats_to_the_Saudi_Oil_Infrastructure.pdf. [Accessed: Apr. 4, 2016].

[99] G. J. Chourio Arocha, M. Mohtadi, and J. B. Ortega, "Evaluation and application of the extended cyclic steam injection as a new concept for Bachaquero-01 reservoir in west Venezuela," *in Proc. of the SPE Reservoir Characterisation and Simulation Conference and Exhibition, Oct. 9-11, 2011, Abu Dhabi, UAE*, [Online]. Texas: Society of Petroleum Engineers, 2011. Available: http://dx.doi.org/10.2118/148083-MS. [Accessed: June 14, 2016].

[100] M. G. Rodriguez and D. D. Mamora, "Increased oil production from Bachaquero-01 by steamflooding using horizontal wells," *in Proc. of the SPE/DOE Improved Oil Recovery Symposium, Apr. 3-5, 2000, Tulsa, Oklahoma*, [Online]. Texas: Society of Petroleum Engineers, 2000. Available: http://dx.doi.org/10.2118/59335-MS. [Accessed: June 14, 2016].

[101] M. G. Rodriguez, *Bachaquero-01 Reservoir, Venezuela — Increasing Oil Production by Switching from Cyclic Steam Injection to Steamflooding Using Horizontal Wells*, Texas: Texas A&M University, 1999.

[102] M. A. Escobar, C. A. Valera, and R. E. Perez, "A large heavy oil reservoir in Lake Maracaibo Basin: Cyclic steam injection experiences," *in Proc. of the International*

Thermal Operations and Heavy Oil Symposium, Feb. 10-12, 1997, Bakersfield, California, [Online]. Texas: Society of Petroleum Engineers, 1997. Available: http://dx.doi.org/10.2118/37551-MS. [Accessed: June 14, 2016].

[103] J. Potma, P. Justiniano, S. Olivares, S. Pizzarelli, O. Gonzalez, S. Schlumberger Oilfield*, et al.*, "Thermal horizontal completions boost heavy oil production," *World oil,* vol. 224, no. 2, pp. 83-85, Feb. 2003. [Online]. Available: http://www.worldoil.com/magazine/2003/february-2003/features/thermal-horizontal-completions-boost-heavy-oil-production. [Accessed: June 14, 2016]

[104] Oil and Gas Journal, "Total seeks to replicate its Sirri development success off Iran," *Oil and Gas Journal,* vol. 97, no. 14, Apr. 1999. [Online]. Available: http://www.ogj.com/articles/print/volume-97/issue-14/in-this-issue/drilling/total-seeks-to-replicate-its-sirri-development-success-off-iran.html. [Accessed: Apr. 12, 2016]

[105] "Sirri Island Oil Fields," *abarrelfull.wikidot.com,* June 29, 2015. [Online]. Available: http://abarrelfull.wikidot.com/sirri-island-oil-fields [Accessed: Apr. 12, 2016]

[106] A. Taheri, M. Zahedzadeh, R. Masoudi, A. Ataei, E. Roayaei, and H. Fakhri, "Simulation and experimental studies of mineral scale formation effects on performance of Sirri-C oil field under water injection," *Iranian Journal of Chemistry and Chemical Engineering,* vol. 30, no. 3, pp. 9-24, Summer 2011. [Online]. Available: http://www.sid.ir/en/vewssid/j_pdf/84320115902.pdf. [Accessed: June 14, 2016]

[107] "Sirri Island," *maroos.net,*[Online]. Available: http://www.maroos.net/page/siri-island.html [Accessed: Apr. 12, 2016]

[108] H. M. El-Houjeiri, K. Vafi, J. Duffy, S. McNally, and A. R. Brandt, "OPGEE V1.1 Draft D: User guide & Technical documentation," *Stanford School of Earth, Energy & Enviromental Sciences*, Oct. 10, 2014 [Online]. Available: https://pangea.stanford.edu/researchgroups/eao/research/opgee-oil-production-greenhouse-gas-emissions-estimator. [Accessed: June 14, 2016].

[109] S. Yeh, S. M. Jordaan, A. R. Brandt, M. R. Turetsky, S. Spatari, and D. W. Keith, "Land use greenhouse gas emissions from conventional oil production and oil sands," *Environmental Science & Technology,* vol. 44, no. 22, pp. 8766-8772, Oct. 2010. [Online]. Available: http://dx.doi.org/10.1021/es1013278. [Accessed: June 14, 2016]

[110] R. Sorkhabi. "The king of giant fields," *GEO ExPro*, pp. 24-29, Vol. 7, No. 4. Available: http://www.geoexpro.com/articles/2010/04/the-king-of-giant-fields. [Accessed: June 15, 2016]

[111] N. G. Saleri and E. H. Bu-Hulaigah, "Knowledge managment in North Ghawar," *in Proc. of the 17th World Petroleum Congress, Sept. 1-5, 2002, Rio de Janeiro, Brazil*, [Online]. London: World Petroleum Congress, 2002. Available: https://www.onepetro.org/conference-paper/WPC-32150 [Accessed: June 15, 2016].

[112] A. Taheri, M. Zahedzadeh, R. Masoudi, F. Alikhani, E. Roayaei, and M. Ghanavati, "Evaluation of reservoir performance under water injection considering the effect of inorganic scale deposition in an Iranian carbonate oil reservoir," *in Proc. of the 8th European Formation Damage Conference, May 27-29, 2009, Scheveningen, Netherlands*,

[Online]. Texas: Society of Petroleum Engineers, 2009. Available: http://dx.doi.org/10.2118/121221-MS. [Accessed: June 14, 2016].

[113] M. I. Al-Eid and S. L. Kokal, "Investigation of increased gas-oil ratios in Ain Dar field," *in Proc. of the 13th Middle East Oil Show & Conference, Apri. 5-8, 2003, Bahrain*, [Online]. Texas: Society of Petroleum Engineers, 2003. Available: http://dx.doi.org/10.2118/81425-MS. [Accessed: June 14, 2016].

[114] "Project: Sirri district Industrial Wastewater Treatment system EPC Project," *samandis-co.com,*[Online]. Available: http://samandis-co.com/2-3.html [Accessed: Apr. 12, 2016]

[115] U.S. Energy Information Administration, *PAD District Imports by Country of Origin,* EPA, May 5, 2016 [Online]. Available: http://www.eia.gov/dnav/pet/pet_move_impcp_a2_r30_epc0_ip0_mbbl_a.htm. [Accessed: Apr. 28, 2016].

[116] R. Soligo and A. M. Jaffe, "Unlocking the Assets: Energy and the Future of Central Asia and the Caucasus," *The James A. Baker III Institute for Public Policy of Rice University*, Apr. 1998 [Online]. Available: http://bakerinstitute.org/files/2753/. [Accessed: May 4, 2016].

[117] Enbridge Pipelines Inc., "Q2 2015 Service Levels On the Enbridge Liquids Pipeline Mainline Network," *Enbridge*, June 2015 [Online]. Available: http://www.enbridge.com/~/media/Rebrand/Documents/Shippers/Enbridge_Mainline_Service_Levels.pdf?la=en. [Accessed: June 14, 2016].

[118] E. Cerić, *Crude oil Assay.*Emir Ceric, 2001. [Online] Available: http://eceric.com/crudeoil.html

[119] Oil and Gas Journal, "Crude Oil Assays," in *Oil and Gas Journal DataBook 2008,* Tulsa, OK: PennWell Books, 2008. [Online] Available: https://books.google.ca/books?id=Vb9VAgAAQBAJ

[120] D. Stratiev, R. Dinkov, K. Petkov, and K. Stanulov, "Evaluation of crude oil quality," *Petroleum & Coal,* vol. 52, no. 1, pp. 35-43, Feb. 2010. [Online]. Available: http://www.vurup.sk/sites/vurup.sk/archivedsite/www.vurup.sk/pc/vol52_2010/issue1/pdf/pc_1_2010_stratiev_051.pdf. [Accessed: June 14, 2016]

[121] Enviroment Canada, *Arabian Light,* Emergencies Science and Technology Division, 1991 [Online]. Available: http://www.etc-cte.ec.gc.ca/databases/Oilproperties/pdf/WEB_Arabian_Light.pdf. [Accessed: May 4, 2016].

[122] "Sea Distance Calculator," *Sea-Distance-org,*[Online]. Available: http://www.sea-distances.org/ [Accessed: Apr. 28, 2016]

[123] T. M. Hamilton. "Oil tanker sizes range from general purpose to ultra-large crude carriers on AFRA scale," *Today in Energy*, Sept. 16, 2014. Available: http://www.eia.gov/todayinenergy/detail.cfm?id=17991. [Accessed: June 15, 2016]

[124] "Saudi Arabia: Hydrocarbon Sector Transport and Storage Facilities," *country-data.com,* Dec. 1992. [Online]. Available: http://www.country-data.com/cgi-bin/query/r-11616.html [Accessed: May 4, 2016]

[125] U.S. Energy Information Administration, *Country Analysis Brief: Venezuela,* EPA, Nov. 25, 2015 [Online]. Available: https://www.eia.gov/beta/international/analysis.cfm?iso=VEN. [Accessed: June 14, 2016].

[126] "Venezuela : Electricity Sector Statistics," *mecometer.com,*[Online]. Available: http://mecometer.com/infographic/venezuela/electricity-sector-statistics/ [Accessed: May 4, 2016]

[127] Deputy for Power & Energy Affairs Power & Energy Planning Department, *Iran and World Energy Facts and Figures, 2012,* Ministry of Energy, 2012 [Online]. Available: http://pep.moe.gov.ir/getattachment/9b9170e5-e842-49fb-8167-4b1934c80443/%DA%A9%D8%AA%D8%A7%D8%A8. [Accessed: June 14, 2016].

[128] Trading Economics. "Electricity production from oil sources (% of total) in Saudi Arabia," *New York,*[Online]. Available: http://www.tradingeconomics.com/saudi-arabia/electricity-production-from-oil-sources-percent-of-total-wb-data.html [Accessed: April 4, 2016]

[129] C. Segar, "Saudi energy mix: renewables augment gas," *IEA Energy: The Journal of the International Energy Agency,* no. 7, p. 40, Nov. 2014. [Online]. Available: http://www.iea.org/ieaenergy/issue7/saudi-energy-mix-renewables-augment-gas.html. [Accessed: June 14, 2016]

[130] I. B. Publications, Middle East Countries Mineral Industry Handbook vol. 1 Strategic Information and Regulations. Washington: LuLu Press, 2015.

[131] M. van Hauwermeiren and D. Vose, *A Compendium on Distributions.*Ghent, Belgium: Vose Software, 2009. [Online] Available: http://www.vosesoftware.com/content/ebookmr4.pdf

[132] "Electricity production from oil sources (% of total) in Saudi Arabia," *tradingeconomics.com,*[Online]. Available: http://www.tradingeconomics.com/saudi-arabia/electricity-production-from-oil-sources-percent-of-total-wb-data.html [Accessed: Apr. 4, 2016]

[133] Flowserve., "Pipeline Transportation Pumps," *Flowserve*, Bulletin FPD-8d (E), Jan. 2015 [Online]. Available: http://www.flowserve.com/files/Files/Literature/ProductLiterature/Pumps/fpd-8-e.pdf. [Accessed: May 16, 2016].

[134] B. Nesbitt, "Flow of Liquids," in *Handbook of Pumps and Pumping: Pumping Manual International*, 1st ed. Oxford, U.K.: Elsevier Science, 2006, pp. 95-124.

[135] H. N. Psaraftis and C. A. Kontovas, "Ship Emission Study prepared for Hellenic Chamber of Shipping," *National Technical University of Athens Laboratory for Maritime Transport*, May 2008 [Online]. Available: http://www.nee.gr/downloads/66ship.emissions.study.pdf. [Accessed: June 14, 2016].

[136] Man Diesel & Turbo., "Basic Principles of Ship Propulsion," *MAN Diesel & Turbo*, 5510-0004-02ppr, Dec. 2011 [Online]. Available: https://marine.man.eu/docs/librariesprovider6/propeller-aftship/basic-principles-of-propulsion.pdf?sfvrsn=0. [Accessed: June 14, 2016].

[137] H. Lindstad, B. E. Asbjørnslett, and A. H. Strømman, "Reductions in greenhouse gas emissions and cost by shipping at lower speeds," *Energy Policy,* vol. 39, no. 6, pp. 3456-3464, June 2011. [Online]. Available: http://dx.doi.org/10.1016/j.enpol.2011.03.044. [Accessed: June 14, 2016]

[138] M. Jafari, A. Badakhshan, V. Taghikhani, D. Rashtchian, C. Ghotbi, and V. A. Sajjadian, "Experimental study and simulation of different EOR techniques in a non-fractured carbonate core from an Iranian offshore oil reservoir " *Iranian Journal of Chemistry and Chemical Engineering,* vol. 27, no. 2, p. 81 to 91, Spring 2008. [Online]. Available: http://www.sid.ir/en/vewssid/j_pdf/84320080209.pdf. [Accessed: June 14, 2016]

[139] S. Ashoori, M. Zahedzadeh, S. Shokrolahzadeh, M. Radmehr, E. Roayaei, and M. Emadi, "Efficiency improvement of sea water injection plant-experience from an offshore oil field," *in Proc. of the 20th World Petroleum Congress, Dec. 4-8, 2011, Doha, Qatar*, [Online]. WPC: World Petroleum Congress, 2011. Available: https://www.onepetro.org/conference-paper/WPC-20-1151?sort=&start=0&q=Efficiency+Improvement+of+Sea+Water+Injection+PlantExperience+from+an+Offshore+Oil+Field&from_year=&peer_reviewed=&published_between=&fromSearchResults=true&to_year=&rows=10# [Accessed: June 14, 2016].

[140] "OPUS® II Technology - A New Innovation For Produced Water And Frac Flowback Treatment," *oilandgasonline.com,*[Online]. Available: http://www.oilandgasonline.com/doc/cophase-cfu-compact-flotation-unit-0001 [Accessed: Apr. 12, 2016]

[141] M. Moshfeghian, "How to Estimate Compressor Efficiency?," *John M. Campbell & Co*, July 1, 2015 [Online]. Available: http://www.jmcampbell.com/tip-of-the-month/2015/07/how-to-estimate-compressor-efficiency/. [Accessed: May 16, 2016].

[142] "Gases - Specific Heat Capacities and Individual Gas Constants," *catalog.conveyorspneumatic.com,*[Online]. Available: http://catalog.conveyorspneumatic.com/Asset/FLS%20Specific%20Heat%20Capacities%20of%20Gases.pdf [Accessed: Feb. 22, 2016]

[143] Division of Oil, Gas & Geothermal Resources, "2009 Annual Report of the State Oil,, & Gas Supervisor," *California Department of Conservation*, 2010 [Online]. Available: http://www.conservation.ca.gov/dog/pubs_stats/annual_reports/Pages/annual_reports.aspx. [Accessed:

[144] K. Sigman, "Introduction to reducing variance in Monte Carlo simulations," *Department of Industrial Engineering and Operations Research*, 2007 [Online]. Available: http://www.columbia.edu/~ks20/4703-Sigman/4703-07-Notes-ATV.pdf. [Accessed: June 14, 2016].

[145] ICF Consulting Canada, "Life Cycle Greenhouse Gas Emissions of Natural Gas: A Litrerature Review of Key Studies Comparing Emissions from Natural Gas and Coal " *The Canadian Natural Gas Initiative*, Dec. 2012 [Online]. Available: www.capp.ca/~/media/capp/customer-portal/documents/215278.pdf. [Accessed: June 14, 2016].

[146] U.S. Energy Information Administration, *International-Total Petroleum and Other Liquids Production*, 2016 [Online]. Available: http://www.eia.gov/beta/international/?fips=MX#pet. [Accessed: Feb. 17, 2016].

[147] Bureau of Safety and Environmental Enforcement, *Field Values for PACIFIC OGORA,* BSEE, 2016 [Online]. Available: https://www.data.bsee.gov/homepg/pubinfo/pacificfreeasci/product/zipped/fixed/PacificOgorFixeddom.asp#Product. [Accessed: May 16, 2016].

[148] U.S. Energy Information Administration, *International Energy Statistics,* EIA [Online]. Available: https://www.eia.gov/cfapps/ipdbproject/iedindex3.cfm?tid=5&pid=53&aid=1&cid=VE,&syid=2004&eyid=2009&unit=TBPD. [Accessed: May 5, 2016].

[149] "East West Crude Oil Pipeline Petroline," *abarrelfull.wikidot.com,* Aug. 16, 2012. [Online]. Available: http://abarrelfull.wikidot.com/east-west-crude-oil-pipeline-petroline [Accessed: Apr. 8, 2016]

Appendix A

Appendix A contains supplementary information for chapter 2.

A1. Base case model modifications

This section describes the modifications made to the original **FU**N**d**amental E**N**gineering Princip**l****E**s-based Mode**L** for Estimation of **G**reen**H**ouse **G**ases in **C**onventional **C**rude **O**ils (FUNNEL-GHG-CCO) and includes the relevant equations.

A1.1 Multistage compressor

Oil and gas compressor efficiencies range from 65% to 90% depending on the type and size of the compressor [28, 141]. This study assumes polytrophic compression with interstage cooling. The polytrophic index is calculated from the compressor efficiency and is used to find the discharge temperature and compression energy requirements. The polytrophic index is calculated using equation A1[141]:

$$\eta_{poly} = \frac{\left(\frac{k-1}{k}\right)}{\left(\frac{n-1}{n}\right)} \quad \textbf{(A1)}$$

where n = polytrophic index; k = heat capacity ratio of natural gas; and η_{poly}= compressor efficiency. The specific heat ratio for NG is 1.27 [142].

A polytrophic index distribution with a mean, minimum, and maximum of 1.36, 1.31, 1.47 is used and represents polytrophic efficiencies of 80%, 70%, and 90% [28, 55, 141]. A maximum compressor ratio (CR) of 5 is used for consistency with the published literature [8, 18]. The number of stages required is calculated using equation A2 [28]:

$$m = ROUNDUP\left[\frac{\ln\left(\frac{P_{out}}{P_{in}}\right)}{\ln(CR_{max})}, 0\right] \quad \textbf{(A2)}$$

where m = the number of stages required; P_{out} = the outlet pressure [MPa]; P_{in} = the inlet pressure [MPa]; and CR_{max} = the maximum compression ratio.

The actual compression ratio is calculated using equation A3 [28]:

$$CR = \left(\frac{P_{out}}{P_{in}}\right)^{1/m} \quad \textbf{(A3)}$$

The inlet temperature for each stage is calculated using equation A4 from OPGEE [18, 28, 141]:

$$T_i = \left[\left(1 - \eta_{coolimg}\right) * T_i * \left(CR^{(n-1/n)} - 1\right)\right] + T_{i-1} \quad \textbf{(A4)}$$

where T_i = the inlet temperature of the ith stage [ºR]; $\eta_{cooling}$ = interstage cooling efficiency; and T_{i-1} = the inlet temperature of the previous stage [ºR]. The interstage cooling efficiency is taken from OPGEE and assumed to be 80% [18]. Conservative minimum and maximum efficiencies were assumed to be 60% and 100%. The inlet temperature of the first stage is assumed for each crude.

The power of compressor is calculated using equation A5 [18, 28, 141]:

$$P_{Comp} = \left(\frac{n}{n-1}\right) * 3.027 * \frac{P_{atm}}{T_{atm}} * \frac{Z}{\eta_{poly}} * \left[CR^{(n-1/n)} - 1\right] * \sum_{i=1}^{m} T_i \quad \textbf{(A5)}$$

where P_{Comp} = the required compressor power [hp-d/MMscf]; P_{atm} = atmospheric pressure [psia], T_{atm} = atmospheric temperature [ºR]; and Z = the compressibility factor. The inlet pressure and temperature are assumed to be 101.4 kPa (14.7 psia) and 15.7 ºC (520 ºR). The compressibility factor is examined for a temperature range of 15.7 to 171.3 ºC (520 to 800 ºR) and a pressure range from 0.69 to 41.37 MPa (100psia to 6000 psia), to represent the industry, resulting in a compressibility factor range of 0.9 to 1.1 with a mean of 1 [84]. The constant 3.027 is a conversion constant with units of hp-d/MMscf-psia.

A1.2 Cogeneration capacity

The peak cogeneration steam production capacity of the Midway-Sunset field is 4.6 million bbl/month and steam consumption is 15.2 million bbl/month [87, 143]. Consequently, the cogeneration facilities can only produce 30% of the field's steam. It is assumed in the current FUNNEL-GHG-CCO refinery analysis that the remaining steam is produced with an NG once-through steam generator (OTSG) [3].

A1.3 Venting, fugitive, and flaring

Additional data were collected to quantify the venting, fugitive, and flaring (VFF) emissions. Canter did a comprehensive examination of the literature and determined that the VFF Gas Volumes for typical North American crudes ranged from 2.1% to 7% of the produced gas volumes, with an average of 4.6% [29]. These values represent the crudes included in this study and are taken as is. The reinjected gas will also have venting and fugitive emissions, but since the reinjected gas is only partially processed, it will have lower emissions than the produced gas. More detail on the reinjected gas is given in section A3.6.

A1.4 Produced gas credit

The gas credit is assumed to be the natural gas (NG) upstream emissions minus the transportation emissions. The transportation emissions are taken from GREET as 5.42 gCO_2eq/MJ [31]; the uncertainty in the credit is due to the uncertainty in the NG upstream emissions only.

A1.5 Crude energy content

The crude higher heating (HHV) value is calculated using equation A6 from Speight [30]:

$$HHV = a - b * SG^2 \quad \textbf{(A6)}$$

where HHV = higher heating value [cal/g], a and b = correlation coefficients, and SG = crude specific gravity. The correlation coefficients a and b are 11160 and 1890 cal/g [30]. PRELIM assumes that the lower heating value (LHV) is 90% of the HHV and converts the units to MJ/kg, which changes a and b to 46.693 and 7.908 MJ/kg [19].

A1.6 Updated base case defaults

Table A1 shows the insensitive emission factor (EF) inputs that have been updated from the previously published FUNNEL-GHG-CCO model. The updated values are from GREET1 2013 [31].

Table A1: Updated emission factors (g/MJ) [31]

Combustion EFs	CO_2	CH_4	N_2O
Diesel engine comb.	73.37	0.004	0.002
Natural gas utility boiler comb.	56.28	0.001	0.001
Natural gas turbine comb.	56.26	0.004	0.001
Diesel upstream	11.94	0.026	0.000
NG upstream	8.05	0.279	0.001
Natural gas upstream transmission	1.73	0.099	0.001
Marine EFs	CO_2	CH_4	N_2O
Origin to dest. comb EF of res. fuel	80.13	0.004	0.002
Dest. to origin comb EF of res. fuel	80.13	0.004	0.002
Residual oil well to pump	11.05	0.100	0.000
Gasoline distribution EFs	CO_2	CH_4	N_2O
Ocean tanker	0.53	0.001	0.000
Barge	0.60	0.001	0.000
Pipeline	0.24	0.000	0.000
Rail	0.10	0.000	0.000
Truck	0.14	0.000	0.000
Diesel distribution EFs	CO_2	CH_4	N_2O
Ocean tanker	0.25	0.000	0.000
Barge	0.36	0.000	0.000
Pipeline	0.21	0.000	0.000
Rail	0.33	0.000	0.000
Truck	0.15	0.000	0.000
Jet distribution EFs	CO_2	CH_4	N_2O
Ocean tanker	0.25	0.000	0.000
Barge	0.35	0.000	0.000
Pipeline	0.21	0.000	0.000
Rail	0.33	0.000	0.000
Truck	0.14	0.000	0.000

The fuel combustion emissions have also been updated using GREET1 2013 to 76.5, 74.7, and 73.2 gCO_2eq/MJ for gasoline, diesel, and jet fuel, respectively [31].

A2. Monte Carlo sampling error

Monte Carlo simulations use random number generators to generate samples that give variations between model runs. This variation is calculated using equation A7 [144]:

$$SE = \frac{2.56 * \sigma}{\sqrt{N}} \quad \textbf{(A7)}$$

where SE = sampling error, σ = standard deviation of the modeled mean, and N= number of samples. The modeled mean then has a 99% probability of being μ±SE. The resulting sampling error for each scenario is shown in Table A2.

Table A2: Monte Carlo sampling error for the WTW emissions

	Maya	Mars	Bow	ANS Current	ANS Historical	Kern Current	Kern Historical
SE (gCO_2eq/MJ)	0.02	0.03	0.04	0.04	0.11	0.03	0.08

A3. Input distributions

This section provides information on how the distributions in Table 2,3, and 4 in chapter 2 were determined.

A3.1 Common inputs distribution generation

The inputs that are used by multiple crudes are categorized into emission factors (EF), electricity EFs, process unit efficiency, surface processing, VFF, and "Other."

A3.1.1 Emission factors inputs

Methane emissions are of special interest as they have a larger effect on global warming than CO_2. Previous studies use a methane **Global Warming Potential** (GWP) of 25 [3, 8, 41]; this means that one tonne of methane has the same global warming effect as 25 tonnes of CO_2. The 2014 Fifth Assessment Report of the Intergovernmental Panel on Climate Change updated the GWP of methane to 34 ± 39% [39, 40]. This will primarily affect produced gas venting and fugitive emissions as the produced gas is mainly methane (78.8%), though it will also affect the natural gas upstream EF. The combustion EFs and electricity EFs will be minimally affected as methane contributes to less than 4% and 0.2%, respectively, of the overall emissions [31, 45].

Natural gas (NG) and produced gas are the main sources of heat for crude recovery and refining, and as a result, the **NG Upstream EF** has a significant effect on the results. Weber and Clavin found that shale gas emissions range from 11.0-21.0 gCO_2eq/MJ with a mean of 14.6 gCO_2eq/MJ, and conventional gas ranges from 12.4-19.5 gCO_2eq/MJ with a mean of 16.0

gCO_2eq/MJ [41]. Since 40% of U.S. NG production comes from shale wells [42], this study used a weighted mean of 15.44 gCO_2eq/MJ. To be conservative, a minimum and maximum of 11.0 and 21.0 gCO_2eq/MJ were used. These emission factors use the former global warming potential (GWP) of 25 for methane and need to be updated to use the new GWP of 34 [39, 40]. The breakdown of emissions from CO_2, CH_4, and N_2O were not available in the Weber and Calvin paper, so the breakdown from GREET was used as an approximation. GREET finds that the U.S. average NG upstream emissions are 52.1% CO_2, 45.1% CH_4, and 2.8% N_2O [31]. Using the GREET ratios, we broke down the original mean of 15.44 gCO_2eq/MJ to 8.04gCO_2/MJ, 0.28 gCH_4/MJ, and 1.45e-3 gN_2O/MJ. For ease of calculation, the minimum and maximum values are converted to 71.2% and 136% of the mean. Assuming a constant share of CO_2, CH_4, and N_2O emissions will introduce error, as the higher upstream emissions tend to have more methane emissions [145]. As a result, the maximum is increased to 140% to compensate.

For the **NG Combustion EF**, Weber and Clavin found that the uncertainty was due to the energy content of the NG and ranged from 55 to 58.1 gCO_2eq /MJ [41]. GREET values of 56.6 and 56.8 gCO_2eq/MJ are used as the mean values for industrial utility boilers and NG turbines, respectively [31]. Weber's and Calvin's values are used as the minimum and maximum values for both combustion EFs since the authors do not specify ranges for specific technologies. The minimum and maximum values are converted to percentages of the mean to account for the change in the GWP of methane.

A3.1.2 Electricity EF

The electricity EF used is dependent on the crude's location and the technology adopted or on-site generation. The mean electricity EF is determined based on the local grid EF; the minimum and maximum are based on the EF for generation technologies that are realistic for the area. GREET is used to determine the electricity EF for various technologies; the upstream EF for the NG, oil, and coal to run the power plants adds an additional 17.4%, 14.7% and 6.4% to the combustion emissions.

For Maya, which uses nitrogen injection and gas lift to produce oil, electricity is the primary energy source. For injection, the Maya nitrogen production facility currently uses an NG combined heat and power plant [43]; therefore, the **Nitrogen Compressor Electricity EF** mean

is assumed to be 471 gCO_2eq/kWh (NG combined cycle (NG CC)) [31]. The minimum and maximum are assumed to be 330 gCO_2eq/kWh (70% of the mean) and 753 gCO_2eq/kWh (NG simple cycle turbine (NG SC) [31]; a wide range was used to be conservative due to a lack of available data. For the **Gas Lift Compressor and Surface Processing**, it was assumed that electricity is generated on the floating platform. An NG SC turbine, 753 gCO_2eq/kWh [31], is assumed as the mean due to space limitations on the platform. An optimistic 471 gCO_2eq/kWh (NG CC) is assumed as the minimum and 1034 gCO_2eq/kWh (oil internal combustion engine (ICE)) is assumed as the maximum [31].

As Mars is also a floating platform, the **Mars Electricity EF** used for the artificial pump lift and surface processing will be the same as the Maya gas lift compressor.

For **Bow River Electricity EF**, the Alberta grid average from 2009-2012 was 1033gCO_2eq/kWh [44]. The original FUNNEL-GHG-CCO model assumed an NG SC turbine (753 gCO_2eq/kWh) was used to produce electricity on site using produced gas [3]. Therefore, this study assumed a mean of 753 gCO_2eq/kWh, a maximum of 1033 gCO_2eq/kWh, and a minimum of 471 gCO_2eq/kWh (NG CC) [31].

For **ANS Electricity EF**, the local grid EF is 224 gCO_2eq/kWh [45]. However, a large amount of hydro is used along the southern coast; the only power plants located in the ANS county are petroleum liquids, NG ICEs, and NG turbines [46]. Therefore, the GREET EFs of 609 gCO_2eq/kWh (NG ICE), 1034 gCO_2eq/kWh (oil ICE), and 471 gCO_2eq/kWh (NG CC) are used as the mean, maximum, and minimum values [31].

Refinery electricity is assumed to be drawn from the grid; therefore, the **Refinery Electricity EF** is dependent on the refinery location. The original FUNNEL-GHG-CCO model assumed that the refineries were located in Los Angeles (L.A.), California for Alaska North Slope and California Kern, Cushing, Oklahoma for Mars and Bow River, and Houston, Texas for Maya. eGrid data from 2004, 2005, 2007, 2009, 2010, and 2012 are averaged to find the mean electricity EFs, which were 318, 739, and 571 gCO_2eq/kWh for L.A., Cushing, and Houston, respectively [45]. For L.A., a conservative minimum and maximum of 200 gCO_2eq/kWh (approximately 3 standard deviations below the average) [45] and 753 gCO_2eq/kWh (NG SC turbine) [31] were assumed. For Cushing, a minimum and maximum of 471 gCO_2eq/kWh (NG CC) and 1051

gCO_2eq/kWh (coal steam turbine) from GREET were assumed [31]. For Houston, a minimum and maximum of 471 gCO_2eq/kWh (NG combined cycle) and 1034 (oil ICE) from GREET were assumed [31].

A3.1.3 Process unit efficiency inputs

Production, surface processing, and refining require a large amount of process heat and steam; therefore, **Boiler and Heater Efficiencies** have a significant effect on the WTW emissions. This study assumes only NG boilers are used. Manufacturer data from Cleaver-Brooks found that small (less than 800Bhp) 860 kPa (125 psig) boilers have efficiencies between 80% and 88% [47]. Larger boilers have lower efficiencies (between 70% and 75%) [48-50]. This study uses a mean of 75% and a maximum of 88% for boiler efficiency. No information was available on the minimum boiler efficiency; however, due to economic and environmental factors, low boiler efficiencies are unlikely and a conservative minimum of 62% (symmetric) is used. Heaters are used to heat various fluids throughout the refinery and surface processing units; this study assumes only NG-fired heaters are used. Drevco Process Heaters advertises heater efficiencies from 70-85% and up to 90% when heat recovery is added [51]. OPGEE and FUNNEL-GHG-CCO assumed an 80% heater efficiency [3, 18]. A report from AMETEK Process Instruments found that energy costs are 65% of the operating costs, thus providing incentives for operators to improve efficiency and making low efficiency heaters unlikely [52]. A mean of 80% a minimum of 70%, and a maximum of 90% are used.

Low Flow Pump Efficiencies are used for smaller pumps during the surface processing stage. Evans reports that smaller centrifugal pumps have efficiencies between 50% and 70% (this range includes motor efficiency) and that motor efficiencies range from 90-97% [53]. Karassik shows that a pump with a gpm/rpm ratio of 0.01 (31gpm glycol pump operating at 1750rpm) would have a maximum hydraulic efficiency of 70% and a minimum efficiency of 40% depending on the pump's specific speed [54]. Due to economics, low efficiencies are unlikely; hence, we selected a mean of 60%, a minimum of 50%, and maximum of 70% for the overall pump efficiency.

High Flow Pump Efficiencies are used for production pumps and main pipeline pumps. OPGEE, Jacobs, and FUNNEL-GHG-CCO use a 65% efficiency for production pumps [1, 15,

18]. Flowserve pumps for the oil and gas sector have gpm/rpm ratios of 0.1 to 10 [133]. Using performance charts from Karassik, we found that ratios of 0.1-10 correspond to peak hydraulic efficiencies for centrifugal pumps of 80% and 85% [54]. Evans stated that medium to large centrifugal pumps have overall efficiencies ranging from 75% to 93% [53]. Additionally, Campbell states that oil and gas centrifugal pumps operate between 70% and 90%, while reciprocating pumps operate between 85% and 92% [55]. These efficiencies are for water. When viscous fluids are pumped, the pump efficiency will drop. Conservative mean, minimum, and maximum efficiencies of 65%, 50%, and 85% were selected.

A3.1.4 Surface processing

After the crude oil reaches the surface, it goes through crude oil stabilization to separate out the gasses and water from the crude. The energy required depends on the crude specific heat capacity, the inlet temperature, and the outlet temperature. Wright developed a correlation for the **Crude Specific Heat Capacity** based on the API and temperature [56]. He also found that the specific heat capacity required a correction factor based on its UOP K factor from 0.84 to 1.5, which were used as the Monte Carlo distribution minimum and maximum. The crude stabilizer **Inlet Temperature** was assumed to have a mean temperature of 48.9 ºC [57]. Limited information is available on the crude inlet temperature, and as a result, a minimum and maximum of 37.8 and 65.6 ºC are assumed. The **Outlet Temperature** mean is assumed to be 173.3 ºC [57], with a minimum and maximum of 93.3 and 204.4 ºC [58].

For crude oil production both **Produced and Imported Water** needs to be treated to remove impurities. Rahman used an average electricity consumption based on work from Vlasopoulos et al., which examined several water treatment technologies [3, 59]. Water treatment involves four stages for produced water and two stages for imported water [3]. To determine a range of energy intensities, the processes with the lowest and highest energy intensities are selected for each stage. Minimum and maximum energy intensities were found to be 0.24 and 0.92kWh/bbl of water for produced water and 0.2 and 0.62kWh/bbl of water for imported water. We selected the averaged values of 0.36 and 0.24 kWh/bbl used by Rahman as the mean values.

A3.1.5 Venting, fugitive, and flaring

The **Vented and Fugitive Gas Volumes** for typical North American crudes range from 2.1% to 7% of the produced gas volume with an average of 4.6%, as stated in section A1.3 [29].

Flared Gas Volumes were determined using country-specific flaring estimates from the National Oceanic and Atmospheric Administration (NOAA) using data from 2004 to 2009 [60]. Oil production data were collected from the Energy Information Administration (EIA) [62, 146] and the National Energy Board (NEB) [63]; the data are shown in Table A3. It is assumed that there is no error in the oil production data and the flaring intensity error is based only on the satellite measurement error from the NOAA [60].

Table A3: Flaring ratios

Crude	Years	Total oil (bbl)	Total flaring (BCM) [60]	NOAA error (BCM) [60]	Flaring intensity (scf/bbl)	Flaring intensity error (scf/bbl)	NOAA region
Maya	2004-2009	7,675,950,000 [146]	14.91	13.62	68.6	62.6	Mexico
Mars	2004-2009	9,710,726,000 [62]	3.56	13.62	13.0	49.5	USA Conus
Bow	2004-2009	5,761,492,955 [63]	10.16	13.62	62.3	83.5	Canada
ANS	2004-2009	1,667,269,000 [62]	9.00	13.62	190.6	288.4	USA Alaska
Kern	2004-2009	9,710,726,000 [62]	3.56	13.62	13.0	49.5	USA Conus

An examination of OPGEE's in-depth analysis of **Flaring Efficiency** found that efficiencies below 80% only occur when there are both high wind speeds and a high gas velocity at the flare tips; this aligns with Carleton University research that found that Alberta's average flaring efficiency is 95%. GHGenius, OPGEE, and the original FUNNEL-GHG-CCO used flaring efficiencies of 95% [1, 14, 18], while GREET used 98% and Jacobs used 99% [15, 31]. High flaring efficiencies are common, but as flare efficiency can degrade quickly at high wind speeds a minimum of 80% is used to be conservative. Since wind speeds follow a Rayleigh distribution [18], wherein high wind speeds have a low probability of occurring, a PERT distribution, which favors values closer to the mean, is used in the Monte Carlo simulation. A mean of 95% and a maximum of 99% are used to align with previous research.

The **Produced Gas Composition** affects the surface processing, venting, and fugitive emissions as these depend on the concentration of methane. The default composition is taken from OPGEE,

which examined 135 oil wells in California [18]. To develop a beta distribution for the methane concentration, ModelRisk data fitting tools were used on the 118 wells that had methane concentrations above 50%. To ensure the gas composition totals 100%, the following method is used.

The component input mol% is generated from the user inputs and the Monte Carlo distributions. The methane concentration is determined from the OPGEE beta distribution, and the remaining components use the insensitive input triangle distributions. The mid calculation concentrations are then calculated as described here. If the methane concentration is higher than 78.8% (the default), then the sum of the component concentrations would be greater than 100%. As a result, the concentrations of nitrogen and heavier hydrocarbons will be reduced. The nitrogen and heavier hydrocarbons components are reduced first because they do not affect the surface processing or VFF calculations. The CH_4 concentration has a maximum of 98.9%; this ensures there is always room for H_2S gas, as this gas will affect the surface processing amine treater emissions. Carbon dioxide emissions are reduced last as they effect the VFF emissions and amine treater emissions.

$$m_{CO2}^{mid} = Max\left[Min\left(m_{CO2}^{in}, 1 - m_{CH4}^{mid} - m_{H2S}^{mid}\right), 0\right] \quad \textbf{(A8)}$$

$$m_{C2}^{mid} = Max\left[Min\left(m_{C2}^{in}, 1 - m_{CH4}^{mid} - m_{H2S}^{mid} - m_{CO2}^{mid}\right), 0\right] \quad \textbf{(A9)}$$

$$m_{C3}^{mid} = Max\left[Min\left(m_{C3}^{in}, 1 - m_{CH4}^{mid} - m_{H2S}^{mid} - m_{CO2}^{mid} - m_{C2}^{mid}\right), 0\right] \quad \textbf{(A10)}$$

$$m_{C4}^{mid} = Max\left[Min\left(m_{C4}^{in}, 1 - m_{CH4}^{mid} - m_{H2S}^{mid} - m_{CO2}^{mid} - m_{C2}^{mid} - m_{C3}^{mid}\right), 0\right] \quad \textbf{(A11)}$$

$$m_{N2}^{mid} = Max\left[Min\left(m_{N2}^{in}, 1 - m_{CH4}^{mid} - m_{H2S}^{mid} - m_{CO2}^{mid} - m_{C2}^{mid} - m_{C3}^{mid} - m_{C4}^{mid}\right), 0\right] \quad \textbf{(A12)}$$

If the methane concertation is below 78.8%, then the sum of the components will be less than 100%; therefore, the remainder shown below is split evenly between the five remaining gasses. The output mol% is used by the model to calculate the VFF and amine treater emissions.

$$m_{remainder}^{mid} = 1 - m_{CH4}^{mid} - m_{H2S}^{mid} - m_{CO2}^{mid} - m_{C2}^{mid} - m_{C3}^{mid} - m_{C4}^{mid} - m_{N2}^{mid} \quad \textbf{(A13)}$$

$$m_{extra}^{mid} = \frac{m_{remainder}^{mid}}{5} \quad \textbf{(A14)}$$

$$m_{CO2}^{out} = m_{CO2}^{mid} + m_{extra}^{mid} \quad \textbf{(A15)}$$

$$m_{C2}^{out} = m_{C2}^{mid} + m_{extra}^{mid} \quad \textbf{(A16)}$$

$$m_{C3}^{out} = m_{C3}^{mid} + m_{extra}^{mid} \quad \textbf{(A17)}$$

$$m_{C4}^{out} = m_{C4}^{mid} + m_{extra}^{mid} \quad \textbf{(A18)}$$

$$m_{CO2}^{out} = m_{N2}^{mid} + m_{extra}^{mid} \quad \textbf{(A19)}$$

A3.1.6 Other inputs

The **Refinery Yield Factor** is the amount of crude, in terms of energy (MJ), required to produce 1 MJ of transportation fuel. Due to losses and the generation of by-products such as fuel oils, the yield factor is greater than one. The refinery yield factor depends on the type of refinery used, the crude properties, and the refinery operating practices. This study assumes a deep conversion refinery is being used, but the yield factor still depends on the refinery configuration [19]. The crude-specific FUNNEL-GHG-CCO value is used as the mean [3]. A PERT distribution with maximums and minimums of ±10% are used based on the variation in refinery yield factors observed when alternative assays are used in Aspen HYSYS for each crude.

Finished products are **Distributed to Bulk Terminals** via ocean tankers, barges, pipelines or freight trains. FUNNEL-GHG-CCO used GREET defaults to calculate the distribution emissions [3, 31]. For gasoline distribution, barges have the highest emission intensity, 0.616 gCO_2eq/MJ, while rail has the lowest, 0.104 gCO_2eq/MJ. Therefore, to determine uncertainty in distribution, a uniform distribution from zero to one was used for the share of gasoline transported by barges. It is also assumed that the only other transportation method used is rail. This same method is used to calculate diesel and jet fuel distribution emissions.

The correlation used to calculate the **Crude's Lower Heating Value** (LHV) was taken as 90% of the higher heating value from Speight, who claimed it was generally accurate to within ±1% [19, 30]. To be conservative, a range of ±5% is used.

A3.2 Maya's input distribution generation

For **Nitrogen Generation and Compression** a MAN turbomachinery report states that 573,957 hp was required to generate and compress 1.2 billion scf/d of nitrogen to 121 bar [43]. An article in Modern Power Systems stated that the entire N_2 generation and compression facility is powered by a 520 MW combined heat and plant [64]. The compressors are driven by a combination of electric motors and steam turbines; a natural gas turbine cogeneration unit is used to produce the electricity and steam [43]. With equations A8 to A10 and the facility information, we calculated the compressor energy intensity (EI), driver efficiency, and facility energy intensity (EI).

$$Compressor\ EI = \frac{P_{Compressor} * 1000\frac{kW}{MW} * 24\frac{hr}{d}}{\dot{V}_{N2}} = 0.00856\frac{kWh}{scf\ N2} \quad \textbf{(A20)}$$

$P_{Compressor}$ = the compressor power required [428 MW] [43] and $\dot{V}_{N2}$= the nitrogen production rate [1.2e6 scf/d] [43].

$$Driver\ Efficiency = \frac{P_{Compressor}}{P_{Facility}} = 82.3\% \quad \textbf{(A21)}$$

$P_{Facility}$ = the facility power consumption [520MW] [64]. The driver efficiency of 82.3% is reasonable as large electric motors have efficiencies above 95% [18], while steam turbine drivers have peak efficiencies from 60% to 80% [65].

$$Facility\ EI = \frac{Compressor\ EI}{Driver\ Efficiency} = 0.0104\frac{kWh * d}{scf\ N2} \quad \textbf{(A22)}$$

The overall N_2 generation and compression energy intensity (kWh/bbl) is calculated by multiplying the required nitrogen injection rate (scf N_2/bbl) by the facility intensity (kWh /scf N_2)

To calculate the uncertainty in the overall N_2 generation and compression energy intensity, we assume that the compressor energy intensity is constant and vary the driver efficiency from 60% to 95%, with a mean of 82.3%.

The **Volume of Nitrogen Injected** is dependent on the field production rate. The fully operational Maya facility injects 1.2 billion scf/d of nitrogen [43]. Limón-Hernández et al. stated that in 1996 production was 1.4 mbpd prior to gas injection. Gas injection was initiated in May, 2000 and fully operational by December 2000 [66]. By October 2000, oil production was up to 1.68 mbpd with a target production rate of 2 mbpd [66]. In 2005 production peaked at 2.1 mbpd and has steadily declined to 1.46 mbpd in 2008 [67]. In 2013 production had decreased to 0.44 mbpd [68]. Hence, an N_2 injection ratio of 822 scf N_2/bbl oil (1.46 mbpd) is used as the mean with a minimum and maximum of 571 and 2727 scf N_2/bbl oil (2.1 and 0.44 mpd). The original FUNNEL-GHG-CCO model used 990 scf N_2/bbl oil and Jacobs used 1200 scf N_2/bbl oil [1, 15], which are included within the selected range.

Maya also uses a gas lift compressor to enhance oil recovery. Although the gas compressibility factor, polytrophic index, and interstage cooling efficiency are insensitive inputs, the same Monte Carlo distributions as ANS crude's are used for consistency.

A3.3 Mars' input distribution generation

Mars uses water flooding to maintain reservoir pressure. The **Water Injection Ratio** was difficult to determine as water was not injected continuously [69]. The planned water injection rate for the field is 86,500 bpd [70]. Between 2005 and 2011 production was at a minimum and maximum of 71 bpd and 120 bpd [69], which gives injection ratios of 1.21bbl/bbl and 0.72 bbl/bbl. Jacobs and Know Your Oil used higher injection ratios of 3 bbl/bbl and 1.5 bbl/bbl [8, 15]. Using production and injection plots for the N/O layer of the Mars field gave an approximate ratio of 0.32 bbl/bbl from June 2005 to June 2008, which is reasonable as Mars has experienced technical difficulties [70]. Data from the Bureau of Safety and Environmental Enforcement (BSEE) were used for the mean and gave an average water injection ratio of 0.70 bbl/bbl [71]. The data analysis is in section A4.1. The minimum and maximum are assumed to be 0.32 bbl/bbl, from the N/O layer, and 1.5 bbl/bbl, from Know Your Oil. Jacobs' ratio of 3 bbl/bbl was ignored as it uses a worldwide average [15].

The **Water Production Ratio** affects how much water needs to be treated at the surface. Jacobs uses 5.5 bbl/bbl and references a personal communication [15], while Know Your Oil used 0.2 bbl/bbl [8]. Reported data from Sousa and Lach showed ratios varied from 0.04 to 0.22 bbl/bbl [69], and 0.02 to 0.05 bbl/bbl [70]. Data from the BSEE gave an average ratio of 0.20 bbl/bbl [71]. To cover the wide range, mean, minimum and maximum values of 0.2, 0.02, and 5.5 are used.

The **Gas-to-Oil Ratio** (GOR) was determined from the BSEE data [71]. The mean of 1133 scf/bbl is from the 2012-20105 data. To be conservative, a minimum and maximum of 800 and 1400scf/bbl are used. More detail is available in section A4.1.

The **Well Lifetime Productivity** is used to amortize the well drilling emissions. For the minimum and mean, values from Know Your Oil (130,000 bbl/well) and the original FUNNEL-GHG-CCO model (533,856 bbl/well) were used [3, 8]. Data from Sousa showed that 41 wells produced a cumulative 950 million bbl of oil as of 2011 [69], which gave 23.2 million bbl/well. This is a conservative maximum as it does not include injection and exploration wells. The field production rate was updated to 95,000 bpd for constituency with the new data [69].

The **Well Depth** will affect the amount of fuel used during drilling, though the fuel amount will have a small effect. A range of 3,048 to 5791 m was taken from Jacobs [15]. These data agree with the data taken from Lach [70].

The water flood injection **Pump Discharge Pressure** effects the pumping energy consumption. Jacobs used 37.9 MPa, while a paper from Weiland found a range of 42.1 to 43.0 MPa [15, 72]. Lach found higher pressures at 42.7 to 47.2 MPa [70]. This study used a mean, minimum, and maximum of 42.0, 37.9, and 47.2 MPa.

A3.4 Bow River's input distribution generation

The **Well Depth** effects the drilling and artificial pump lift emissions. Data from the Alberta Energy Regulator show the average well depth for areas 3 and 4 from 2002 to 2013 is 954m, with a minimum and maximum of 712m and 1306m [73]. Areas 3 and 4 are used as the Bow River crude is produced from both areas. The National Energy Board (NEB) found the average depth was 1047m with a minimum and maximum of 880m and 1720m for the Bow River

Pekisko field [74]. Due to the limited data coverage, a mean, minimum, and maximum of 1000m, 600m, and 1800m were used.

The **Reservoir Pressure** is used to determine the energy requirements of the artificial pump lift and water injection pump. FUNNEL-GHG-CCO used an average pressure of 7.83 MPa, which is used as the mean [3]. Data from a Viking field well show a minimum pressure of 4.39 MPa [75], while Pekisko data show a range of 11.03 to 17.24 MPa [76]. To be conservative, a minimum and maximum of 4.14 and 17.24 MPa are assumed.

The **Water Production Ratio** was determined from data for typical heavy oil water floods in Alberta and Saskatchewan. Renouf et al. found the average WOR was 15 bbl/bbl, with the average field operating with a WOR greater than 4 bbl/bbl for 53% of the time [77, 78]. This study uses a mean, minimum and maximum of 15, 4, and 20 bbl/bbl.

A3.5 Alaska North Slope input distribution generation

ANS uses gas alternating water injection, and data show a large amount of water and gas in the production streams [79]. The **Water Production and Injection Ratios** and the **Gas Production and Injection Ratios** have a significant effect on the results. Monthly production data for Prudhoe Bay and Kuparuk were used as these two fields are responsible for approximately 75% of the Alaska North Slope Production [80]. The analysis of the ANS data can be found in section A4.2. ModelRisk fitting tools were used to develop the distributions, and ModelRisk copulas were used to relate the production and injection ratios. The gas production and injection ratios were strongly correlated with a correlation coefficient of 0.99. The water production and injection ratios showed a weaker correlation with a 0.69 correlation coefficient.

ANS injects large amounts of gas into the reservoir; hence, the compressor inputs have a significant effect on the results. The mean compressor **Inlet Temperature** is assumed to be 15ºC [8, 15]. A conservative minimum of 0ºC (cold day) and maximum of 40ºC (hot day) are assumed for this study. The **Discharge Pressure** for the injection and gas lift compressors uses a mean, minimum, and maximum of 18.6, 15.5, and 21.7 MPa. The maximum and mean are from the Alaska Department of Administration [83], and the minimum is determined assuming a symmetric distribution due to lack of data.

For the compressor calculations the **Polytrophic Index**, **Compressibility Factor**, and **Interstage Cooling Efficiency** are required. A polytrophic index distribution with a mean, minimum, and maximum of 1.36, 1.31, 1.47 is used and represents polytrophic efficiencies of 80%, 70% and 90% [28, 55, 141]. A compressibility factor range of 0.9 to 1.1 is assumed with a mean of 1 for this study [84]. The interstage cooling efficiency is assumed to be 80% with a minimum and maximum efficiency of 60% and 100%.

The venting and fugitive analyses by Canter only examine the produced gas that is not reinjected and assumes there are no venting and fugitive emissions from the reinjected gas. It is expected that the **Reinjected Gas Venting and Fugitive** volumes will be lower than the remaining produced gas since the reinjected gas is not processed to the same extent as the produced gas, but the volume will not be negligible. A GHGenius model update found that oil well fugitives and basic surface processing losses are 0.316% of the produced gas [86]; which correspond to 1.3 gCO_2eq/scf of gas processed. OPGEE found that a dehydrator can emit up to 0.4 gCO_2eq/scf [18]. Weber and Clavin found that a typical natural gas plant produces an average of 2.7 gCO_2eq/scf of fugitive emissions at the well and a minimum of 0.8 gCO_2eq/scf at the plant [41]. The lower estimate was chosen for the plant since the injected gas is not treated as thoroughly. As a result, mean, minimum, and maximum values of 1.3, 0.4, and 3.5 gCO_2eq/scf are used. The non-injected gas equivalent emissions are 18.6 gCO_2eq/scf when a venting and fugitive loss of 4.6% is used.

A3.6 California Kern input distribution generation

Kern uses steam injection to produce the heavy oil. The **Steam Injection Ratio**, **WOR**, and **GOR** were determined from monthly production data for the Midway Sunset oilfield [87]. A detailed analysis is provided in section A4.3. The WOR and SOR were also found to have a correlation coefficient of 0.91; a BiFrank copula was determined using the same methodology used in the ANS scenario.

Since Kern requires a large amount of heat for steam injection, cogeneration can be used to increase efficiency. The California Department of Conservation found that 415MW of NG cogenerated electricity is produced in the Midway Sunset field [143]. The **Natural Gas**

Consumption and **Electricity/Steam Ratio** were determined from the data; the analysis is in section A4.4.

The **Steam Energy Required** is used to convert the steam injection ratio to steam energy. The mean value of 1944 kJ/kg was determined from a typical Midway Sunset Cogeneration facility with a steam quality of 80% [89]. The steam energy required was most sensitive to the quality of steam produced; hence, the minimum and maximum values of 1682 kJ/kg and 2321 kJ/kg are for 60% and 100% quality steam [90].

The **Cogeneration Steam Capacity** determines the percentage of Kern's steam generation that uses cogeneration. The mean uses 30% from the average monthly steam consumption of 15.2 million bbl/month and the total cogeneration steam production rate of 4.6 million bbl/month [87, 143]. The minimum and maximum assumptions are no cogeneration and 100% cogeneration.

The cogeneration unit produces more electricity than the production and surface processing facilities require; the excess electricity is sold to the grid and receives a credit for offsetting the grid electricity. The **Electricity Credit** uses the local grid EF, which for California is 318 gCO_2eq/kWh [45]. A minimum of 200 gCO_2eq/kWh is assumed as a conservative lower limit. The maximum is assumed to be 471 gCO_2eq/kWh (NG combined cycle turbine) [31].

A4. Input distributions data analysis

In order to determine some of the Monte Carlo distributions, the raw data had to first be filtered, combined, or adjusted. The following sections summarize how the distributions were determined from the raw data.

A4.1 Mars data

The Mars offshore field is defined by the BSEE codes 764 and 807 [69]. Well statues codes were filtered to include only 04 (water injecting) and 08 (oil producing) wells [147]. Data were analyzed for the years 2012-2015 [71]. The average injection WOR was determined to be 0.70 bb/bbl and was constant over the four-year period. The GOR data showed a wider range of values that oscillated over the four-year time period. As a result, a wider range was used for the GOR distribution to be conservative.

A4.2 Alaska data

Monthly production data were gathered for the period January 2013 to December 2015 from the Alaska Department of Administration [79]. The data included the monthly crude, water, and gas production volumes and water and gas injection volumes [79]. Only the data from Prudhoe Bay and Kuparuk were used, as these two fields are responsible for approximately 75% of Alaska North Slope's production [80]. Over the three years analyzed, there was no correlation to time. The data were further filtered to ensure only fields that used water alternating gas injection were included.

The data showed that for the high production wells the ratios were relatively stable, but for the low production wells there was a significant amount of variation. This can be seen for the Production WOR in Figure A1. Consequently, wells producing less than 3 million bpd, approximately 20% of the total production, were excluded from the analysis. ModelRisk data fitting tools were used to produce distributions from the remaining data. Due to limitations in the data fitting software and the data coverage, the standard deviation for the distributions was multiplied by 1.5, making the distribution wider to be more conservative.

Excel's Data Analysis correlation function was used to examine the relationship between the production and production ratios. The gas production and injection ratios were strongly correlated with a correlation coefficient of 0.99. The water production and injection ratios showed a weaker correlation with a 0.69 correlation coefficient. ModelRisk BiFrank copulas were used to model the dependence between the production and injection ratios. The BiFrank copula requires the correlation parameter theta. The simulated Injection/Production ratio was determined using the copula and compared to the actual Injection/Production ratio in an iterative method until an acceptable theta was determined. For the gas ratios theta is assigned the maximum value of 35 due to the strong correlation. For the water ratios a theta of 5.6 was used; a more conservative approach was used for water as it is less sensitive variable.

For the historical scenarios the data from Prudhoe Bay are used as its cumulative production is five times larger than Kuparuk River's [79]. Similar to the current scenarios, the ratios are modelled as normal distributions. The mean values are determined from the 2015 cumulative production and injection volumes. Due to the lack of information, the standard deviation is

assumed to be the same as the current scenario's. For example, the injection WOR standard deviation was ±28% for the current scenario, so the historical scenario standard deviation is assumed to also be ±28%.

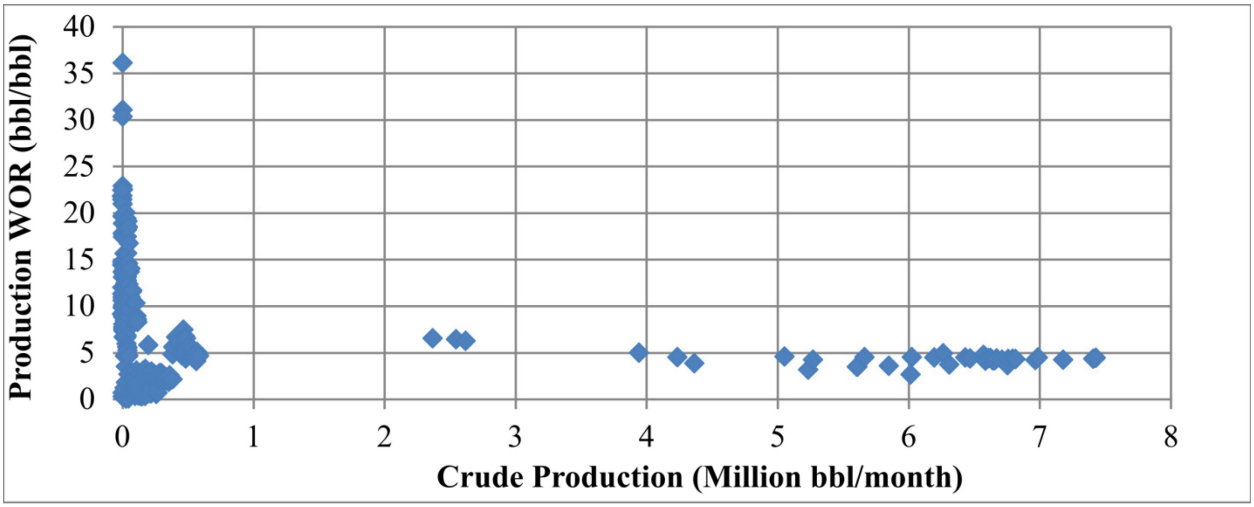

Figure A1: Alaska North Slope water production ratio

A4.3 Kern data

Data were collected from monthly production reports from January 2011 to September 2015 for the Midway Sunset oilfield [87]. The data included monthly volumes of crude, GOR, and water cut production data. For the steam injection data, the volume of steam injected was collected for both steam flooding and cyclic steam injection. The data showed an increasing trend with time; hence, the December data were used and were collected for 1996 and 2005 to 2010. The additional data confirmed that the crude production has been steadily declining while steam injection and water production have been increasing. The GOR showed a sharp rise in 2009 but leveled off afterward.

Due to the strong time dependence of the steam injection and WOR, ModelRisk data fitting tools were not used. The Monte Carlo distribution mean and minimum are determined from the averages and minimums in the 2011-2015 data. The maximum is determined by projecting a linear trend five years into the future. Since the GOR stabilized during the 2011-2015 timeframe, it was possible to fit a normal distribution to the data. The standard deviation was doubled to be conservative and account for the limited data availability. The steam injected and water produced

showed a strong dependence with a correlation coefficient of 0.91. Using the same method as for the ANS scenario, we created a BiFrank copula with a theta of 13.

Historical scenario ratios are determined from the Midway Sunset field cumulative data [87]. The minimum and maximum values are determined using the same methodology as for the ANS historical case.

A4.4 Kern cogeneration data

The data from the California Department of Conservation included the peak power consumption, mass flow rate of steam produced, and the volume of natural gas used. The amount of electricity produced was determined assuming a 90% use. The energy added to the steam was calculated from the change in enthalpy. It was assumed that the boiler is a constant pressure system and the water entered at 100C and exited at 285C [89]. The system produces 80% quality steam at 6.89 MPa [89], resulting in an enthalpy change of 1944 kJ/kg [90]. The electricity/steam ratio (MWh/MWh) was used to eliminate the three outliers that had large ratios (9.9) or small ratios (0.2) compared to the remaining plants, which had ratios between 0.54 and 0.75. The three outliers represented 16% of the peak power production. The natural gas consumption in scf/MWh was determined from the natural gas volume divided by the electricity and steam energy. ModelRisk data fitting tools were used to produce distributions for the natural gas consumption intensity and the electricity/steam ratio.

A5. Diesel and jet fuel results

The diesel and jet fuel results are similar to the gasoline emissions and are included here for completeness. The VFF and WTR emissions are the same for all three fuels. The only difference between the gasoline, diesel, and jet fuel emissions is in the refining, distribution and combustion emissions.

A5.1 Refinery tornado plots

Table A4 and A5 provide the data needed to generate the refinery tornado plots for the diesel and jet fuel scenarios.

Table A4: Diesel refinery tornado plot data

gCO_2eq/MJ Diesel	Maya		Mars		Bow		ANS		Kern	
Input	**Min**	**Max**	**Min**	**Max**	**Min**	**Max**	**Min**	**Max**	**Min**	**Max**
NG boiler EF	15.08	15.47	12.35	12.67	13.67	14.02	10.66	10.95	12.02	12.35
Boiler efficiency	14.95	15.66	12.23	12.81	13.53	14.18	10.54	11.09	11.89	12.49
Electricity EF	14.88	15.79	12.13	12.91	13.42	14.29	10.45	11.17	11.78	12.60
CH_4 GWP	14.84	15.75	12.04	13.04	13.33	14.42	10.42	11.36	11.77	12.78
NG upstream EF	14.44	16.26	11.84	13.31	13.10	14.74	10.18	11.54	11.48	13.02
Heater efficiency	14.44	16.26	11.83	13.30	13.09	14.71	10.18	11.52	11.47	13.01
Conditional mean	15.29		12.52		13.85		10.81		12.19	

Table A5: Jet refinery tornado plot data

gCO_2eq/MJ Jet	Maya		Mars		Bow		ANS		Kern	
Input	**Min**	**Max**	**Min**	**Max**	**Min**	**Max**	**Min**	**Max**	**Min**	**Max**
NG boiler EF	9.43	9.67	7.91	8.11	8.98	9.21	6.79	6.98	7.62	7.83
Boiler efficiency	9.34	9.79	7.84	8.20	8.89	9.31	6.72	7.06	7.53	7.94
Electricity EF	9.31	9.85	7.76	8.27	8.82	9.39	6.66	7.12	7.47	7.99
CH_4 GWP	9.27	9.85	7.72	8.34	8.78	9.45	6.65	7.22	7.47	8.10
Heater efficiency	9.02	10.16	7.56	8.52	8.59	9.68	6.48	7.35	7.28	8.24
NG upstream EF	9.02	10.16	7.58	8.53	8.60	9.69	6.49	7.35	7.28	8.26
Conditional mean	9.55		8.02		9.10		6.89		7.73	

A5.2 Diesel WTW tornado plots

The diesel WTW emission tornado plots use a functional unit of gCO_2eq/**MJ of Diesel**.

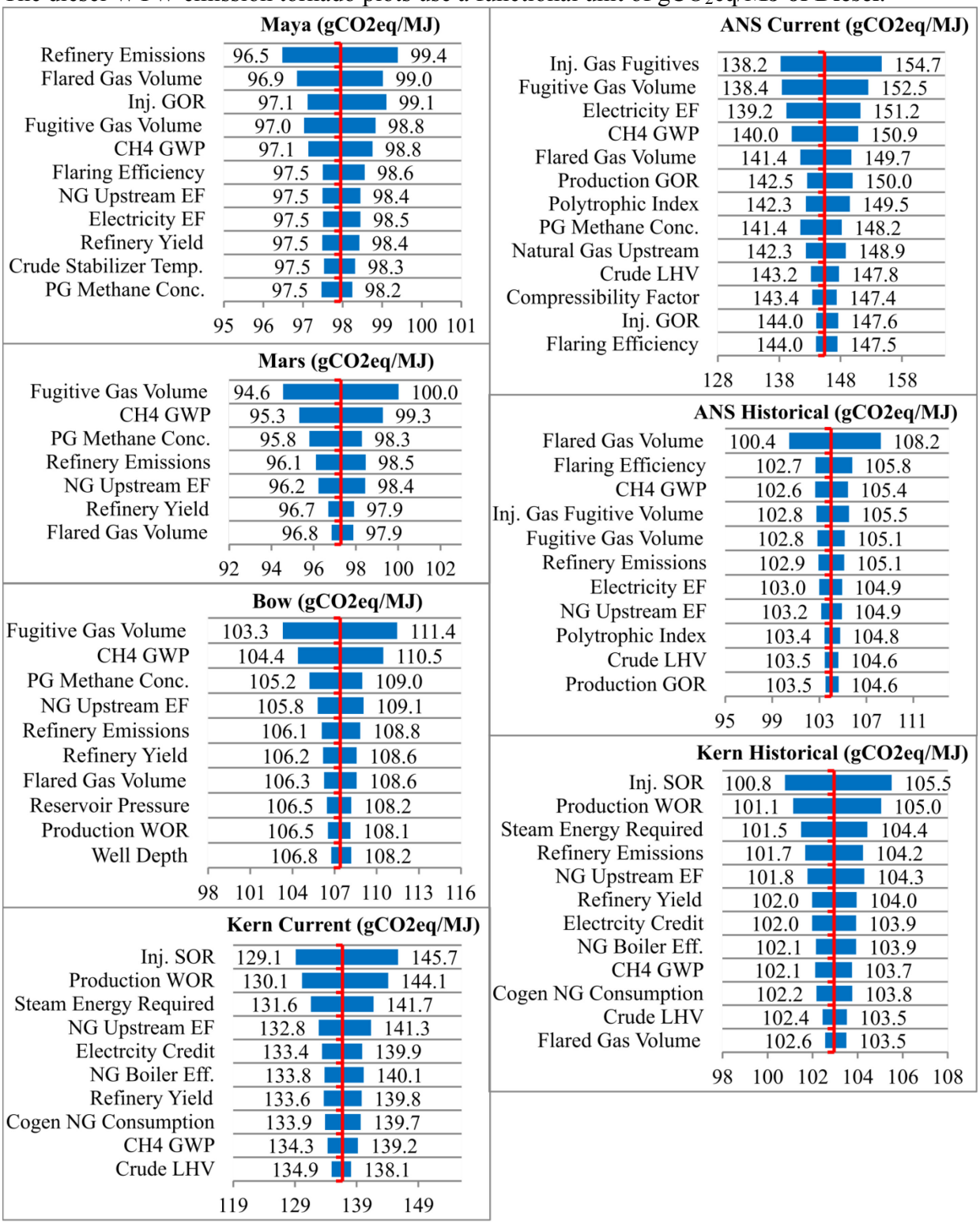

Figure A2: Diesel WTW emission tornado plots

A5.3 Jet WTW tornado plots

The jet WTW emission tornado plots use a functional unit of gCO_2eq/**MJ of Jet**.

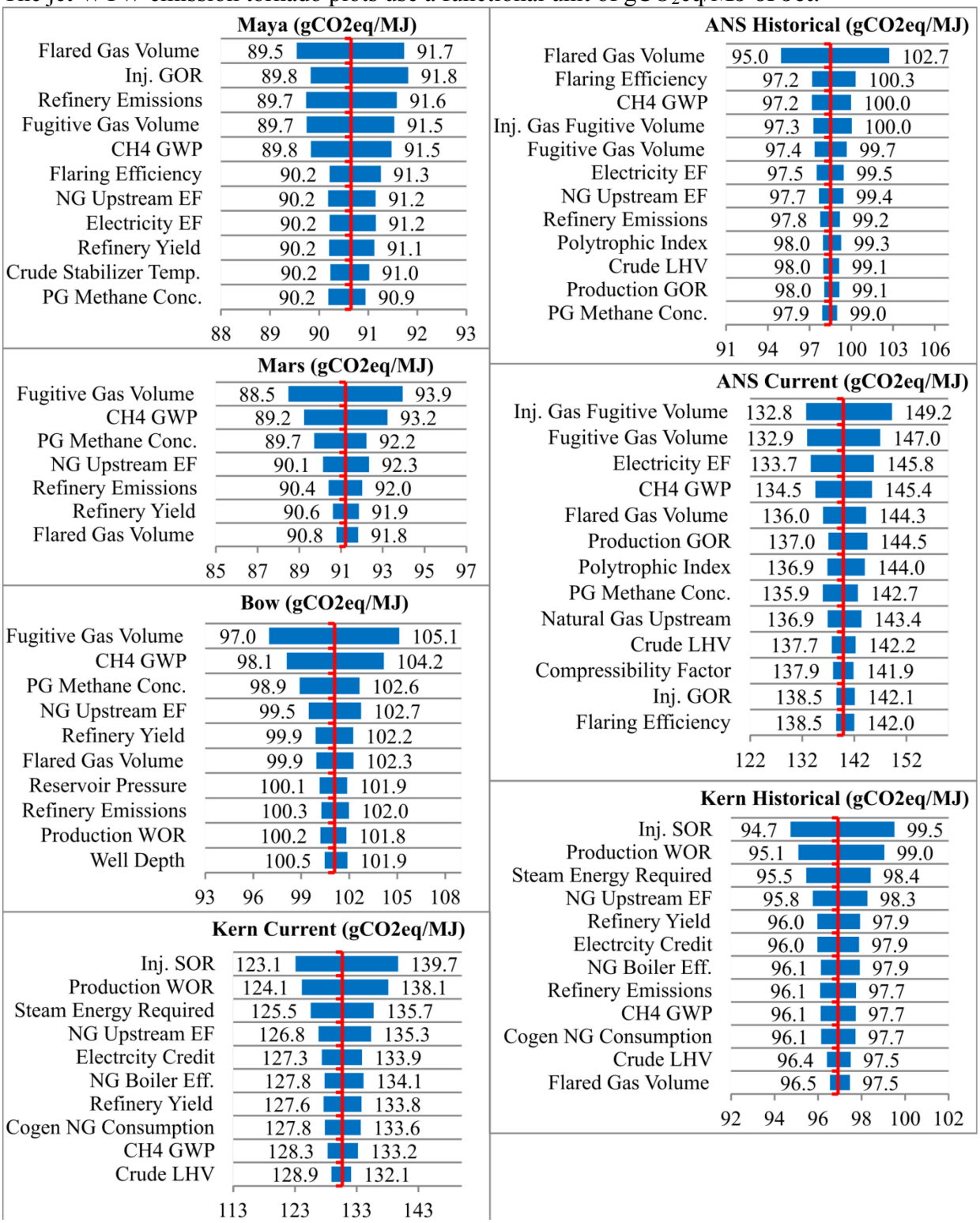

Figure A3: Jet WTW emission tornado plots

Appendix B

Appendix B contains supplementary information for chapter 3.

B1. Monte Carlo sampling error

Monte Carlo samples are generated at random from the input distribution; therefore, if the same model is run multiple times the results will have variations due to the random number generator. The Monte Carlo sampling error represents the amount of variation that will occur between simulations and is calculated using equation B1 [144]:

$$SE = \frac{2.56 * \sigma}{\sqrt{N}} \quad \textbf{(B1)}$$

where SE = sampling error, σ = standard deviation of the mean, and N= number of samples. The constant 2.56 is used to ensure the modeled mean has a 99% probability of being μ±SE. This study used 50,000 samples for each scenario. The sampling error for the four scenarios is shown in Table B1.

Table B1: Monte Carlo sampling error for the well-to-wheel emissions

	Vene HS	Vene LS	Sirri	Arab Light
SE (gCO_2eq/MJ)	0.09	0.03	0.03	0.02

B2. Monte Carlo crude specific distributions

This section reviews how the input distributions are defined from the reference material for the crude specific inputs.

B2.1 Saudi Arabia distributions

The original **Production GOR** for the Arab-D field was 97.95 m^3/m^3 [97]. A study of Arab-D crude from the Ain Dar section of the Ghawar field showed that the GOR ranges from 37.58-214.25 m^3/m^3 with a mean of 101.51 m^3/m^3; however, the wells with high gas flow rates ranged from 89.05 to 115.76 m^3/m^3 [113]. A modified PERT distribution was used with a minimum, maximum, and mean of 37.56, 241.25, 98.84 m^3/m^3 and a lambda of 15. This resulted in a distribution with a mean, P25, and P75 of 101.51, 89.05, and 114.76 m^3/m^3.

The **Injection WOR** varies from 1 to 4 m^3/m^3, with an average of 1.8 m^3/m^3 in the Ain Dar field [97]. The injection WOR range is similar to the TIAX scenario (2.7 m^3/m^3), and the Bow (3.47 m^3/m^3) and Mars (0.3-1.5 m^3/m^3) scenarios previously studied [17]. The **Production WOR** varies significantly across the Ain Dar field with water cuts ranging from close to 0% up to 99% with average of 42% (0.72 m^3/m^3) [97]. Since Saudi Arabia has to import 0.64 million m^3/d of seawater to aid injection [15] and the majority of the wells in Ain Dar have moderate water cuts, it was assumed that that the injection WOR would be higher than the production WOR [97]. Hence the injection WOR was assumed to have a mean, minimum, and maximum of 1.8, 1, and 5 m^3/m^3, and the production WOR was assumed to have a mean, minimum and maximum of 0, 0.72, and 5 m^3/m^3. A BiFrank copula was used to model a weak dependence between the water injection and production ratios; this will result in a more conservative uncertainty range.

The **Water Injection Pressure** was approximated from the reservoir pressure of 20.58 MPa [113]. Jacobs assumes the injection pressure is 2.66 MPa above the reservoir pressure [15]. Therefore, this study assumed a mean injection pressure of 20.58 MPa with a minimum and maximum of 17.83 and 23.34 MPa.

The **Produced Gas Composition** for Ain Dar wells was found to have an average methane concentration of 44.3 mol% compared to the default 78.8% [3, 113]. The gas composition was approximated from the wells' produced fluid compositions presented by Al-Eid [113]. The gas was assumed to be made up of the N_2, CO_2, H_2S, C1, C2, C3, and C4 components, and the C5+ components were removed. Al-Eid also found that the methane concentration varied from 32.5% to 47.6%. As a result, methane concentration was assumed to have a triangular distribution with a mean, minimum, and maximum of 44.3%, 32.5%, and 47.6%. The default gas composition is shown in Table B2.

Table B2: Arab Light produced gas composition

Component	Produced fluid	Approximated PG
N_2	0.1%	0.3%
CO_2	5.9%	10.9%
H_2S	1.9%	3.4%
C1	23.9%	44.3%
C2	9.8%	18.1%
C3	7.5%	13.8%
C4	4.9%	9.1%
C5	4.0%	0%
C6	3.3%	0%
C7+	38.7%	0%
Total	54.0%	100%

B2.2 Venezuela distributions

The Bachaquero **Injection SOR** varied significantly across the literature from 0.05 to 4.8 m^3/m^3 [99-102]. Therefore, two scenarios are used, low steam and high steam. The low steam scenario uses simulated data from Chourio et al., who showed that injection SOR varied from 0.05 to 0.41 m^3/m^3 depending on the steam flooding method used [99]. Rodriguez et al. reported that the cumulative injection SOR for three steam injection areas varied from 0.2 to 0.42 m^3/m^3 [100, 101]. To be conservative, the low steam scenario used a mean, minimum, and maximum of 0.25, 0.01 and 0.7 m^3/m^3. For the high steam scenario simulation, using data from Rodriguez et al. for steam flooding with horizontal wells we found the injection SOR varied from 1.2 to 4.8 m^3/m^3, with an average of 2.1 m^3/m^3 [100, 101]. To be conservative the high steam scenario used a mean, minimum, and maximum of 2.1, 1, and 5 m^3/m^3. The **Production WOR** was taken from Chourio et al. and ranged from 0.3 to 3 m^3/m^3 [99]; a mean of 2 m^3/m^3 was used for both scenarios. To be conservative a BiFrank copula was used to model dependence between the injection and production WORs.

In 1948 the American Association of Petroleum Geologists reported that the field average **Production GOR** was 97.95 m^3/m^3 [97]. In 2000 Potma et al. reported that horizontal wells were producing 69.46 m^3/m^3 by 2000 [103]. While. Rodriguez et al. found that the current GOR ranges from 142.48 to 164.38 m^3/m^3 [101]. To be conservative a mean, minimum, and maximum of 97.95, 53.43, 178.09 m^3/m^3 is used.

The **Steam Energy Required** depends on the steam pressure, water inlet temperature, and quality. Steam quality has the largest effect on the energy requirement and pressure has the smallest effect. Rodriguez used 75% at reservoir face [100, 101], while Escobar et al. stated that the steam was generated at 80% at the surface [102]. Since the well is 914 m deep there will be significant heat loss as the steam is injected, resulting in the quality decreasing. Therefore, we use a minimum, and maximum quality of 70% and, 90%. The inlet temperature is assumed to range from 37.8 to 100 ºC. Reservoir pressure in Bachaquero has dropped from its initial pressure of 9.45 to 4.83 MPa, and Escobar et al. state that the steam generators operate at 17.24 MPa [102]. Therefore, we assumed the injection pressure would vary from 4.83 to 17.24 MPa. Using 17.24 MPa injection of 70% quality steam with boiler feed water at 100 ºC results in a minimum steam energy of 1659 kJ/kg [90]. Using 4.83 MPa injection of 90% quality steam with boiler feed water at 37.8 ºC results in a maximum steam energy of 2434 kJ/kg [90]. The mean was assumed to be the average of 2046 kJ/kg.

B2.3 Sirri Iran Distributions

Simulation data for Siri C wells found that the **Production WOR** can vary from 0.1 to 1.5 m^3/m^3, and a rate of 4 m^3/m^3 was considered the cutoff point for the wells [106]. Data from Taheri et al. showed that water injection rates started at 0.1 m^3/m^3 and then rose to 5.7 m^3/m^3 [106, 112]. Due to the lack of information, a conservative triangular distribution with a mean, minimum, and maximum of 1, 0.1, 5.7 m^3/m^3 is used. The Sirri C&D fields water treatment facility is designed to produce 11,920 m^3/d of water for injection, while the fields produce a combined 4,450 m^3/d of oil [139]; this results in an **Injection WOR** of 2.7 m^3/m^3. A simulation of Sirri C wells found that the injection WOR would start at 1 m^3/m^3 and decline to 2 m^3/m^3 over 60 years [106]. Due to lack of information, a conservative triangular distribution with a mean, minimum, and maximum of 0.5, 2.7, 5.7 m^3/m^3 is used. The maximum of 5.7 is used to align with the production WOR. The water injection and production WORs are modeled with a BiFrank copula to account for dependence between the two inputs. This is a conservative approach that will result in a wider uncertainty range. Simulation data from Taheri et al. used **Water Injection Pressures** of 27.58 MPa, with a minimum injection pressure of 17.93 MPa and a maximum allowable injection pressure of 30.93 MPa [106, 112]. Due to the lack of data, these values are used for this study.

Little information is available on the **Production GOR** for Sirri. The Sirri C field had a production GOR of 57.70 m^3/m^3 in the 1970s [106]. The Sirri D field has a production GOR of 57.88 to 68.57 m^3/m^3 [138]. Water injection simulations by Tahrie et al. found that the production GOR starts at 133.57, reaches a peak at 195.90, and stabilizes at 142.48 m^3/m^3 [112].

Sirri currently does not reinject its produced waste water; instead it reduces the oil content to below 10 ppm and releases it into the ocean [114]. For the **Produced Water,** Sirri currently uses compact floatation units (CFU) [114]. CFUs combine the hydrocyclone and degassing/floatation units into a single compact unit [140]. Typically, produced water has to go through four filtration stages before being fed into a boiler [3, 59]; however, the CFU represents the first two stages only [59]. As a result, the produced water filtration uses a mean, minimum, and maximum energy intensity of 0.31, 0.63, and 1.26 kWh/m^3 from the ranges specified by Vlasopoulos et al. for stage 1 and 2 technologies [59].

B3. Monte Carlo general input distributions

This section reviews how the input distributions are defined from the reference material for the general inputs.

B3.1 Flaring intensity distributions

The flared gas volumes are obtained from the National Oceanic and Atmospheric Administration (NOAA), and the crude oil production volumes are determined from EIA government reports for each region [60, 148]. The error in the flaring intensity is assumed to be due to the error in the flared volumes, and while the oil production volumes are assumed to have no error.

Table B3: Flaring intensity error

Crude	Years	Total oil (m^3) [148]	Total flaring (BCM) [60]	NOAA error (BCM) [60]	Flaring intensity (m^3/m^3)	Flaring intensity Error (m^3/m^3)
Venezuela	2004-2009	961,233,705	14.25	13.62	14.82	14.16
Iran	2004-2009	1,444,317,045	67.19	13.62	46.52	9.42
Saudi Arabia	2004-2009	3,135,979,260	20.40	13.62	6.50	4.35

B3.2 Transportation distributions

The transportation distributions have been updated for new crudes from this study and for the North American crudes from chapter 2.

B3.2.1 Pipeline distributions

The **Pipeline Velocities** were separated into three groups, Heavy, Light/Medium, and Middle Eastern Light. Data from Enbridge showed that heavy oil pipelines operated with velocities between 0.8 and 2.0 m/s, with an average of 1.4 m/s, and light and medium oil pipelines ranged from 1.3 to 3.1 m/s, with an average of 2.0 m/s [117]. Data from Rice University found that Middle Eastern pipelines operate at velocities up to 3.8 m/s [116]. The Saudi Arabia Petroline delivers 0.8 million m^3/d through two parallel pipelines with diameters of 1220 and 1422 mm [54]. Assuming the friction losses are equal for both lines, the 1220 mm pipeline transports 0.32 million m^3/d at 3.15 m/s and the 1422 mm line transports 0.48 million m^3/d at 3.47 m/s. As a result, the Middle Eastern pipelines use a mean, minimum and maximum velocity of 3.3, 2.0, and 3.8 m/s to be conservative. Table B4 shows which ranges are used for each scenario.

Table B4: Pipeline velocity groups for each scenario

Crude	Maya	Mars	Bow	ANS	Kern	Vene	Sirri	Arab Light
Pipeline 1	L/M	L/M	L/M	L/M	H	H	MEL	MEL
Pipeline 2	L/M	L/M	L/M	L/M	H	H	L/M	L/M
H = Heavy L/M = Light/Medium MEL = Middle Eastern Light								

The **Pipeline Throughput** determines the diameter of the pipeline, which affects the friction losses. In order to provide a conservative estimate, a range of throughputs is used. An analysis of data from an Enbridge report shows an average throughput of 63,590 m^3/d with a minimum and maximum of 15,900 and 127,190 m^3/d [117]. The Saudi Arabia Petroline is a special case and uses a 0.48 million m^3/d throughput with a ±10% uncertainty range [149]. The **Pipeline Length** uses a ±10% uncertainty range to be conservative.

Research found that pipeline pumps are generally centrifugal, and some are reciprocating [133, 134]. The specific speeds for Flowserve centrifugal pipeline pumps was found to be 0.1-10 (gpm/rpm), which results in a **Pipeline Pump Efficiency** of 80-85% according to Karassik et al.

[54, 133]. Reciprocating pumps were found to have efficiencies of 85%-92% [55]. To be conservative, a mean efficiency of 85% and a peak efficiency of 92% are assumed. The minimum efficiency was assumed to be 75% as lower efficiencies would increase costs.

B3.2.2Marine distributions

The **Marine Distance** uses a ±10% uncertainty range to be conservative. The **Ocean Tanker Capacity** ranges are based on the range of typical VLCC and ULCC vary from 160,000 to 320,000 DWT [123]. For Saudi Arabia, port-specific data give a range of 280,000 to 350,000 DWT [124]. The **Tanker Velocity** ranges for typical VLCC and ULCC varies from 22.2 to 31.5 with a mean of 27.8 km/hr. [123, 135-137].

The distributions for the **Marine EF** and **Residual Oil Energy Density** were taken from the GREET uncertainty ranges [13]. The marine EF distribution was calculated from the GREET LHV, density, and carbon content distributions and results in a minimum and maximum of 97.6% and 102.6% of the mean [13]. To be conservative, a minimum and maximum of 95% and 105% were used. The residual oil energy density (kg/MJ) distribution was calculated from the GREET LHV (MJ/L) and density (g/L) distributions. The LHV is approximated by GREET as 93.5% of the HHV [13].

B3.3.3 Electricity distributions

The electricity distributions were updated for the F-2 crudes to ensure consistent boundaries were used between the F2 and F3 models. The electricity EF depends on the type of power plant used. This study uses GREET, eGrid, and the Canadian National Inventory Report to determine the electricity EF for the various crudes [13, 44, 45]. The electricity EF includes the plant combustion emissions and the fuel upstream emissions. If the power is produced offsite, then a 6.5% transmission loss is added. Table B5 shows the updated electricity EF for the F-2 models.

Saudi Arabia's electricity grid uses natural gas and oil to produce 43% and 57% of its electricity, respectively [132]; hence, the natural gas and oil average scenarios from GREET were used to determine the mean **Arab Light Electricity EF** of 869 gCO_2eq/MJ [13]. As the production wells cover a large area, it was assumed that electricity was generated offsite and transmission losses were included. To be conservative, a natural combined cycle (NG CC) and oil gas turbine was assumed for the minimum and maximum values. The **Arab Light Petroline Electricity EF** is

767 gCO_2eq/MJ and represents an onsite simple cycle natural gas turbine [130]. A minimum and maximum of 90% and 110% of the mean are used.

The Venezuelan grid is made of 68.5% hydro, 14.3% oil, and 17.2% NG power generation [126]. Since the hydroelectricity is produced in the southeast and the Bachaquero crude is produced from the northwest, it was assumed that the mean **Vene Production Electricity EF** would use only half of the country's hydroelectricity. The oil and natural gas generation used the GREET default technology shares [13]. For the minimum scenario it was assumed no hydroelectric was used and for the maximum scenario the Venezuelan grid mix was used. It was assumed electricity was generated offsite.

The Sirri grid uses 69.2% natural gas and 35.6% oil with the remainder using renewable energy [127]. The overall conversion efficiency was 33.8% for the oil and gas power plants in Iran while the GREET default technology share uses 39.7%. The GREET default technology share was adjusted by decreasing the NG CC and increasing the natural gas simple cycle (NG SC) technology share until an overall efficiency of 33.8% was achieved [13]. The adjusted technology share was used for the **Sirri Electricity EF** mean value. The minimum and maximum values used the EFs for an NG SC and an oil gas turbine generator. It was assumed all electricity is generated offsite.

Table B5: F-2 updated electricity EF (gCO_2eq/kWh)

Location	Min	Mean	Max
Maya N_2 inj.	336	479	767
Maya SP/pipeline 1	479	767	1,140
Maya refinery/pipeline 2	502	656	804
Mars pre-refinery	479	767	1,140
Mars pipeline 2	502	699	961
Mars/Bow refinery	502	741	1,119
Bow production/SP	502	990	1,119
Bow pipeline	502	834	1,119
ANS pre-refinery	502	721	972
ANS/Kern/refinery/pipeline 2	236	337	804
Kern cogen credit	236	337	502

B4. Diesel and jet fuel results

The diesel and jet uncertainty results are included here for interested readers. The results are similar to the gasoline results; the refinery emissions show the largest variation among the three fuel types. Diesel (A) and jet (B) WTW emissions show that the Sirri WTW emissions are higher than the Vene LS WTW emissions for diesel and jet fuel while for gasoline the opposite is true. This difference is a result of the refinery configuration and crude composition. The heavier Venezuelan crude requires more energy to produce gasoline compared to the lighter Sirri crude. Figures B2 and B3 show the tornado plots for the diesel and jet fuel scenarios. The main difference between the gasoline, diesel, and jet fuel tornado plots is the severity of the refinery emissions.

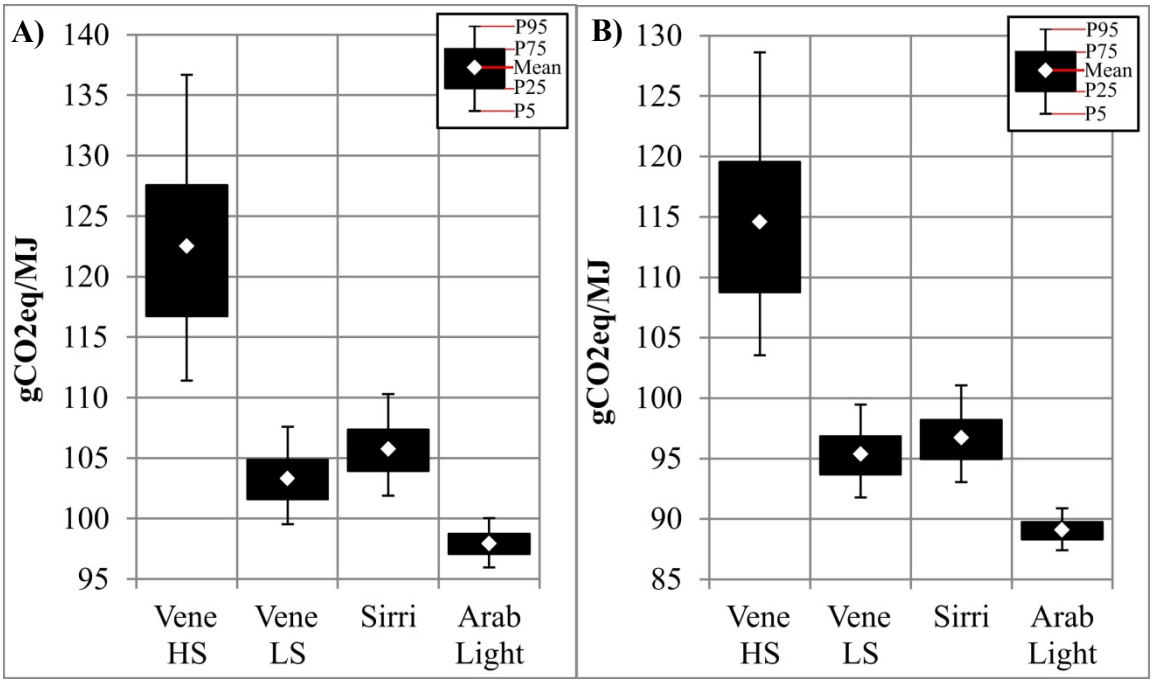

Figure B1: Diesel (A) and jet (B) WTW emissions

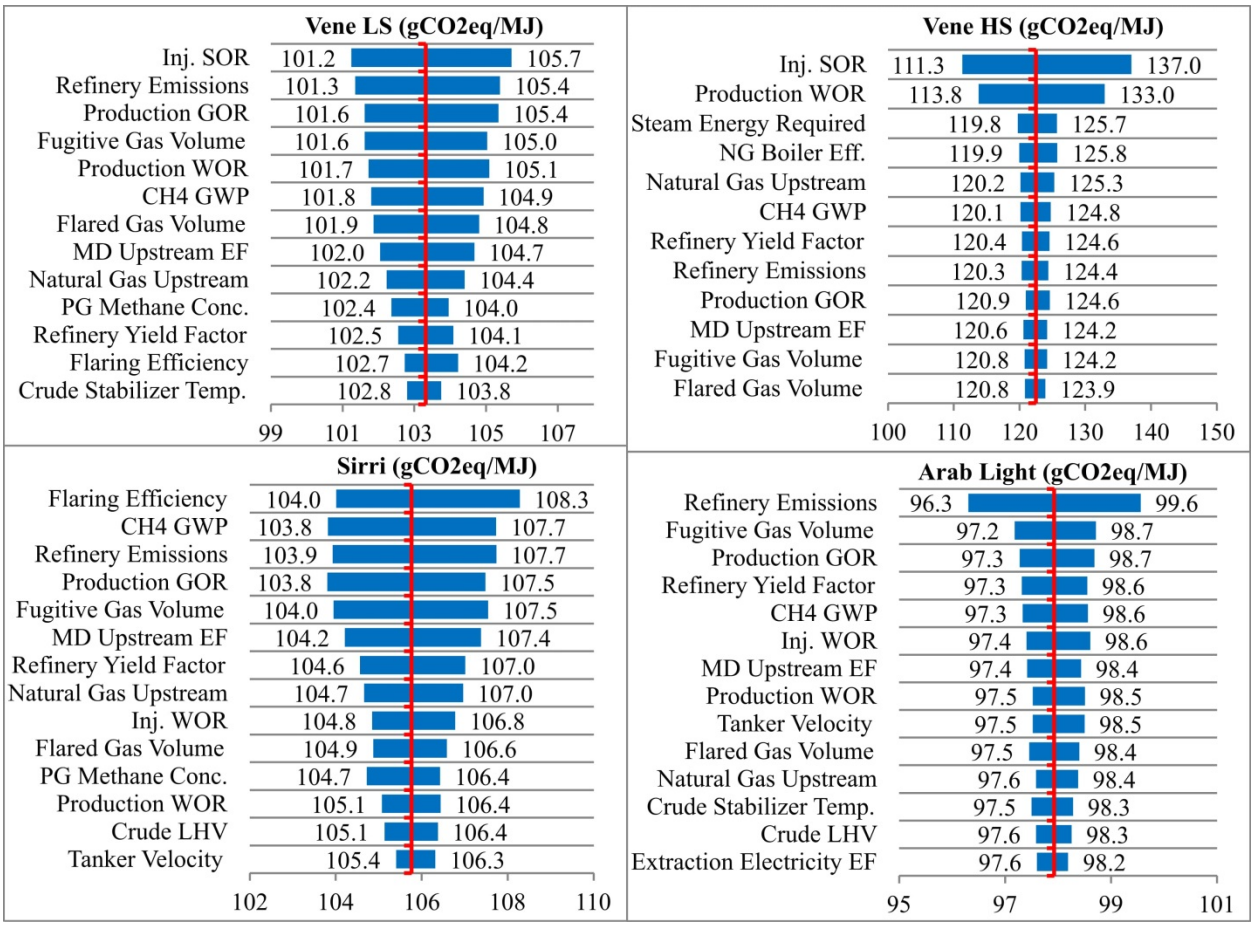

Figure B2: Diesel fuel WTW tornado plots

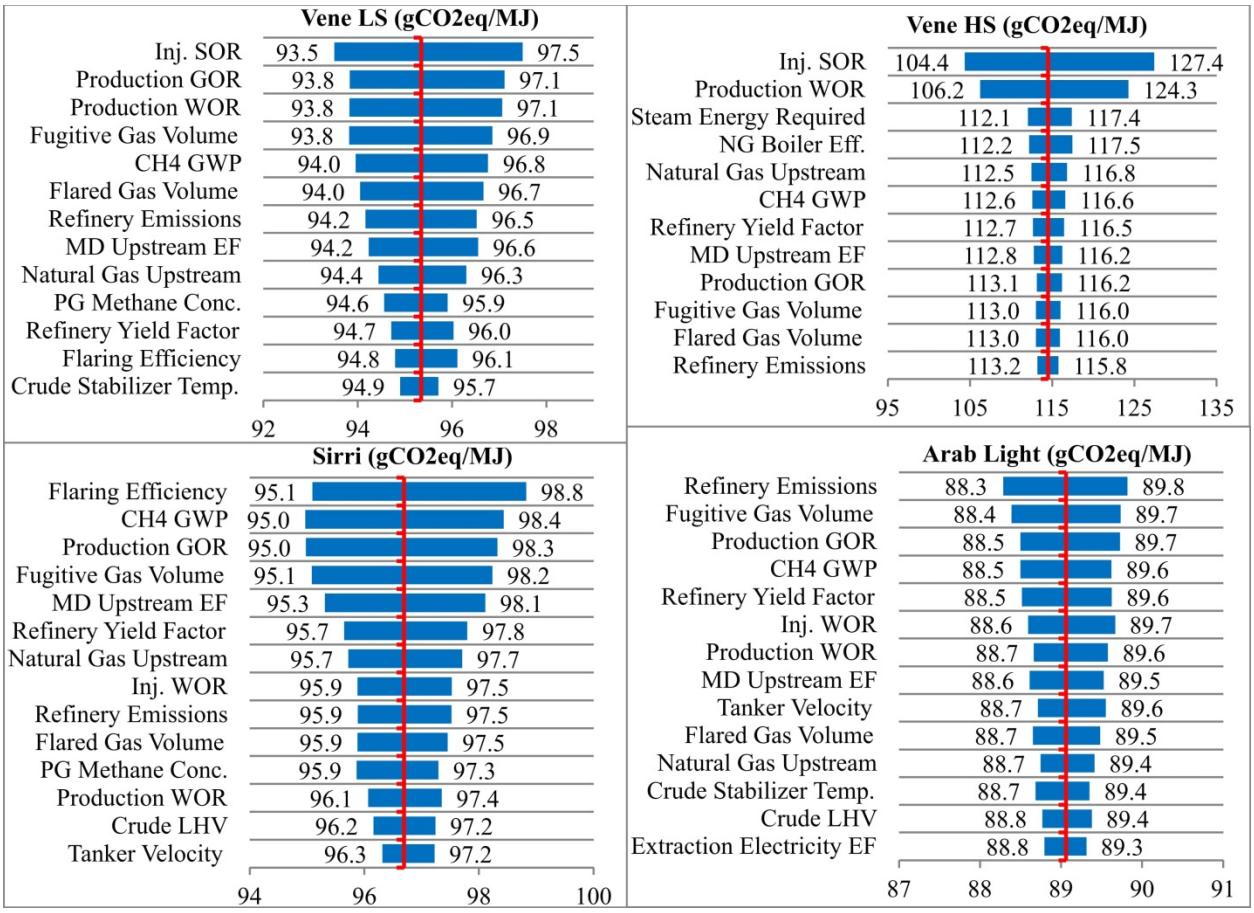

Figure B3: Jet fuel WTW tornado plots